

UCLA

UCLA Electronic Theses and Dissertations

Title

Studies on the role of macrophages in the toxicity induced by diesel exhaust particles, and on cardiovascular effects triggered by electronic cigarettes

Permalink

<https://escholarship.org/uc/item/4xx7m70b>

Author

Bhetraratana, May

Publication Date

2018

Supplemental Material

<https://escholarship.org/uc/item/4xx7m70b#supplemental>

Peer reviewed|Thesis/dissertation

UNIVERSITY OF CALIFORNIA

Los Angeles

Studies on the role of macrophages
in the toxicity induced by diesel exhaust particles,
and on cardiovascular effects triggered by electronic cigarettes

A dissertation submitted in partial satisfaction of the
requirements for the degree Doctor of Philosophy
in Molecular Toxicology

by

May Bhetraratana

2018

© Copyright by

May Bhetraratana

2018

ABSTRACT OF THE DISSERTATION

Studies on the role of macrophages in the toxicity induced by diesel exhaust particles,
and on cardiovascular effects triggered by electronic cigarettes

by

May Bhetraratana

Doctor of Philosophy in Molecular Toxicology

University of California, Los Angeles, 2018

Professor Jesus A. Araujo, Chair

Worldwide, cardiovascular disease is the leading cause of death, with air pollution and smoking being major contributors. Epidemiological studies on air pollution have demonstrated that people living in areas with poorer air quality are at greater risk for hospitalizations, morbidities, and mortality due to cardiovascular and respiratory events. Tobacco cigarette smokers are also at risk for similar events, while users of the increasingly popular electronic cigarette (e-cig) are known to experience symptoms such as coughing and reduced lung function.

While much is known about the cardiovascular health effects of air pollution and tobacco cigarette smoking, though, there remain important knowledge gaps – (1) what are the molecular mechanisms linking air pollution with disease that extends beyond the lungs, and (2) are e-cig users still at risk for developing cardiovascular disease like tobacco smokers?

Our research with a model air pollutant, diesel exhaust particles (DEP), therefore focused on the role of a particular cell type, the macrophage, in the mechanism behind the toxicity of air pollution. This portion of the work utilized experiments conducted on cells and mice to dissect gene-environment interactions. For our research regarding e-cigs, this focused on analyzing heart rate and oxidative status to look at cardiovascular function. For the work here, two groups of subjects, habitual e-cig smokers and non-smokers, were compared.

In this dissertation, Chapter 1 will lay out the foundation for the issues of air pollution and smoking, particularly e-cig smoking, and explain the need to study the toxicological mechanisms behind their health effects. Chapter 2 describes an *in vitro* study that takes advantage of two powerful tools for studying the role of genes in responses – the Hybrid Mouse Diversity Panel (HMDP) and Affymetrix microarrays. Peritoneal macrophages isolated from HMDP mice were treated with an extract of DEP, and their gene expressions profiles were analyzed and compared in order to determine key pathways. Following that discussion, Chapter 3 describes a study using myeloid-specific *Nrf2* (nuclear factor, erythroid derived 2, like 2) knockout (mNrf2 KO) mice, which were developed using the Cre-Lox technique, in order to determine the role of this antioxidant transcription factor in hyperacute *in vivo* responses. To characterize the physiological responses, echocardiographies and cardiac catheterizations were performed. Additionally, to characterize the genetic responses in the lungs, we used a recently established tool called Drop-seq to perform single cell RNA sequencing (scRNA-seq). And lastly, Chapter 4 focuses on the cardiovascular effects of e-cig smoking in human subjects. The work here is the result of a collaborative effort between our lab and a clinical team led by Dr. Holly Middlekauff.

Two supplementary video files are also a part of this dissertation. Both videos relate to Chapter 3 and show the behavior of mice exposed to DEP, with one of the mice being a genotypic control mouse (DEP-Treated-Control-Mouse.MOV) and the other being an mNrf2 KO mouse (DEP-Treated-KO-Mouse.MOV).

Overall, our results demonstrated that DEP treatment elicited *in vitro* responses in macrophages that were driven by the NRF2 antioxidant transcription factor and conducive to polarization into a Mox or Mox-like macrophage subtype. Additionally, mice that were knocked out for *Nrf2* in macrophages and other myeloid cells were highly susceptible to DEP exposure, showing signs of diastolic dysfunction and a dysregulated inflammatory response resulting in pro-inflammatory macrophages. Our results also showed that e-cig use led to harmful effects on the cardiovascular system, including reduced heart rate variability and increased systemic oxidative stress in the form of increased oxidizability of low-density lipoproteins (LDL).

The research work carried out here offers insight into a potential mechanism explaining DEP-induced cardiovascular effects and why certain people could be more susceptible to air pollution exposures. Our work also provides a greater understanding of the little-known chronic consequences of using e-cigs and could be a warning to those considering using these devices.

The dissertation of May Bhetraratana is approved.

Oliver Hankinson

Peter John Tontonoz

Xia Yang

Jesus A. Araujo, Committee Chair

University of California, Los Angeles

2018

“Eureka!”

–Archimedes

This one-word quote has been my favorite since childhood. It especially encompasses my time at UCLA since the past several years have been a time of discovery for me, both personally and professionally. Thank you to my parents, Cholladda and Wiroj, and to my little sister, Mint, for supporting my lifelong journey of seeking my own “Eureka” moments. I want to also thank Praking and my granduncle, Thaworn, for taking me in and taking care of me during my last years of the program. My work here is truly dedicated to all of them.

And I finally have an answer to the perpetual question, “When will you be done?”

Now. I am done, now.

TABLE OF CONTENTS

LIST OF FIGURESIX

LIST OF TABLESXI

LIST OF ABBREVIATIONSXII

ACKNOWLEDGEMENTS XIII

VITA XVII

CHAPTER 1 – BACKGROUND..... 1

 Introduction..... 1

 Air Pollution Components and Sources 2

 Health Effects of Air Pollution Particulates..... 6

 Prevalence of Tobacco and Electronic Cigarette Smoking..... 8

 Health Effects of Tobacco and Electronic Cigarette Smoking 10

 References..... 12

CHAPTER 2 – MACROPHAGE RESPONSES AGAINST DIESEL EXHAUST PARTICLES 17

 Abstract 17

 Introduction..... 17

 Materials and Methods..... 19

 Results..... 23

 Discussion..... 28

 Figures..... 33

 Tables..... 42

 References..... 50

CHAPTER 3 – DELETION OF NRF2 IN MYELOID CELLS INDUCES ABNORMAL	
CARDIOPULMONARY RESPONSES.....	55
Abstract.....	55
Introduction.....	55
Materials and Methods.....	57
Results.....	66
Discussion.....	74
Figures.....	86
Tables.....	107
References.....	113
CHAPTER 4 – CARDIOVASCULAR EFFECTS OF ELECTRONIC CIGARETTES	120
Introduction.....	120
Published JAMA Cardiology Article	123
Published JAMA Cardiology Article Supplement.....	130
References (for the Introduction).....	139
CHAPTER 5 – CONCLUSIONS AND FUTURE DIRECTIONS	140

LIST OF FIGURES

Figure 1-1: Global map of annual mean PM _{2.5} levels.	3
Figure 1-2: Map of the annual mean PM _{2.5} levels in the United States.	4
Figure 1-3: E-cig use among high school students in the United States in 2017.	9
Figure 2-1: Quality of selected AFFX control probes.	33
Figure 2-2: Quality of replicate microarrays.	33
Figure 2-3: Selected plots of genes with varied patterns of differential expression after DEPe treatment.	34
Figure 2-4: Top 20 Reactome pathways of the 1,284 genes upregulated with DEPe treatment.	35
Figure 2-5: Top 20 Reactome pathways of the 1,428 genes downregulated with DEPe treatment.	36
Figure 2-6: Transcription factor network of selected genes upregulated with DEPe.	37
Figure 2-7: Gene expression of macrophage markers in peritoneal macrophages after DEPe exposure.	39
Figure 2-8: Expression of macrophage markers following OxPAPC treatment.	40
Figure 2-9: Expression of macrophage markers following LPS treatment.	41
Figure 3-1: Nrf2 and its constructs.	86
Figure 3-2: Alveolar and peritoneal macrophages mRNA and protein expression.	87
Figure 3-3: Whole tissue gene expression.	88
Figure 3-4: Appearance of perfused lungs following exposures.	88
Figure 3-5: Appearance of mice following oropharyngeal aspiration of DEP.	89
Figure 3-6: Cytospin slides of bronchoalveolar lavage cells.	89
Figure 3-7: Bronchoalveolar lavage numbers following exposures.	90
Figure 3-8: H&E-stained lung sections following exposures.	91
Figure 3-9: Alveolar macrophage gene expression and BALF cytokine concentration after exposures.	92
Figure 3-10: Echocardiography left ventricular measurements.	93
Figure 3-11: Heart rates as measured by cardiac catheterization.	94
Figure 3-12: Ventricular pressures.	94

Figure 3-13: Cardiac catheterization pressure curves of the left ventricles.	95
Figure 3-14: Ventricular developed pressures.	96
Figure 3-15: Mean pulmonary arterial pressure (MPAP).	97
Figure 3-16: Plasma PON1 activity.	97
Figure 3-17: Clustering of cells analyzed in scRNA-seq.....	100
Figure 3-18: Distribution of general lung cell types for scRNA-seq.	101
Figure 3-19: Violin plots of Nrf2 expression.....	102
Figure 3-20: Number of unique differentially expressed genes (DEGs) by cell type.....	103
Figure 3-21: Common DEGs across three or more cell types in DEP- vs. PBS-treated control.	105
Figure 3-22: Violin plots of selected genes for the alveolar macrophages 1 cluster.....	106

LIST OF TABLES

Table 2-1: Samples used for Affymetrix microarrays.....	42
Table 2-2: Top 20 genes differentially expressed with DEPe treatment in peritoneal macrophages.	43
Table 2-3: Top 40 genes upregulated with DEPe treatment.	44
Table 2-4: Top 40 genes downregulated with DEPe treatment.	45
Table 2-5: Differentially expressed Mox marker genes with DEPe treatment.	46
Table 2-6: Differentially expressed M1 marker genes with DEPe treatment.	48
Table 2-7: Differentially expressed M2 marker genes with DEPe treatment.	49
Table 2-8: Summary of macrophage polarization by treatment.....	49
Table 3-1: C57BL/6J vs. LysM-Cre measurements.....	107
Table 3-2: Primers and probes for quantitative real-time PCR.....	107
Table 3-3: Distribution of lung cell types for scRNA-seq.	108
Table 3-4: DEP-treated vs. PBS-treated control DEGs and enriched pathways.....	109
Table 3-5: DEP-treated vs. PBS-treated KO DEGs and enriched pathways.	110
Table 3-6: PBS-treated KO vs. PBS-treated control DEGs and enriched pathways.....	111
Table 3-7: DEP-treated KO vs. DEP-treated control DEGs and enriched pathways.....	112

LIST OF ABBREVIATIONS

DEG	Differentially expressed gene
DEP	Diesel exhaust particles
DEPe	Diesel exhaust particles extract
DLAM	Division of Laboratory Animal Medicine (UCLA)
EPA	Environmental Protection Agency
FDR	False Discovery Rate
GCLM	Glutamate-cysteine ligase, modifier subunit
HDL	High-density lipoprotein
HMDP	Hybrid Mouse Diversity Panel
HMOX1	Heme oxygenase 1
KO	Knockout
LDL	Low-density lipoproteins
LPS	Lipopolysaccharide
NRF2	Nuclear factor, erythroid derived 2, like 2
OxPAPC	Oxidized 1-palmitoyl-2-arachidonoyl-sn-glycero-3-phosphatidylcholine
PM	Particulate matter
PON1	Paraoxonase 1
SRXN1	Sulfiredoxin 1 homolog (<i>S. cerevisiae</i>)
TXNRD1	Thioredoxin reductase 1
WHO	World Health Organization

ACKNOWLEDGEMENTS

I am thankful for the opportunity to have been in the Molecular Toxicology program, with special appreciation to our department chair, Dr. Oliver Hankinson, and to my advisor, Dr. Jesus Araujo, for taking a chance on me. On my journey to the end, I was helped by so many people, and I would like to acknowledge their professional contributions.

First, thank you to all who have been in the Araujo Lab. During my time, several students have joined our laboratory to offer their knowledge and assistance. I am grateful for our undergraduate students, all of whom were overachievers who gave their best and to whom I wish I had given more of mine: Benjamin Nguyen, Benjamin Yang, Jasmine Sidhu, Noa Park, Anjali Logue, and Karla Luna. All of these undergraduates have assisted me in genotyping my mice and performing cell studies. Ben Nguyen and Ben Yang were additionally particularly indispensable during my numerous mouse experiments. I am also grateful for the graduate students who have come through the lab during my time: Dawoud Sulaiman, Jenna Harrigan, Hiromi Murata, Gerardo Gutierrez, and Sara Erwin. They are all intelligent individuals and I know each one of them will go far in their careers. And many, many thanks to my colleagues: Dr. Min Zhang and Rajat Gupta; they have each offered so much guidance and time that I could never repay.

The mouse exposures and Affymetrix microarrays in Chapter 2 were conducted by a former post-doctoral scholar in the laboratory, Dr. Luz Orozco. Dr. Xia Yang introduced me to R, without which none of the work in Chapters 2 and 3 would have been possible.

Chapter 3 was the most grueling, but it would have been much more so had I not had the assistance and expertise of several individuals. $Nrf2^{fl/fl}$ mice were provided by Dr. Jingbo Pi. LysM-Cre mice, as well as general advice for all things research-related were generously provided by Dr. Min Zhang; she was a source of knowledge and friendship during my entire time

as a graduate student. Credit for many weeks of Western blot troubleshooting which finally resulted in a decent blot is due to Rajat Gupta. My right-hand man in the exposures, tissue collections, and analyses was Ben Yang; his help was truly invaluable. Cardiac measurements were conducted by Dr. Soban Umar. Analysis of the lung histology was performed by Dr. Nora Rozengurt. And the single-cell sequencing could not have been done without the help of Dr. Xia Yang and her lab: Dr. Jason Hong, Dr. Graciela Diamante, Dr. Sana Majid, and Dr. In Sook Ahn.

Chapter 4 is an article reprint from *JAMA Cardiology* 2.3, 278-84 (2017) entitled “Increased Cardiac Sympathetic Activity and Oxidative Stress in Habitual Electronic Cigarette Users.” The work was the result of a collaborative effort between our lab and the clinical team led by Dr. Holly Middlekauff. I also appreciate the work of Dr. Roya Moheimani and Dr. Jeffrey Gornbein, and analyses in our lab were also performed by Dr. Fen Yin. I thank Kacey Peters for coordinating everything with the patients, and I want to especially thank her and the nurses at the Clinical & Translational Research Center for making the trek up to our 4th floor lab from their B-floor clinic countless times to deliver the blood samples to us.

I greatly appreciate all the support I have received financially from the following: the UCLA Graduate Division Dr. Ursula Mandel Scholarship (2011-2012), the National Institute of Environmental Health Sciences Training Grant in Molecular Toxicology (2014-2017), and the UCLA Graduate Division Dissertation Year Fellowship (2017-2018). And, after all these years, thanks also must go to all members of my committee for their time and help in guiding me through my projects: Dr. Jesus Araujo, Dr. Oliver Hankinson, Dr. Peter Tontonoz, and Dr. Xia Yang. I am especially forever grateful for Dr. Jesus Araujo’s mentorship. His critical analysis of my work and the writing of my dissertation have undoubtedly made me a better scientist. My appreciation could never be fully put into words. I would not be here without all his help.

Lastly, I would like to conclude by offering my gratitude to those who have provided friendship, assistance, and mentorship outside of my research projects.

I am so grateful to have gone through the Molecular Toxicology program with my fellow cohort member, Lisa. Our journey took us through classes and seminars and conferences together, multiple discussions over meals, and culminated in us finishing the program just months apart. Her success encouraged my own.

I am also grateful for my friendship with Evelyn. We started our respective doctoral programs at the same time, were co-teaching assistants, and served the campus community together. Over the past couple years, we enthusiastically played (and conquered! ☺) all the racket sports available at UCLA (tennis, squash, racquetball, badminton, and table tennis) and also memorably went to the Indian Wells tourney. We have had so many discussions about graduate student life on the court, at restaurants, and in the car, encouraging each other in our academic paths. In the end, we fittingly defended our dissertations just a day apart. Cheers!

I would like to also thank the professors and teaching assistants with whom I have had the pleasure of teaching alongside. Thank you to Professors Raffaella D'Auria and Ed Rhodes for giving me the opportunity to be a teaching assistant for the Introduction to Environmental Science course. I want to also thank Professors Kevin McKeegan, Noah Garrison, and Suzanne Paulson for their guidance and for serving as excellent teachers when they later joined the course teaching team. I had a lot of fun being a teaching assistant alongside Evelyn and Therese and learned much from watching them interact with our undergraduate students.

Thank you to the Mobile Clinic Project. Being a part of this organization has taught me much about some of society's most pressing issues. I am grateful I got to team up with the best public health-minded coordinators for several years: Jennifer H. and Amie (2012-2013); Jenna

A. and Stephanie (2013-2014); Jenna v.D. and Tessa (2014-2015); and Dana and Maureen (2016-2017). And, although I did not serve as a student officer alongside the following individuals, I remain appreciative to have still worked with them: Chiara, Chiao-Wen, and Mindy (2015-2016); and Elsa, Amanda, and Caryssa (2017-2018). Being a public health coordinator requires a lot of time and effort, and for that I am thankful these ladies all stepped up to the plate and made that commitment. And finally, I must especially thank Dr. Michael Prelip of the Community Health Sciences (CHS) department. He has worked tirelessly for the mission of the Mobile Clinic and provided so much guidance and support to our public health student volunteers and also personally to myself in my career goals. Thank you to everyone with the Mobile Clinic for your dedication to the Los Angeles homeless community.

Also, thank you to the elected officials of the Graduate Student Association for entrusting me to serve the campus community. I learned I have a surprising interest in finances and reviewing funding applications. But, more importantly, I am grateful to have served alongside other students, staff, and faculty as our work together has affirmed my belief in the value of teamwork and diverse voices.

I will forever cherish all my experiences and friendships from UCLA as they have helped me become more mindful of my role as a researcher and as a citizen in our society.

Thank you everyone.

If creativity is squashed,

Desire is lost,

Gone is the inspiration,

And with it the motivation,

Forging a new path ahead is a must.

May Bhetraratana

EDUCATION

- University of California, Berkeley** May 2009
B.A. Molecular and Cell Biology
B.S. Microbial Biology
Minor: Toxicology
- Johns Hopkins Bloomberg School of Public Health** May 2010
M.H.S. Reproductive and Cancer Biology
Certificate: Vaccine Science and Policy

PUBLICATIONS

- Li, Rongsong, Kaveh Navab, Greg Hough, Nancy Daher, Min Zhang, David Mittelstein, Katherine Lee, Payam Pakbin, Arian Saffari, **May Bhetraratana**, Dawoud Sulaiman, Tyler Beebe, Lan Wu, Nelson Jen, Eytan Wine, Jesus A. Araujo, Alan Fogelman, Constantinos Sioutas, Mohamed Navab, and Tzung K. Hsiai. "Exposure to Atmospheric Ultrafine Particles Promotes Intestinal Free Oxidative Fatty Acid Production." *Environmental Health Perspectives* 123.1 (2015): 34-41.
- Moheimani, Roya S., **May Bhetraratana***, Fen Yin, Kacey M. Peters, Jeffrey Gornbein, Jesus A. Araujo, and Holly R. Middlekauff. "Increased Cardiac Sympathetic Activity and Oxidative Stress in Habitual Electronic Cigarette Users." *JAMA Cardiology* 2.3 (2017): 278-84. *Shares first authorship with RSM.
- Boas, Zachary, Pawan Gupta, Roya S. Moheimani, **May Bhetraratana**, Fen Yin, Kacey M. Peters, Jeffrey Gornbein, Jesus A. Araujo, Johannes Czernin, and Holly R. Middlekauff. "Activation of the "Splenocardiac Axis" by Electronic and Tobacco Cigarettes in Otherwise Healthy Young Adults." *Physiological Reports* 5.17 (2017): 1-9.
- Moheimani, Roya, **May Bhetraratana**, Kacey Peters, Benjamin Yang, Fen Yin, Jeffrey Gornbein, Jesus Araujo, and Holly Middlekauff. "Sympathomimetic Effects of Acute E-Cigarette Use: Role of Nicotine and Non-Nicotine Constituents." *Journal of the American Heart Association* 6.9 (2017): 1-10.
- Asanad, Kian, Jimmy Zheng, Alec Chan-Golston, Eric Tam, **May Bhetraratana**, Chiao-Wen Lan, Mindy Zhao, Ridwa Abdi, Farah Abdi, Elena Vasti, and Michael L. Prelip. "Assessing quality of care through client satisfaction at an interprofessional student-run free clinic." *Journal of Interprofessional Care* 32.2 (2017): 203-10.
- Araujo, Jesus A., and **May Bhetraratana**. (2018) Chronic Vascular Pathology and Toxicology. In: McQueen, C. A., *Comprehensive Toxicology*, Third Edition. Vol. 13, pp. 297–313. Oxford: Elsevier Ltd.

Zhang, Min, Kojiro Nakamura, Shoichi Kageyama, Akeem O. Lawal, Ke Wei Gong, **May Bhetraratana**, Takehiro Fujii, Dawoud Sulaiman, Hirofumi Hirao, Subhashini Bolisetty, Jerzy W. Kupiec-Weglinski, and Jesus A. Araujo. "Myeloid HO-1 Modulates Macrophage Polarization and Protects Against Ischemia-Reperfusion Injury." *JCI Insight* 3.19 (2018): e120596.

ABSTRACTS

Bhetraratana M, Umar S, Yang B, Park N, Eghbali M, Araujo JA. "Effects of diesel exhaust particles exposure on myeloid-specific Nrf2 knockout mice." Presented at the UCLA Cardiovascular Symposium (Sep 25, 2017) and the UCLA Department of Medicine Research Day (Oct 7, 2017).

Bhetraratana M, Hong J, Orozco LD, Diamante G, Majid S, Yang X, and Araujo JA. "The role of Nrf2 in responses to diesel exhaust particles exposures as demonstrated by microarray and Drop-seq analyses." Presented at the UCLA Department of Medicine Research Day (Sep 29, 2018).

TEACHING

"Introduction to Interventions for At-Risk Populations"
Community Health Sciences 187B, UCLA
Teaching Assistant, Spring 2014

"Introduction to Environmental Science"
Environment M10, UCLA
Teaching Assistant, Fall 2013, Fall 2014, Fall 2015
Teaching Associate, Fall 2016

SERVICE

- **Mobile Clinic Project (MCP)**, UCLA, Public Health Coordinator and Volunteer, Jan 2012 – Sep 2017
- **Community Activities Committee (CAC)**, UCLA, Graduate Representative, Sep 2013 – Jun 2014
- **Community Activities Committee (CAC)**, UCLA, Chair, Sep 2014 – Jun 2015
- **Graduate Student Association (GSA)**, UCLA, Director of Discretionary Funding, Sep 2015 – Jun 2016
- **Student Fee Advisory Committee (SFAC)**, UCLA, Graduate Representative, Sep 2016 – Jun 2017

SCHOLARSHIPS/FELLOWSHIPS

- **Dr. Ursula Mandel Scholarship**, Graduate Division, UCLA, Sep 2011 – Jun 2012
- **National Institute of Environmental Health Sciences Training Grant in Molecular Toxicology**, Dept of Pathology & Laboratory Medicine, UCLA, Jul 2014 – Jun 2017
- **Dissertation Year Fellowship**, Graduate Division, UCLA, Jul 2017 – Jun 2018

CHAPTER 1 – **BACKGROUND**

Introduction

Air pollution is arguably the largest global public health issue today. Virtually no matter where one lives, air pollution is a tangible concern. The World Health Organization (WHO) has estimated that 9 in 10 people are living in areas where the air quality is worse than acceptable standards (World Health Organization 2018). It is no wonder then that pollutant levels are rigorously monitored and regulated by many government agencies, such as the United States Environmental Protection Agency (EPA). Despite these efforts though, worldwide air pollution emissions over the past several years have shown mixed trends. While emissions have declined in Europe and in the United States by 1.5-4% from 2000 to 2009, emissions in Asia and the Pacific have increased instead, according to the latest report from the Intergovernmental Panel on Climate Change (IPCC) (IPCC 2013). With this, the threat of air pollution on human health remains. In fact, poor atmospheric quality is estimated to lead to 3.3 million premature deaths globally annually (Lelieveld et al. 2015), especially due to cardiopulmonary events. It is therefore important to study the health effects of these inhaled pollutants to better understand the mechanisms behind their toxicity.

At a much more personal level, there is another potential inhalation toxicant emerging as a separate public health issue. Humans have been smoking tobacco for many centuries, but since the beginning of the 21st century, the electronic cigarette (e-cig) has become a more attractive and modern way to smoke. The WHO estimates that 7 million people annually die from tobacco use, due to cardiovascular disease, lung cancer, and other conditions (World Health Organization

2017). On the other hand, the morbidity and mortality risks of using e-cigs are unknown, and thus there is a necessity for research studies to be conducted on these new devices.

Worldwide, cardiovascular disease is the leading cause of death (World Health Organization 2014), with air pollution and smoking being major contributors. Much of this Background Chapter will be about air pollution – the components of air pollution, its known health effects, and the key mechanisms of the health effects. Following that will be a discussion on cigarettes, particularly e-cigs and its growing popularity in society and potential health implications of their use.

Air Pollution Components and Sources

Atmospheric pollutants are a diverse mixture of gaseous compounds and particulate matter, with the composition varying by location and thus the local sources of emissions. In general, the gaseous contributions to air pollution include carbon monoxide (CO), nitrogen dioxide (NO₂), sulfur dioxide (SO₂), and ozone (O₃). The particulate matter (PM) components are categorized by size and include PM₁₀ (“coarse” particulates less than 10 µm in diameter), PM_{2.5} (“fine” particulates less than 2.5 µm in diameter), and “ultrafine” particulates (less than 0.1 µm, or 100 nm, in diameter). Our research deals specifically with the PM fraction since particulates have been implicated in various health issues, as will be described later.

The United States EPA has designated several of the gases and particulates as “criteria pollutants,” meaning that the agency has strict standards for regulating their concentration in the atmosphere, at levels that above which the pollutants are generally considered to be harmful to human health. PM is among these criteria pollutants, with PM_{2.5} and PM₁₀ standard levels set at 35 µg/m³ over a 24-hour period and at 150 µg/m³ over a 24-hour period, respectively (United

States Environmental Protection Agency 2016). PM_{2.5} also has two standards for the annual mean levels (averaged over 3 years); one standard is set at 15 µg/m³ to protect the public's welfare, while a stricter standard is set at 12 µg/m³ to protect the public's health (United States Environmental Protection Agency 2016). Some of the most polluted cities in the world are concentrated in the Middle East and Asia, with PM_{2.5} levels that can exceed the EPA standards by more than ten times, such as the city of Zabol, Iran, with an annual mean PM_{2.5} concentration of 216.7 µg/m³ (**Figure 1-1**) (World Health Organization 2016). Within the United States, there are also places that surpass the EPA guidelines, with the poorest air quality often found in the state of California, such as in Visalia and Porterville, with an annual mean PM_{2.5} concentration of 17.9 µg/m³ (**Figure 1-2**) (World Health Organization 2016).

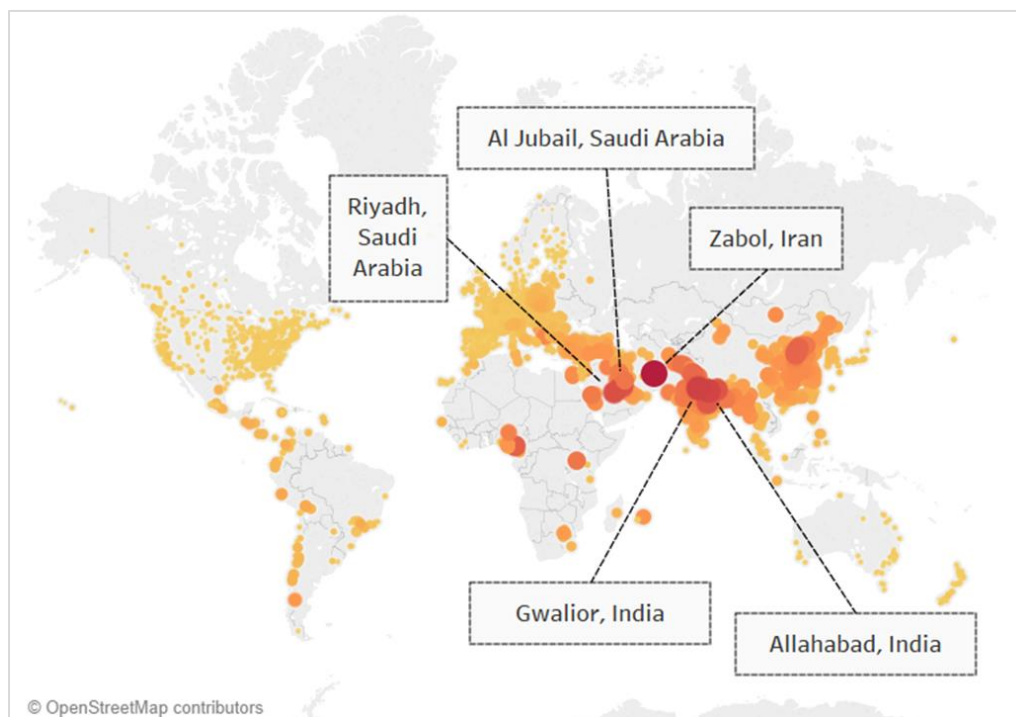


Figure 1-1: Global map of annual mean PM_{2.5} levels. The darker the color and larger the circle, the higher the particulate concentration. The five cities with the highest annual mean PM_{2.5} levels are indicated: Zabol, Iran (216.7 µg/m³); Gwalior, India (176.1 µg/m³); Allahabad, India (169.7 µg/m³); Riyadh, Saudi Arabia (155.5 µg/m³); and Al Jubail, Saudi Arabia (151.7 µg/m³). Note that the US EPA standards for PM_{2.5} are 15 µg/m³ to protect the public's welfare, and 12.0 µg/m³ to protect the public's health (United States Environmental Protection Agency 2016). The figure was created using Tableau software (with OpenStreetMap geodata) to map PM_{2.5} values from the WHO, with the data for each city last updated between 2008-2015 (World Health Organization 2016).

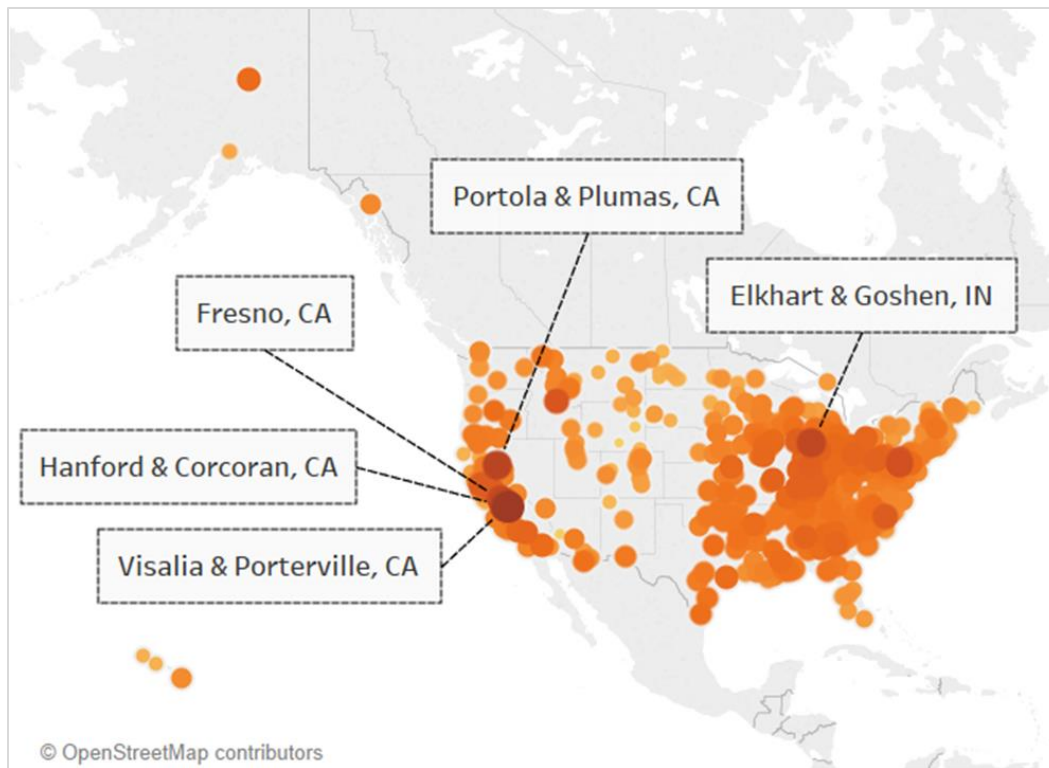


Figure 1-2: Map of the annual mean PM_{2.5} levels in the United States. The darker the color and larger the circle, the higher the particulate concentration. The five cities with the highest annual mean PM_{2.5} levels are indicated: Visalia & Porterville, California (17.9 $\mu\text{g}/\text{m}^3$); Hanford & Corcoran, California (16.45 $\mu\text{g}/\text{m}^3$); Portola & Plumas, California (15.6 $\mu\text{g}/\text{m}^3$); Fresno, California (15.13 $\mu\text{g}/\text{m}^3$); and Elkhart & Goshen, Indiana (15.1 $\mu\text{g}/\text{m}^3$). Note that the US EPA standards for PM_{2.5} are 15 $\mu\text{g}/\text{m}^3$ to protect the public's welfare, and 12.0 $\mu\text{g}/\text{m}^3$ to protect the public's health (United States Environmental Protection Agency 2016). The figure was created using Tableau software (with OpenStreetMap geodata) to map PM_{2.5} values obtained from the WHO (World Health Organization 2016), with the data for each city last updated in 2014.

There are many man-made and natural sources of particulate matter in air pollution, including traffic vehicles, road dust, industrial and construction work, fires, volcanoes, and sea spray (salt), among various other anthropogenic and environmental sources (Brook et al. 2004). Emissions from personal, commercial, and industrial/construction vehicles are consistently major contributors to PM_{2.5}. Firefighters may encounter around 100-480 $\mu\text{g}/\text{m}^3$ of airborne particulates in their fire stations, while locomotive staff may similarly breathe in high concentrations of 39-191 $\mu\text{g}/\text{m}^3$ of respirable particles (National Toxicology Program 2016). Miners who work with heavy equipment in confined spaces probably have the highest occupational exposures at 1,280

$\mu\text{g}/\text{m}^3$ of diesel exhaust particles (National Toxicology Program 2016). Even just living around major roadways can be hazardous. For instance, people near UCLA around Wilshire and Sunset Boulevards may be subjected to concentrations around $40 \mu\text{g}/\text{m}^3$ of $\text{PM}_{2.5}$ (Shirmohammadi et al. 2017).

The two main types of fuel currently used to power vehicles are gasoline and diesel. Worldwide, many large stationary machines as well as transportation vehicles run on diesel, while a large proportion of passenger vehicles in many countries rely on this fuel. In fact, diesel was the fuel type for over 50% of new passenger cars in Italy in 2013 and over 50% of all passenger cars in France in 2015 (Eurostat 2017). Other diesel-run vehicles include planes, trains, boats, and heavy equipment in construction sites (Kean et al. 2000). Compared to gasoline engines, diesel engines historically contribute more to $\text{PM}_{2.5}$ formation (Zheng et al. 2002, Gentner et al. 2012). The average diameter of diesel exhaust particles (DEP) is $0.2 \mu\text{m}$, with median values between $0.05 - 1 \mu\text{m}$ (Li et al. 2002). Within each particle is a core of carbon, upon which are absorbed many organic chemicals, such as polycyclic aromatic hydrocarbons (PAHs), as well as some non-organics, like metals (Wichmann 2007). DEP are also described in the National Toxicology Program's Report on Carcinogens as "reasonably anticipated to be a human carcinogen" (National Toxicology Program 2016). However, the recent addition of filters in newer diesel-powered vehicles are fortunately reducing their particulate emissions to be even lower than those from gasoline engines (Platt et al. 2017). Although undoubtedly, there remain countless older diesel vehicles without filters still being used today.

Clearly there is a high prevalence of diesel engines for industrial, commercial, and personal use. Diesel fuel is also a major source of particulates, and, as will be described in the next section, particulates are often attributed to morbidities and mortalities, especially due to

negative impacts on cardiovascular health. Because of these reasons, we have decided to use DEP as our model pollutant in the studies performed in Chapters 2 and 3.

Health Effects of Air Pollution Particulates

PM has been frequently associated with human health issues, especially cardiovascular abnormalities (Brook et al. 2010). The widely-cited Harvard Six Cities Study demonstrated an association between PM_{2.5} levels and mortality (Dockery et al. 1993), which helped push the EPA to set new air quality standards (Dockery 2009). Those living in the study's most PM_{2.5}-polluted city of Steubenville, Ohio had a significant 1.26 increased risk of mortality, compared to those living in the cleanest city in the study, Portage, Wisconsin (Dockery et al. 1993), amounting to a loss of two to three years in lifespan (Dockery 2014). The increased risk of death was attributed primarily to cardiopulmonary diseases and lung cancer (Dockery et al. 1993).

Since that landmark paper, there continue to be studies showing positive associations between levels of air pollution with morbidity and mortality due to cardiovascular/respiratory events. For instance, studies all over the world confirm that increased particulates are associated with increased rate of hospitalizations, including those done in the U.S. (Wellenius et al. 2005, Dominici et al. 2006, Bell et al. 2009), Australia (Morgan et al. 1998), Hong Kong (Wong et al. 1999), and Turkey (Tecer et al. 2008).

Those studies are supported by other epidemiological research looking at relationships between air pollution and the physiological basis for specific cardiopulmonary diseases. A study in Los Angeles demonstrated that residents living in areas with higher PM_{2.5} levels had, on average, thicker carotid arteries, indicative of increased risk for developing atherosclerosis (Kunzli et al. 2005). Other studies have shown associations between poor air quality with

increased blood pressure (Ibald-Mulli et al. 2001), altered heart rates (Peters et al. 1999, Gold et al. 2000), increased plasma viscosity (Peters et al. 1997), and reduced lung function (Schwartz 1989).

The American Heart Association released their first statement on “Air Pollution and Cardiovascular Disease” in 2004, in which they acknowledge that while there are many studies linking high levels of particulates with poor cardiovascular health, the mechanisms explaining these links were uncertain (Brook et al. 2004). Over a decade later, the mechanisms can still be described as just potential and plausible explanations (Fiordelisi et al. 2017). There are at least a few major hypotheses under consideration. One, the particulates may cause pulmonary inflammation that expands into systemic inflammation and oxidative stress (Brook et al. 2004, Araujo et al. 2009, Fiordelisi et al. 2017). Two, PM may affect pulmonary reflexes, subsequently altering the nervous system’s control on heart function (Brook et al. 2004, Araujo et al. 2009, Fiordelisi et al. 2017). And three, particles may directly translocate from the pulmonary spaces of the lungs and into the circulation (Nemmar et al. 2002, Fiordelisi et al. 2017). The evidence regarding these mechanisms have so far been either inconsistent or too limited to make any definitive conclusions.

Because of the uncertainty about the exact cellular and molecular processes surrounding the widely accepted public health implications of air pollutants, our projects in Chapters 2 and 3 focus on a couple of key cellular and molecular players to define a potential link between pulmonary exposures and cardiovascular diseases.

Prevalence of Tobacco and Electronic Cigarette Smoking

Another source of inhaled toxicants is cigarette smoke. In fact, it has been estimated that environmental tobacco smoke contributes approximately 1-2% of the PM in the atmosphere (Zheng et al. 2005, Polichetti et al. 2009), so both active and passive (secondhand) smoking are of public health concern. Tobacco smoking has been around for many centuries, but over the past several years, it has become less common. The results of the National Health Interview Survey (NHIS) showed a reduction in the percentage of current adult cigarette smokers in the United States from 20.9% in 2005 to 15.5% in 2016 (Jamal et al. 2018). The prevalence of cigarette smoking has also been dropping among high schoolers in the U.S. from 15.8% in 2011 to 7.6% in 2017 according to the National Youth Tobacco Survey (NYTS) (Wang et al. 2018).

However, within the last 15 years, the e-cig has emerged as an increasingly popular, yet potentially toxic, nicotine-delivery system. In fact, the modern form of the e-cig was invented by Hon Lik in 2003 as an "alternative to smoking cigarettes" (Boseley 2015). While tobacco cigarettes rely on combustion, e-cigs work by way of a battery-powered unit that heats up the so-called e-juice (a flavored liquid often containing nicotine) into inhalable vapors. The National Adult Tobacco Survey (NATS) estimated the percentage of adults who use e-cigs "every day" or "some days" as 1.9% in 2012-2013 (Agaku et al. 2014). When NATS ended in 2014, questions on e-cig smoking were subsequently included into NHIS, and this latter survey showed that the percentage of current e-cig use jumped to 3.7% in 2014, although there was a significant decrease to 3.2% later in 2016 (Bao et al. 2018).

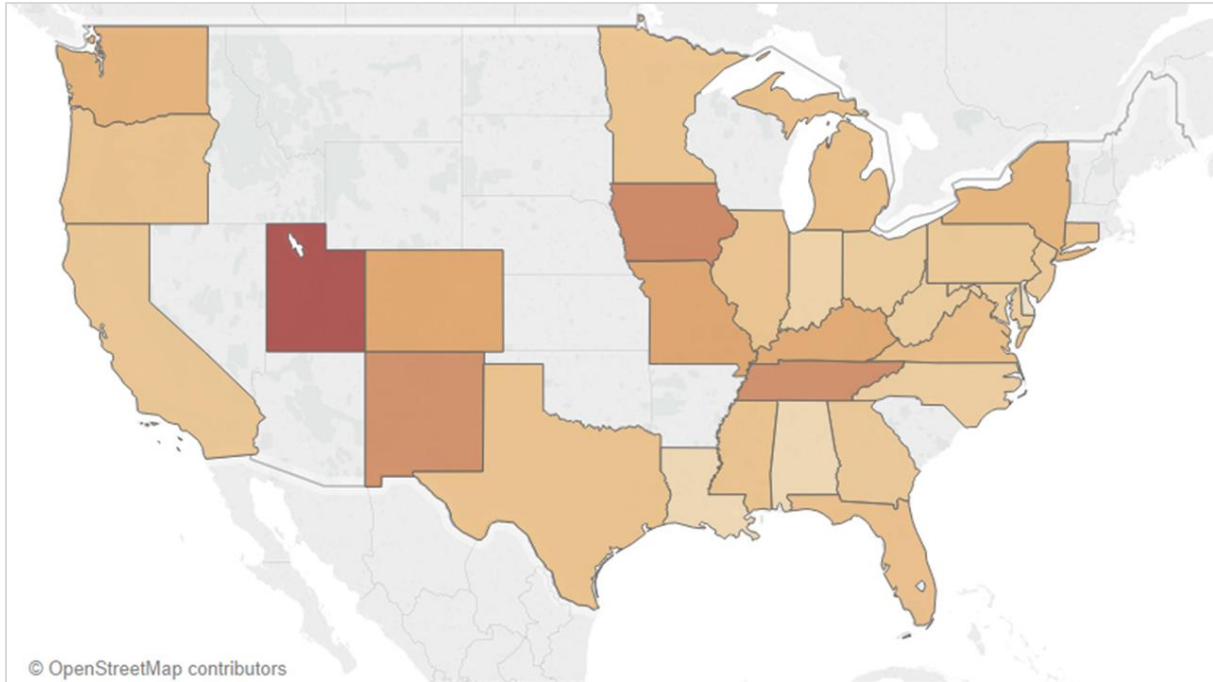


Figure 1-3: E-cig use among high school students in the United States in 2017. The darker the color, the higher the percentage of high school students with current e-cig use. States that were missing values are uncolored (and include Alaska and Hawaii, which are not present in this figure). Nine states had prevalence levels higher than the national average of 11.7%. Those states were Utah (40.1%), Iowa (26.4%), Tennessee (24.2%), New Mexico (23.9%), Missouri (18.2%), Colorado (17.2%), Kentucky (16.7%), Washington (13.7%), and New York (13.6%). Delaware had the lowest e-cig use rate at 1.6%. The figure was created using Tableau software (with OpenStreetMap geodata) to map values obtained from the 2017 National Youth Tobacco Survey (NYTS) (Office on Smoking and Health 2017).

A much more pronounced e-cig use trend has been observed among youth. According to the NYTS, the percentage of high school students who currently use these devices rapidly rose from 1.5% in 2011 to 16% in 2015 (U.S. Department of Health and Human Services 2016). Although e-cig use among students dropped for the first time in 2016 to 11.3% (Jamal et al. 2017), it remained steady the following year at 11.7% in 2017 (Wang et al. 2018). Despite the drop, e-cigs were still the most popular tobacco product last year among high schoolers (Wang et al. 2018). That being said, there is large variability in the prevalence of youth e-cig use in each state, with Utah by far surpassing the rest of the states that were surveyed; 41.1% of high schoolers in Utah were e-cig users, compared to the second-place state, Iowa at 26.4% (**Figure**

1-3). Overall, it is clear there is a generational difference in the preference of these devices, with teenagers currently using e-cigs more favorably compared to adults. Therefore, over the next several years, the percentage of people that use them will likely rise, underscoring the need to study their effects on health.

Health Effects of Tobacco and Electronic Cigarette Smoking

Active and passive (secondhand) cigarette smoking have long been known to lead to health issues and death. Smokers are at risk for numerous conditions including, but not limited to, coronary heart disease, stroke, cancers of the lung and other organs, chronic obstructive pulmonary disease (COPD), and reproductive dysfunctions (U.S. Department of Health and Human Services 2014). For non-smokers, passive exposure to secondhand smoke still can result in cardiopulmonary consequences including lung cancer, coronary heart disease, and stroke, among others (U.S. Department of Health and Human Services 2014). The carcinogenic and toxic properties of tobacco smoke may be due to any one or combination of the >4,000 known compounds found in tobacco smoke such as nicotine, ammonia, benzene, phenols, radioactive elements, and many other chemicals (National Toxicology Program 2016). In addition, tobacco smoke also contains particulates in the PM₁₀, PM_{2.5}, and ultrafine ranges (Invernizzi et al. 2004), which themselves can be harmful. The main question then is this: are e-cigs any better?

Currently, e-cigs have elicited mixed reactions from the public, from being touted as a safer alternative to tobacco cigarettes, to being a cause for concern with only a limited amount of research having been done on their effects on health (Cahn et al. 2011). An online PubMed search of the term “electronic cigarettes” reveals that from 2007 to 2011, there were less than 10 total published research studies referring to this topic. Since 2012, though, the number of

“electronic cigarettes” research articles has shot up exponentially, peaking so far at 335 articles published just within the 2016 year. As of October 1, 2018, there were 1,565 total articles on “electronic cigarettes” published since 2007 in the PubMed database. On the other hand, there are over 28,000 studies published on the topic of “tobacco cigarettes” that are currently in PubMed. Clearly, there is still much more work to be done to better understand the personal and public health impacts of e-cigs.

E-cig vapors comprise many free radicals and compounds, including nicotine, propylene glycol, glycerol, formaldehyde, acrolein, nitrosamines, and others, all at levels presumably less than those found in tobacco cigarette smoke (Callahan-Lyon 2014, Goniewicz et al. 2014). However, the degree to which the concentration of each compound is reduced compared with cigarette smoke may vary widely. For instance, the concentration of acetaldehyde in e-cig vapor was determined to be 450 times less than in tobacco cigarette smoke, while formaldehyde was just nine times less (Goniewicz et al. 2014). Even with the lower concentrations, e-cig vapors from nicotine- and flavor-containing e-juices have been shown to still be cytotoxic to cultured skin and lung cells, much like cigarette smoke (Cervellati et al. 2014). Additionally, e-cig vapors are also harmful enough to increase oxidative stress in mouse lungs, promote macrophage migration into the alveoli, and reduce capacity of macrophages to clear a pulmonary bacterial infection (Sussan et al. 2015). These negative effects could also be due to the particulate component of e-cig vapors, which have been shown to contain a large number of ultrafine particles with an average diameter of less than 500 nm (Ingebrethsen et al. 2012).

In humans, some acute health issues due to e-cig use have been documented, such as irritation of the oral cavity, coughing, increased cytokines, and reduced forced expiratory volume (Callahan-Lyon 2014). But there is virtually no data on the ability of e-cigs to trigger

cardiovascular health effects. Chapter 4 addresses the need to fill in this research gap by testing the cardiovascular effects of e-cigs on individuals who have been using these devices for at least one year.

References

Agaku, I. T., B. A. King, C. G. Husten, R. Bunnell, B. K. Ambrose, S. S. Hu, E. Holder-Hayes and H. R. Day (2014). "Tobacco product use among adults--United States, 2012-2013." MMWR Morb Mortal Wkly Rep **63**(25): 542-547.

Araujo, J. A. and A. E. Nel (2009). "Particulate matter and atherosclerosis: role of particle size, composition and oxidative stress." Part Fibre Toxicol **6**: 24.

Bao, W., G. Xu, J. Lu, L. G. Snetselaar and R. B. Wallace (2018). "Changes in Electronic Cigarette Use Among Adults in the United States, 2014-2016." Jama **319**(19): 2039-2041.

Bell, M. L., K. Ebisu, R. D. Peng, J. M. Samet and F. Dominici (2009). "Hospital admissions and chemical composition of fine particle air pollution." Am J Respir Crit Care Med **179**(12): 1115-1120.

Boseley, S. (2015). "Hon Lik invented the e-cigarette to quit smoking – but now he's a dual user." Retrieved May 31, 2018.

Brook, R. D., B. Franklin, W. Cascio, Y. Hong, G. Howard, M. Lipsett, R. Luepker, M. Mittleman, J. Samet, S. C. Smith, Jr. and I. Tager (2004). "Air pollution and cardiovascular disease: a statement for healthcare professionals from the Expert Panel on Population and Prevention Science of the American Heart Association." Circulation **109**(21): 2655-2671.

Brook, R. D., S. Rajagopalan, C. A. Pope, 3rd, J. R. Brook, A. Bhatnagar, A. V. Diez-Roux, F. Holguin, Y. Hong, R. V. Luepker, M. A. Mittleman, A. Peters, D. Siscovick, S. C. Smith, Jr., L. Whitsel and J. D. Kaufman (2010). "Particulate matter air pollution and cardiovascular disease: An update to the scientific statement from the American Heart Association." Circulation **121**(21): 2331-2378.

Cahn, Z. and M. Siegel (2011). "Electronic cigarettes as a harm reduction strategy for tobacco control: a step forward or a repeat of past mistakes?" J Public Health Policy **32**(1): 16-31.

Callahan-Lyon, P. (2014). "Electronic cigarettes: human health effects." Tob Control **23 Suppl 2**: ii36-40.

Cervellati, F., X. M. Muresan, C. Sticozzi, R. Gambari, G. Montagner, H. J. Forman, C. Torricelli, E. Maioli and G. Valacchi (2014). "Comparative effects between electronic and

cigarette smoke in human keratinocytes and epithelial lung cells." Toxicol In Vitro **28**(5): 999-1005.

Dockery, D. (2014). Landmark air pollution study turns 20. The Big 3. K. Feldscher. Boston, MA, Harvard T.H. Chan School of Public Health.

Dockery, D. W. (2009). "Health effects of particulate air pollution." Ann Epidemiol **19**(4): 257-263.

Dockery, D. W., C. A. Pope, 3rd, X. Xu, J. D. Spengler, J. H. Ware, M. E. Fay, B. G. Ferris, Jr. and F. E. Speizer (1993). "An association between air pollution and mortality in six U.S. cities." N Engl J Med **329**(24): 1753-1759.

Dominici, F., R. D. Peng, M. L. Bell, L. Pham, A. McDermott, S. L. Zeger and J. M. Samet (2006). "Fine particulate air pollution and hospital admission for cardiovascular and respiratory diseases." Jama **295**(10): 1127-1134.

Eurostat. (2017). "Passenger cars in the EU." Eurostat Retrieved December 27, 2017, from http://ec.europa.eu/eurostat/statistics-explained/index.php/Passenger_cars_in_the_EU.

Fiordelisi, A., P. Piscitelli, B. Trimarco, E. Coscioni, G. Iaccarino and D. Sorriento (2017). "The mechanisms of air pollution and particulate matter in cardiovascular diseases." Heart Fail Rev **22**(3): 337-347.

Gentner, D. R., G. Isaacman, D. R. Worton, A. W. Chan, T. R. Dallmann, L. Davis, S. Liu, D. A. Day, L. M. Russell, K. R. Wilson, R. Weber, A. Guha, R. A. Harley and A. H. Goldstein (2012). "Elucidating secondary organic aerosol from diesel and gasoline vehicles through detailed characterization of organic carbon emissions." Proc Natl Acad Sci U S A **109**(45): 18318-18323.

Gold, D. R., A. Litonjua, J. Schwartz, E. Lovett, A. Larson, B. Nearing, G. Allen, M. Verrier, R. Cherry and R. Verrier (2000). "Ambient pollution and heart rate variability." Circulation **101**(11): 1267-1273.

Goniewicz, M. L., J. Knysak, M. Gawron, L. Kosmider, A. Sobczak, J. Kurek, A. Prokopowicz, M. Jablonska-Czapla, C. Rosik-Dulewska, C. Havel, P. Jacob, 3rd and N. Benowitz (2014). "Levels of selected carcinogens and toxicants in vapour from electronic cigarettes." Tob Control **23**(2): 133-139.

Ibald-Mulli, A., J. Stieber, H. E. Wichmann, W. Koenig and A. Peters (2001). "Effects of air pollution on blood pressure: a population-based approach." Am J Public Health **91**(4): 571-577.

Ingebrethsen, B. J., S. K. Cole and S. L. Alderman (2012). "Electronic cigarette aerosol particle size distribution measurements." Inhal Toxicol **24**(14): 976-984.

Invernizzi, G., A. Ruprecht, R. Mazza, E. Rossetti, A. Saso, S. Nardini and R. Boffi (2004). "Particulate matter from tobacco versus diesel car exhaust: an educational perspective." Tob Control **13**(3): 219-221.

IPCC (2013). Climate Change 2013: The Physical Science Basis, Working Group I Contribution to the Fifth Assessment Report of the Intergovernmental Panel on Climate Change. T. F. Stocker, D. Qin, G.-K. Plattner et al. New York: 1535.

Jamal, A., A. Gentzke, S. S. Hu, K. A. Cullen, B. J. Apelberg, D. M. Homa and B. A. King (2017). "Tobacco Use Among Middle and High School Students - United States, 2011-2016." MMWR Morb Mortal Wkly Rep **66**(23): 597-603.

Jamal, A., E. Phillips, A. S. Gentzke, D. M. Homa, S. D. Babb, B. A. King and L. J. Neff (2018). "Current Cigarette Smoking Among Adults - United States, 2016." MMWR Morb Mortal Wkly Rep **67**(2): 53-59.

Kean, A. J., R. F. Sawyer and R. A. Harley (2000). "A fuel-based assessment of off-road diesel engine emissions." J Air Waste Manag Assoc **50**(11): 1929-1939.

Kunzli, N., M. Jerrett, W. J. Mack, B. Beckerman, L. LaBree, F. Gilliland, D. Thomas, J. Peters and H. N. Hodis (2005). "Ambient air pollution and atherosclerosis in Los Angeles." Environ Health Perspect **113**(2): 201-206.

Lelieveld, J., J. S. Evans, M. Fnais, D. Giannadaki and A. Pozzer (2015). "The contribution of outdoor air pollution sources to premature mortality on a global scale." Nature **525**(7569): 367-371.

Li, N., M. Wang, T. D. Oberley, J. M. Sempf and A. E. Nel (2002). "Comparison of the pro-oxidative and proinflammatory effects of organic diesel exhaust particle chemicals in bronchial epithelial cells and macrophages." J Immunol **169**(8): 4531-4541.

Morgan, G., S. Corbett and J. Wlodarczyk (1998). "Air pollution and hospital admissions in Sydney, Australia, 1990 to 1994." Am J Public Health **88**(12): 1761-1766.

National Toxicology Program (2016). Report on Carcinogens. Research Triangle Park, NC, U.S. Department of Health and Human Services, Public Health Service.

Nemmar, A., P. H. Hoet, B. Vanquickenborne, D. Dinsdale, M. Thomeer, M. F. Hoylaerts, H. Vanbilloen, L. Mortelmans and B. Nemery (2002). "Passage of inhaled particles into the blood circulation in humans." Circulation **105**(4): 411-414.

Office on Smoking and Health (2017). 2017 National Youth Tobacco Survey. N. C. f. C. D. P. a. H. Promotion. Atlanta, GA, Centers for Disease Control and Prevention, U.S. Department of Health & Human Services.

Peters, A., A. Doring, H. E. Wichmann and W. Koenig (1997). "Increased plasma viscosity during an air pollution episode: a link to mortality?" Lancet **349**(9065): 1582-1587.

Peters, A., S. Perz, A. Doring, J. Stieber, W. Koenig and H. E. Wichmann (1999). "Increases in heart rate during an air pollution episode." Am J Epidemiol **150**(10): 1094-1098.

Platt, S. M., I. El Haddad, S. M. Pieber, A. A. Zardini, R. Suarez-Bertoa, M. Clairotte, K. R. Daellenbach, R. J. Huang, J. G. Slowik, S. Hellebust, B. Temime-Roussel, N. Marchand, J. de Gouw, J. L. Jimenez, P. L. Hayes, A. L. Robinson, U. Baltensperger, C. Astorga and A. S. H. Prevot (2017). "Gasoline cars produce more carbonaceous particulate matter than modern filter-equipped diesel cars." *Sci Rep* **7**(1): 4926.

Polichetti, G., S. Cocco, A. Spinali, V. Trimarco and A. Nunziata (2009). "Effects of particulate matter (PM(10), PM(2.5) and PM(1)) on the cardiovascular system." *Toxicology* **261**(1-2): 1-8.

Schwartz, J. (1989). "Lung function and chronic exposure to air pollution: a cross-sectional analysis of NHANES II." *Environ Res* **50**(2): 309-321.

Shirmohammadi, F., D. Wang, S. Hasheminassab, V. Verma, J. J. Schauer, S. M. M. and C. Sioutas (2017). "Oxidative potential of on-road fine particulate matter (PM2.5) measured on major freeways of Los Angeles, CA, and a 10-year comparison with earlier roadside studies." *Atmospheric Environment* **148**: 102-114.

Sussan, T. E., S. Gajghate, R. K. Thimmulappa, J. Ma, J. H. Kim, K. Sudini, N. Consolini, S. A. Cormier, S. Lomnicki, F. Hasan, A. Pekosz and S. Biswal (2015). "Exposure to electronic cigarettes impairs pulmonary anti-bacterial and anti-viral defenses in a mouse model." *PLoS One* **10**(2): e0116861.

Tecer, L. H., O. Alagha, F. Karaca, G. Tuncel and N. Eldes (2008). "Particulate matter (PM(2.5), PM(10-2.5), and PM(10)) and children's hospital admissions for asthma and respiratory diseases: a bidirectional case-crossover study." *J Toxicol Environ Health A* **71**(8): 512-520.

U.S. Department of Health and Human Services (2014). *The Health Consequences of Smoking - 50 Years of Progress: A Report of the Surgeon General: Executive Summary*. Atlanta, GA.

U.S. Department of Health and Human Services (2016). *E-Cigarette Use Among Youth and Young Adults: A Report of the Surgeon General: Executive Summary*. Atlanta, GA, U.S. Department of Health and Human Services, Centers for Disease Control and Prevention, National Center for Chronic Disease Prevention and Health Promotion, Office on Smoking and Health.

United States Environmental Protection Agency. (2016). "NAAQS Table." Retrieved November 3, 2017, from <https://www.epa.gov/criteria-air-pollutants/naaqs-table>.

Wang, T. W., A. Gentzke, S. Sharapova, K. A. Cullen, B. K. Ambrose and A. Jamal (2018). Tobacco Product Use Among Middle and High School Students - United States, 2011-2017. *Morbidity and Mortality Weekly Report (MMWR)*. **67**: 629-633.

Wellenius, G. A., J. Schwartz and M. A. Mittleman (2005). "Air pollution and hospital admissions for ischemic and hemorrhagic stroke among medicare beneficiaries." *Stroke* **36**(12): 2549-2553.

Wichmann, H. E. (2007). "Diesel exhaust particles." *Inhal Toxicol* **19 Suppl 1**: 241-244.

Wong, T. W., T. S. Lau, T. S. Yu, A. Neller, S. L. Wong, W. Tam and S. W. Pang (1999). "Air pollution and hospital admissions for respiratory and cardiovascular diseases in Hong Kong." Occup Environ Med **56**(10): 679-683.

World Health Organization. (2014). "The top 10 causes of death." Fact sheets Retrieved May 26, 2014, from <http://www.who.int/mediacentre/factsheets/fs310/en/>.

World Health Organization. (2016). "WHO Global Urban Ambient Air Pollution Database (update 2016)." Retrieved November 26, 2017, from http://www.who.int/phe/health_topics/outdoorair/databases/cities/en/.

World Health Organization (2017). WHO Report on the Global Tobacco Epidemic, 2017: Monitoring tobacco use and prevention policies. Switzerland.

World Health Organization. (2018). "Air pollution." Retrieved August 13, 2018, from <http://www.who.int/airpollution/en/>.

Zheng, M., G. R. Cass, J. J. Schauer and E. S. Edgerton (2002). "Source apportionment of PM_{2.5} in the Southeastern United States using solvent-extractable organic compounds as tracers." Environ Sci Technol **36**(11): 2361-2371.

Zheng, M., L. G. Salmon, J. J. Schauer, L. Zeng, C. S. Kiang, Y. Zhang and G. R. Cass (2005). "Seasonal trends in PM_{2.5} source contributions in Beijing, China." Atmospheric Environment **39**(22): 3967-3976.

CHAPTER 2 –
MACROPHAGE RESPONSES AGAINST DIESEL EXHAUST PARTICLES

Abstract

For nearly a decade now, the Hybrid Mouse Diversity Panel (HMDP) has been utilized as a valuable tool to analyze the role of genetic diversity on disease phenotypes, allowing the results of mouse studies to be better extrapolated to explain the health of the human population. Perhaps the most ubiquitous disease-causing factor worldwide is air pollution, which is known to lead to various cardiopulmonary morbidities and increased mortality. Indeed, there have been many cell, animal, and human studies on different components of air pollution, such as diesel exhaust particles extract (DEPe), but none of these studies have done a comprehensive genetic profiling of multiple mouse strains to determine biological response pathways to these toxins. In this study, we looked at 24 strains from the HMDP to analyze the genetic effects of DEPe on macrophages, a key cell type that is responsive to air pollution. Our results demonstrate that despite the varied genetic backgrounds of the 24 mouse strains, the responses to DEPe are commonly driven by *Nrf2*-mediated responses and the likely polarization of macrophages into the Mox subtype across all strains.

Introduction

The Hybrid Mouse Diversity Panel (HMDP) consists of over 100 inbred strains which were selected among hundreds of mouse strains for their suitability in conducting association studies (Bennett et al. 2010, Ghazalpour et al. 2012, Lusi et al. 2016). Utilization of this panel allows for the analysis of complex traits that are influenced by more than one gene (these

phenotypes may also be described as multigenic, polygenic, or non-Mendelian) (Bennett et al. 2010). The HMDP has been used to identify candidate genes of several traits, such as atherosclerosis (Bennett et al. 2015), bone mineral density (Farber et al. 2011), microbiota composition (Org et al. 2015), and inflammation (Orozco et al. 2012).

Of particular interest when studying complex traits are gene-environment interactions. In fact, many chronic diseases are thought to result from oxidative stress responses to xenobiotic electrophiles (Kensler et al. 2007). One major environmental source of oxidants is air pollution, and exposure to this has been associated with worsened respiratory and cardiovascular outcomes, as described in Chapter 1. Despite the major health effects of atmospheric pollutants being quite clear, the mechanisms relating inhaled particulate exposures to adverse events beyond the lungs, particularly in the cardiovascular system, remain uncertain.

For our purpose of exploring the molecular responses to air pollution, our study takes advantage of the utility of the HMDP for elucidating the basis of complex traits. There are multiple cell types in the lungs, and among those that initially respond to air pollutants are lung alveolar and interstitial macrophages. Thus, we isolated macrophages from 24 different HMDP strains; the macrophages were harvested from the peritoneal cavity, where they are more abundant and easier to collect than from the lungs. These cells were then treated with either media only or an extract of diesel exhaust particles (DEPe), which is our model air pollutant. We then compared the genetic expression profiles of the peritoneal macrophages using Affymetrix microarrays. While the relatively small number of HMDP strains we used here do not have enough power for disease gene discovery, they do allow us to analyze the influence of genetic variation on molecular pathways mediating the responses to DEPe.

Materials and Methods

Mice

Peritoneal macrophages were harvested from 24 strains of mice from the HMDP. Among these 24 strains, 13 were classic inbred strains and 11 were recombinant inbred strains (**Table 2-1**). The recombinant strains were the result of crosses of either: A/J with C57BL/6J (resulting in the AXB recombinant strain), C57BL/6J with DBA/2J (resulting in the BXD recombinant strain), and C57BL/6J with C3H/HeJ (resulting in the BXH recombinant strain). These 24 strains were a part of a larger study by Orozco et al. (2012) evaluating the effects of various compounds on inflammatory responses in macrophages. However, that published study only analyzed data from lipopolysaccharide (LPS) and oxidized phospholipid (oxidized 1-palmitoyl-2-arachidonoyl-sn-glycero-3-phosphatidylcholine, OxPAPC) treatments, utilizing 86 HMDP strains for the control group (treated with media only), 89 strains for the LPS-treated group, and 80 strains for the OxPAPC-treated group (Orozco et al. 2012). The DEPe-treated group had not been analyzed until now.

Peritoneal Macrophage Collection and Culture Conditions

Mice were injected with thioglycollate to elicit macrophage infiltration into the peritoneal cavity (Orozco et al. 2012). Thioglycollate induces peritonitis by stimulating the production of advanced glycation end products which are detected by the resident immune cells of the peritoneal cavity and lead to an immune response (Misharin et al. 2012). Within 24 hours following thioglycollate injection, there generally is a high amount of neutrophil infiltration, which later makes way for rising macrophage numbers that peak at around three to four days after injection (Lam et al. 2013). Thus, in this study, four days after thioglycollate injection, we

collected peritoneal macrophages by intraperitoneal lavage and cultured them in DMEM media containing 1% FBS, with cells from different mice of the same strain pooled together (Orozco et al. 2012).

The following day, cells were then treated with either 25 µg/mL DEPe or media-only for four hours. The DEPe had been made via methanol extraction as described previously (Li et al. 2002). Most of the 24 strains used in the study had experimental replicates (duplicates or triplicates) (**Table 2-1**).

Affymetrix Microarrays

Following the DEPe and media-only treatments, the RNA was isolated from the peritoneal macrophages as described previously by Bennett et al. (2010), and the genetic profiles were analyzed using Affymetrix HT MG-430A arrays. These arrays contained 22,416 probe sets, which each probe set having eleven pairs of probes, and with each pair containing a perfect match and a mismatch for a particular transcript/sequence (Affymetrix 2009). Pre-processing of the microarray dataset utilized robust multi-array average (RMA) normalization. This method performs background correction, quantile normalization, and linear model fitting to the dataset (Irizarry et al. 2003).

Since the DEPe-treated group was conducted as part of a larger study looking at the gene expression profiles of LPS and OxPAPC treatments compared with control, it is important to note that an analysis of the Affymetrix data comparing those three (control, LPS, and OxPAPC) have been published (Orozco et al. 2012), with the RMA-normalized data from these three groups made publicly available on the Gene Expression Omnibus (GEO) repository website (<https://www.ncbi.nlm.nih.gov/geo/>), under the GEO Accession number GSE38705. However,

the DEPE-treated cells were not analyzed in that study, nor deposited into GEO, but the DEPE dataset will be evaluated here.

Microarray Quality Control and Cleanup

The Affymetrix HT MG-430A arrays used in this study contained several dozen control probe sets, indicated with the AFFX prefix; these may be used to detect housekeeping genes such as *β -actin* and *Gapdh*, or used as hybridization or poly-A controls (Affymetrix 2007). The 5':3' ratio of the control probe sets were plotted for each sample to ensure sample quality. In addition, a quality assessment was performed on the experimental replicates by plotting replicates against each other and calculating the slope of the line of best fit and the R-squared values.

After checking for quality, the expression values of the experimental replicates were then averaged, resulting in 24 control/DEPE-treated strain pairs. Then the microarray dataset was trimmed by removing all NULL/NA probes from the dataset, leaving 21,812 probe sets left in the analysis. In addition, since 5,152 of the genes were each being detected by more than one probe, only unique genes were reported, resulting in a dataset of 13,278 genes.

Differential Gene Expression Analysis

Differential gene expression analysis was performed on the dataset using the *limma* package in R. The *limma* package performs linear modeling of the microarray data to determine differentially expressed genes between conditions (Smyth et al. 2018). The significance values reported were adjusted for multiple testing using the Benjamini & Hochberg correction, which controls the false discovery rate (FDR) (Smyth et al. 2018).

Pathway analysis on enriched genes was conducted using the online Gene Ontology (GO) Consortium resource (Ashburner et al. 2000), which currently uses PANTHER (Protein ANalysis THrough Evolutionary Relationships) tools for evaluating gene set enrichment (The Gene Ontology Consortium 2017). Genes were mapped to pathways using the PANTHER Overrepresentation Test against the Reactome version 65 database, with pathway significance assessed using Fisher's exact test with FDR correction for multiple testing. Pathways with $FDR < 0.05$ were considered significant.

Transcription Factor Enrichment Analysis

The Expression2Kinases (X2K) software was used to relate differentially expressed genes with transcription factors that may regulate their expression (Chen et al. 2012). Chen et al. (2012) developed this software using a database of transcription factor interactions based on ChIP-seq/chip experimental results from several dozen publications. The X2K program performs an enrichment analysis of the list of genes inputted by the user against this database. Transcription factors with $p < 0.05$ were considered significant. The resulting transcription factor and gene interactions were then visualized using the Cytoscape software (Shannon et al. 2003).

Macrophage Polarization Subtypes Analysis

A list of markers characteristic of the M1, M2, and Mox macrophage subtypes were acquired from the study published by Kadl et al. (2010). Their marker lists were generated from Affymetrix array analysis of polarized bone marrow-derived macrophages and contained 1,255 M1 marker genes, 265 M2 markers, and 119 Mox markers (Kadl et al. 2010). Some of the gene names from that 2010 paper have since been changed in the National Center for Biotechnology

Information (NCBI) Gene database (<https://www.ncbi.nlm.nih.gov/gene>) or determined as no longer valid gene names when the NCBI website was last accessed in January 2018; the M1, M2, and Mox lists were accordingly updated for our analyses. From there, we had lists of 924 M1 markers, 182 M2 markers, and 92 Mox markers. We then determined which genes from these lists had corresponding probe sets in our Affymetrix HT MG-430A arrays, and in the end, we worked with lists of 644 M1 markers, 143 M2 markers, and 64 Mox markers for our analyses. These macrophage marker lists were used to subset the microarray dataset and analyze patterns of upregulation and downregulation within these macrophage subtypes following DEPe, LPS, and OxPAPC exposures. Heat maps of the \log_2 (fold change) values were visualized in R.

Results

Quality of Microarrays

Analysis of the AFFX control probes indicated that the samples were of sufficient quality. The AFFX control probe sets can detect 5' and 3' signals of select housekeeping genes, and hybridization and poly-A controls, and it is ideal to get 5':3' signal ratios of 1, although ratios between 0 and 3 remain acceptable (Roy et al. 2002). The 5':3' signal ratios for all AFFX control probes tested across all microarrays in the study were around 1, with a minimum of 0.57 and a maximum of 1.41 (**Figure 2-1**).

Additionally, the qualities of the experimental replicates were measured by plotting them against each other and calculating their correlations. The slopes for all experimental replicate comparisons were all around 1 (with the lowest value being 0.9431, and the highest being 1.0150), and the R-squared values ranged from 0.9395 to 0.9944, indicating a good reproducibility of replicates (**Figure 2-2**).

Differentially expressed genes in macrophage responses to DEPe

Out of the 13,278 unique genes that were detectable by the Affymetrix arrays, 2,712 genes were determined to be differentially expressed with DEPe exposure (FDR < 0.05). **Table 2-2** contains a list of the top 20 differentially expressed genes. **Figure 2-3** illustrates the expression patterns of select genes: the top four differentially expressed genes from **Table 2-2**, which are all antioxidant genes (*Hmox1*, heme oxygenase 1; *Txnrd1*, thioredoxin reductase 1; *Srxn1*, sulfiredoxin 1 homolog (*S. cerevisiae*); and *Gclm*, glutamate-cysteine ligase, modifier subunit); *Ier2* (immediate early response 2), the most significantly downregulated gene with DEPe treatment (ranked 13 in **Table 2-2**); and *Lmx1b* (LIM homeobox transcription factor 1 β), a gene that was not consistently differentially expressed with DEPe treatment across all strains (**Figure 2-3**).

Of the 2,712 differentially expressed genes, 1,284 were upregulated with DEPe treatment, while 1,428 were downregulated with DEPe treatment, as averaged across all 24 mouse strains (FDR < 0.05). The top 40 upregulated genes are listed in **Table 2-3** while the top 40 downregulated genes are in **Table 2-4**.

For the upregulated genes, 238 Reactome pathways were identified, categorized into 103 hierarchical groups, with the top 20 groups graphed in **Figure 2-4**. The most prominent upregulated pathways are involved in cellular responses to external stimuli, including stress and heat stress, represented by genes like *Txnrd1*, *Prdx1* (peroxiredoxin 1), and *Gsr* (glutathione reductase), which are also among the top 40 individually upregulated genes (**Table 2-3**). Reactome pathway analysis of the 1,428 downregulated genes resulted in the identification of 174 Reactome pathways, categorized into 68 hierarchical groups, with the top 20 groups graphed in **Figure 2-5**. Metabolism is the most significant category of downregulated pathways, and this

group specifically includes pathways involved in the metabolism of lipids and of fatty acids. This Reactome category is represented by genes like *Abcd1* (ATP-binding cassette, sub-family D (ALD), member 1) and *Itpkb* (inositol 1,4,5-trisphosphate 3-kinase B), which are also among the top 40 individually downregulated genes (**Table 2-4**). This dysregulation is consistent with previous studies that have shown impaired lipid metabolism with air pollution exposure, leading to increased concentrations of low-density lipoproteins (LDL) and triglycerides in the blood, for instance (Yitshak Sade et al. 2016).

Although more than half of the differentially expressed genes are downregulated with DEPe, the genes with the most prominent responses are upregulated. In fact, more than half of the 75th and of the 90th percentiles of all differentially expressed genes are specifically upregulated (374 out of 678 genes, and 175 out of 272 genes, respectively). And indeed, out of the top 20 differentially expressed genes, all except for one are upregulated (**Table 2-2**). Therefore, it is of great interest to determine the transcription factors that would be mediating these increased responses as these would control responses by multiple genes.

A set of genes that (1) were significantly upregulated (FDR < 0.05), and (2) had at least a 1.5-fold change with DEPe treatment, were selected to run through the X2K software to determine the main transcription factors responsible for mediating the expression of the most responsive upregulated genes. This list of genes fitting both criteria contained 227 genes, representing about 18% of all upregulated genes. The X2K analysis of this subset resulted in 97 transcription factors identified as being significantly ($p < 0.05$) involved in regulating the expression of these genes. The network of transcription factors with the 227 upregulated genes is illustrated in **Figure 2-6**, with the blue diamonds representing transcription factors. The transcription factor that was most significantly associated with this set of upregulated genes was

NRF2 (nuclear factor, erythroid derived 2, like 2). Indeed, *Nrf2* has been shown in previous studies to be important in protective responses against air pollution (Aoki et al. 2001, Li et al. 2004, Wittkopp et al. 2016).

DEPe Treatment May Polarize Macrophages to the Mox Subtype

NRF2 transcriptional regulation has also been demonstrated to drive macrophage polarization to the macrophage subtype, Mox. Mox was first identified by Kadl et al. (2010) based on this cell type's unique properties following stimulation with oxidized phospholipids like OxPAPC, such as reduced phagocytic ability. The gene expression profile of this subtype is in large part regulated by *Nrf2*, which triggers the mRNA expression of antioxidants such as *Hmox1*, *Srxn1*, and *Txnrd1* (Kadl et al. 2010). Kadl et al. (2010) proposed a list of 119 Mox markers determined by OxPAPC-induced upregulation of genes that did not correspond to M1 or M2 polarization; from their list, we were able to analyze the expression of 64 Mox marker genes in our Affymetrix arrays. Nearly three-fourths of the Mox markers were differentially expressed (47 out of 64 genes had FDR < 0.05), with over half of these being upregulated (34 had FDR < 0.05 and fold change > 1.5). This high number of upregulated Mox genes is apparent with the heat map in **Figure 2-7a**. A list of the 47 Mox markers that were differentially expressed (both upregulated and downregulated) with DEPe treatment is in **Table 2-5**. Since Kadl et al. (2010) identified the Mox macrophage subtype from OxPAPC-treated bone-marrow derived macrophages, we also compared the Mox marker profile of our DEPe-treated peritoneal macrophages with the Affymetrix microarray data of OxPAPC-treated peritoneal macrophages from the paper by Orozco et al. (2012). Indeed, microarray data from these OxPAPC treatments similarly indicate more of a Mox phenotype, as nearly half of the Mox markers were

significantly upregulated (27 out of 64 genes had $FDR < 0.05$ and fold change > 1.5) (**Figure 2-8**). Thus, the macrophage response to DEPe clearly shows the importance of oxidative stress response genes, with the gene expression profile demonstrating characteristics very similar to the Mox macrophage subtype. Surprisingly, the DEPe-treated peritoneal macrophages had an even stronger Mox expression profile than the OxPAPC-treated cells in terms of percentage of upregulated Mox markers (53.13% vs. 42.19%).

We also visualized the expression profiles of two other known macrophage subtypes – M1 and M2. Macrophages treated with IFN- γ and LPS can be polarized to a pro-inflammatory M1 phenotype, which has important roles in innate immunity (Martinez et al. 2014). We looked at 644 M1 marker genes, derived from the list identified by Kadl et al. (2010), and determined that less than 5% of the M1 markers were significantly upregulated (30 out of 644 had $FDR < 0.05$ and fold change > 1.5) with DEPe treatment (**Figure 2-7b**). A list of the differentially expressed M1 marker genes following DEPe treatment is found in **Table 2-6**.

In comparison, the Affymetrix arrays from LPS-treated cells from the paper by Orozco et al. (2012) showed a prominent M1 marker pattern in most strains, with over 57% of the M1 markers having an $FDR < 0.05$ and a fold change > 1.5 , as expected for an M1 stimulus (**Figure 2-9**). It should be noted, though, that there are six mouse strains that showed a much more muted LPS response, due to their genetics. In fact, one of the six LPS-hyporesponsive strains is C3H/HeJ, which has been known to contain a dominant negative mutation that prevents these mice from responding to LPS (Vogel et al. 1999). Crossing C3H/HeJ with other strains can thus result in progeny that show a range of responses to LPS, from significantly reduced to full activity (Vogel et al. 1999). Indeed, in our data, the other five LPS-hyporesponsive strains are

the result of crosses involving C3H/HeJ (including B6cC3-1/KccJ, which is noted in The Jackson Laboratory as a recombinant congenic BXH strain (The Jackson Laboratory).

For M2 macrophages, IL-4 and IL-13 can mediate polarization to this anti-inflammatory subtype (Gordon 2003, Martinez et al. 2014). Of the 182 M2 marker genes from the list derived from Kadl et al. (2010), 143 were detected in our Affymetrix arrays. Similar to the M1 markers, less than 5% of the M2 markers were significantly upregulated with DEPe treatment (5 out of 143 had $FDR < 0.05$ and fold change > 1.5) (**Figure 2-7c**). **Table 2-7** contains a list of the differentially expressed M2 marker genes following DEPe treatment.

Based on our data, it is clear that DEPe does not lead to either an M1 or an M2 macrophage phenotype, but instead leads to a Mox-like phenotype. This characteristic is also apparent when comparing DEPe treatment with LPS and OxPAPC treatments. **Table 2-8** contains a summary of the percentage of upregulated macrophage markers under DEPe, LPS, and OxPAPC conditions.

Discussion

Our studies here demonstrate that macrophages exhibit strong responses to DEPe. Across multiple strains of mice from the HMDP, these reactions are similar, including being dominated by oxidative stress response systems led by *Nrf2* and having a Mox-like macrophage subtype.

Our work in this chapter focused specifically on evaluating macrophage responses to our model air pollutant, DEPe, because previous studies have shown that myeloid lineage cells such as macrophages are among the cell types in the lungs that can have particularly robust responses to air pollution. For instance, exposure to pollutants can lead to greater macrophage infiltration in the alveoli of the lungs (Farina et al. 2013, Yanamala et al. 2013, Rizzo et al. 2014), where these

cells can phagocytose foreign particles (Strom et al. 1990, Finch et al. 2002, Suwa et al. 2002, Kulkarni et al. 2006). Indeed, infiltration of immune cells in the lungs feature prominently in many diseases associated with air pollution, such as asthma and chronic obstructive pulmonary disease (COPD) (Becker et al. 2002).

The use of multiple mice from the HMDP as the source for our macrophages has been beneficial in allowing us to look at the effects of our air pollutant at a population level. The HMDP has been used in several previous studies to lend weight to the genetic basis of certain traits, as described earlier. And, as referred to in multiple instances in this chapter, the most relevant HMDP study was conducted by Orozco et al. (2012) in which they treated peritoneal macrophages with OxPAPC and LPS to evaluate the genetic basis of inflammatory responses and consequently identified a candidate gene, *2310061C15Rik*, now known as COX assembly mitochondrial protein 2 (*Cmc2*). In this chapter, while we were not able to use our dataset to perform gene discovery due to the relatively small number of strains (24), we were still able to determine likely molecular pathways that comprised macrophage responses to air pollution. In our study, we have demonstrated that oxidative stress responses to DEPe are present across all of the 24 HMDP strains in the study. For instance, each strain had increased expression of several antioxidant genes, including *Hmox1*, *Txnrd1*, *Srxn1*, and *Gclm* (**Figure 2-3**), which were the top four significantly upregulated genes (**Table 2-2**). Accordingly, the top group of enriched Reactome pathways are involved in responses to external stimuli, which includes stress (**Figure 2-4**). These results are consistent with previous studies that show DEPe can elicit oxidative stress responses (Sagai et al. 1993, Takano et al. 1997, Li et al. 2002, Marano et al. 2002, Xiao et al. 2003, Araujo 2010). For instance, rat alveolar macrophages exposed to DEP extract (DEPe) showed increased expression of genes involved in the antioxidant system – *Hmox1*, *Hmox2*,

peroxiredoxin 1 (*Prdx1*), NAD(P)H quinone dehydrogenase 1 (*Nqo1*), and a subunit of glutathione S-transferase (*Gstp1*) (Koike et al. 2002). And, DEPe treatment led RAW 264.7 macrophages and THP-1 monocytes to have a reduced ratio of glutathione to glutathione disulfide (GSH/GSSG ratio), indicative of increased oxidative stress since GSH acts as a scavenger of reactive oxygen species (Li et al. 2002, Li et al. 2002).

In our study, we have also demonstrated that *Nrf2* is the most significant transcriptional regulator of the top DEPe-upregulated genes (**Figure 2-6**), and indeed it has been demonstrated that the NRF2 transcription factor is important in regulating oxidative stress responses, such as driving the expression of *Hmox1* (Li et al. 2004). How this transcription factor functions is that under normal, unstressed conditions, the NRF2 protein is bound to KEAP1 (Kelch-like ECH-associated protein 1) in the cellular cytoplasm. KEAP1 acts to repress the activity of NRF2 by promoting its proteasomal degradation. On the other hand, under conditions of electrophilic stress, NRF2 is released from KEAP1 to translocate into the nucleus and promote the transcription of genes containing the antioxidant response element (ARE) in their promoter region, with several of these genes including antioxidant and Phase II detoxifying genes (Nguyen et al. 2009). An especially high oxidative stress load that overwhelms NRF2 and other protective enzymes can lead to cell death, and accordingly, studies have illustrated the cytotoxicity of air pollutants on macrophages and monocytes (Hiura et al. 1999, Li et al. 2002).

Expanding on the role of *Nrf2*, our study has additionally shown that macrophages exposed to DEPe respond similarly as they do when exposed to oxidized phospholipids, based on gene expression profiles. In fact, DEPe treatment polarizes macrophages to more of a Mox subtype, which is so named for its polarization following oxidized phospholipid-exposure and is dominated by *Nrf2* regulation (Kadl et al. 2010). This polarization to a Mox-like phenotype is

illustrated with the Mox, M1, and M2 marker heat maps for DEPe treatment, in which the patterns are similar for all strains (**Figure 2-7**), underscoring that there is a conserved, common reaction to this ubiquitous insult. This presence of Mox-like cells is also confirmed as there is a similarity in macrophage marker patterns between the DEPe and OxPAPC treatments, with DEPe treatment perhaps even acting as a stronger Mox polarization stimulus than OxPAPC under our conditions (**Table 2-8**). And, while we did not test an M2-stimulus, we can say that DEPe did not induce an M1 phenotype especially when compared with the M1-stimulus, LPS (**Figure 2-9; Table 2-8**). As Mox macrophages have a unique phenotype compared to other subtypes, further studies could be done to explore whether DEPe-treated macrophages also have reduced migrating and phagocytic capabilities like oxidized phospholipid-treated macrophages do (Kadl et al. 2010). We have attempted to evaluate the phagocytosis of fluorescent beads in DEPe-treated macrophages, using the ImageStream Mark II Imaging Flow Cytometer in the UCLA Janis V. Giorgi Flow Cytometry Core Laboratory for quantification of uptake of the beads, but further refinement of this technique and our conditions are necessary.

While DEPe treatment has promoted robust and distinct genetic responses in our cells, it is worth noting that the type of macrophages used in this study are thioglycollate-elicited peritoneal macrophages. While the use of thioglycollate has been an established method to increase the number of macrophages in the peritoneal cavity (Zhang et al. 2008), this agent can affect macrophage function such as reducing their antimicrobial ability (Hoover et al. 1984), and it is unknown whether thioglycollate could induce macrophage polarization to a certain phenotype. Thus, this makes the distinct Mox profiling of these peritoneal cells much more compelling. Using bone marrow-derived macrophages instead may even strengthen the expression of the Mox markers upon DEPe treatment.

In this chapter, our results showed that macrophage responses to DEPe are dominated by stress-responsive genes and a Mox-like phenotype, properties that are both driven by the antioxidant transcription factor NRF2. With *Nrf2* playing such a prominent role in determining how macrophages react to air pollutants, it would also be intriguing to perform gene expression profiling of cells knocked out for this gene and treated with DEPe to determine if the Mox marker pattern would be ablated, which would confirm the key role of this transcription factor in macrophage responses to pollutants. In the next chapter, we evaluate the role of *Nrf2* expression in myeloid cells including macrophages in in vivo responses to air pollution.

Figures

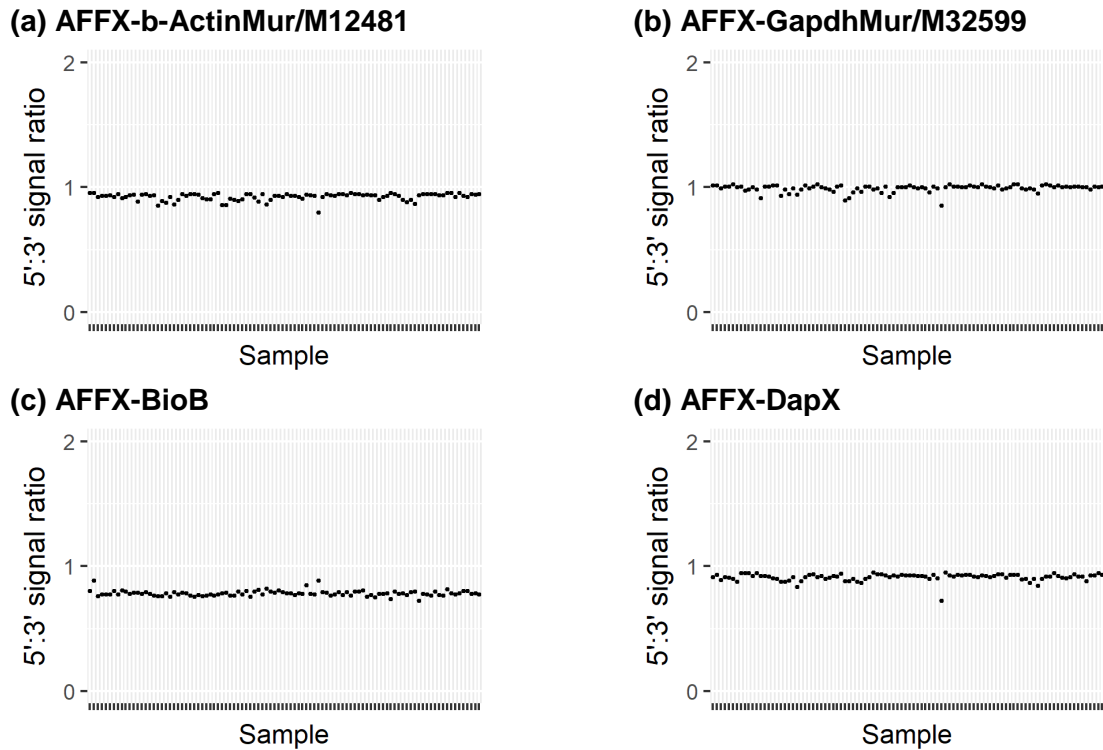


Figure 2-1: Quality of selected AFFX control probes. Plots of 5':3' signal ratios of control probes for the housekeeping genes (a) *β-actin* (denoted with probe ID AFFX-b-ActinMur/M12481 in the Affymetrix array) and (b) *Gapdh* (AFFX-GapdhMurM32599), (c) the hybridization control *bioB* (AFFX-BioB), and (d) the poly-A control *dapX* (AFFX-DapX), showed that all samples had ratios around 1, indicating a high degree of array quality.

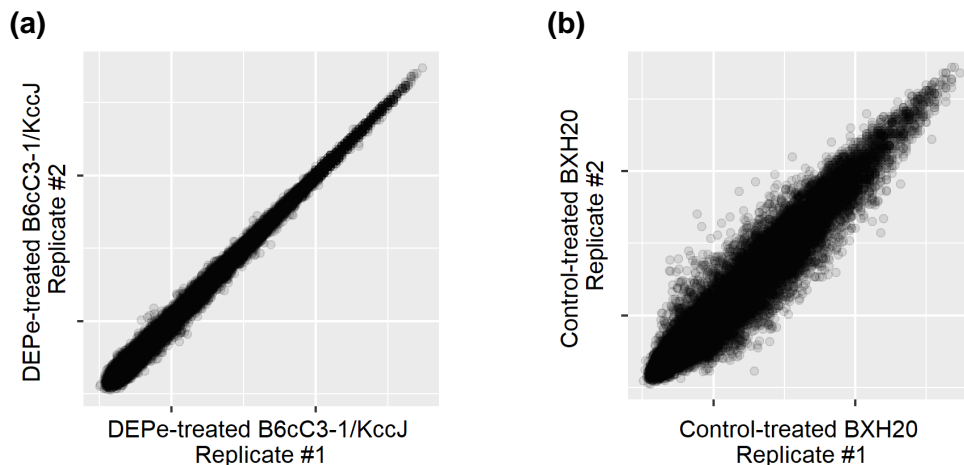
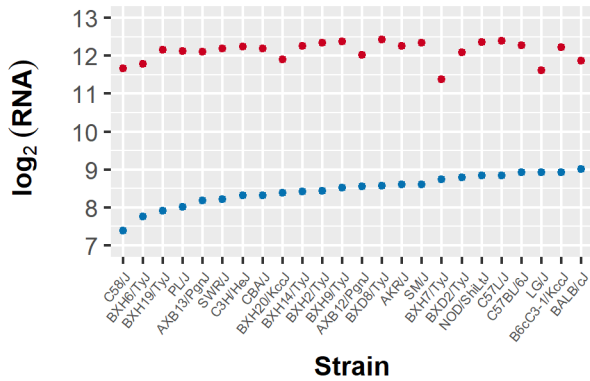
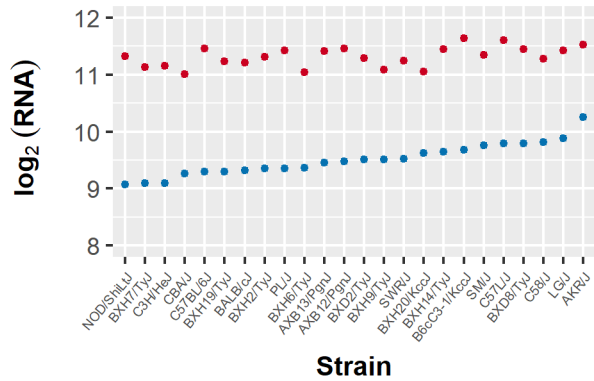


Figure 2-2: Quality of replicate microarrays. Selected plots of replicate microarrays of (a) the DEPE-treated samples from the B6cC3-1/KccJ strain and (b) the control-treated samples from the BXH20 strain. Among all replicates in the microarray dataset, these two comparisons had (a) the highest R-squared value at 0.9944 and (b) the lowest R-squared value at 0.9395.

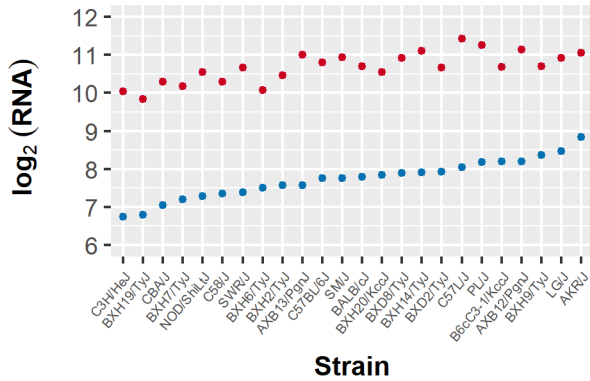
(a) *Hmox1*



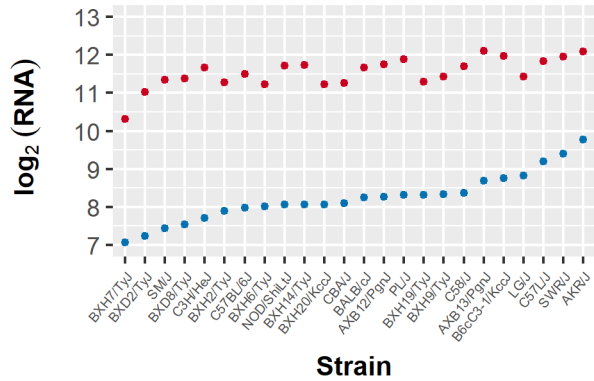
(b) *Txnrd1*



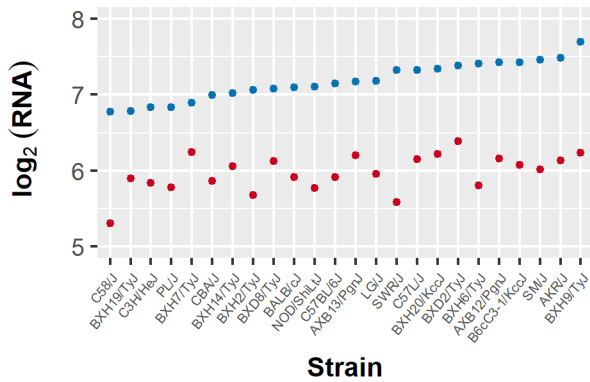
(c) *Srxn1*



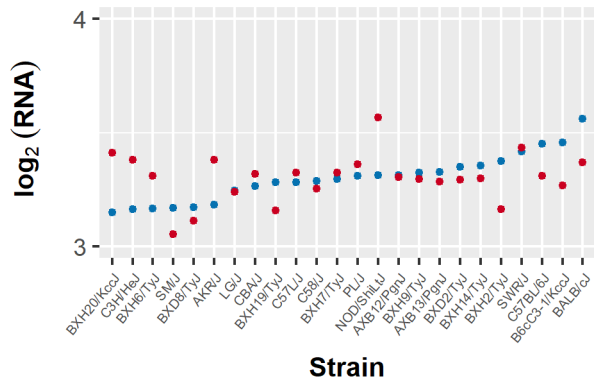
(d) *Gclm*



(e) *Ier2*



(f) *Lmx1b*



● Control ● DEPe

Figure 2-3: Selected plots of genes with varied patterns of differential expression after DEPe treatment. Strains on the x-axis are listed in order of increasing $\log_2(\text{RNA})$ expression of the control treatment. Four antioxidant genes were the most significantly upregulated with DEPe treatment across all strains: (a) *Hmox1*, (b) *Txnrd1*, (c) *Srxn1*, and (d) *Gclm*. (e) *Ier2* is the most significantly downregulated gene with DEPe treatment, and (f) *Lmx1b* is an example of a gene that shows a more strain-specific response, with no consistent pattern across all groups based on treatment.

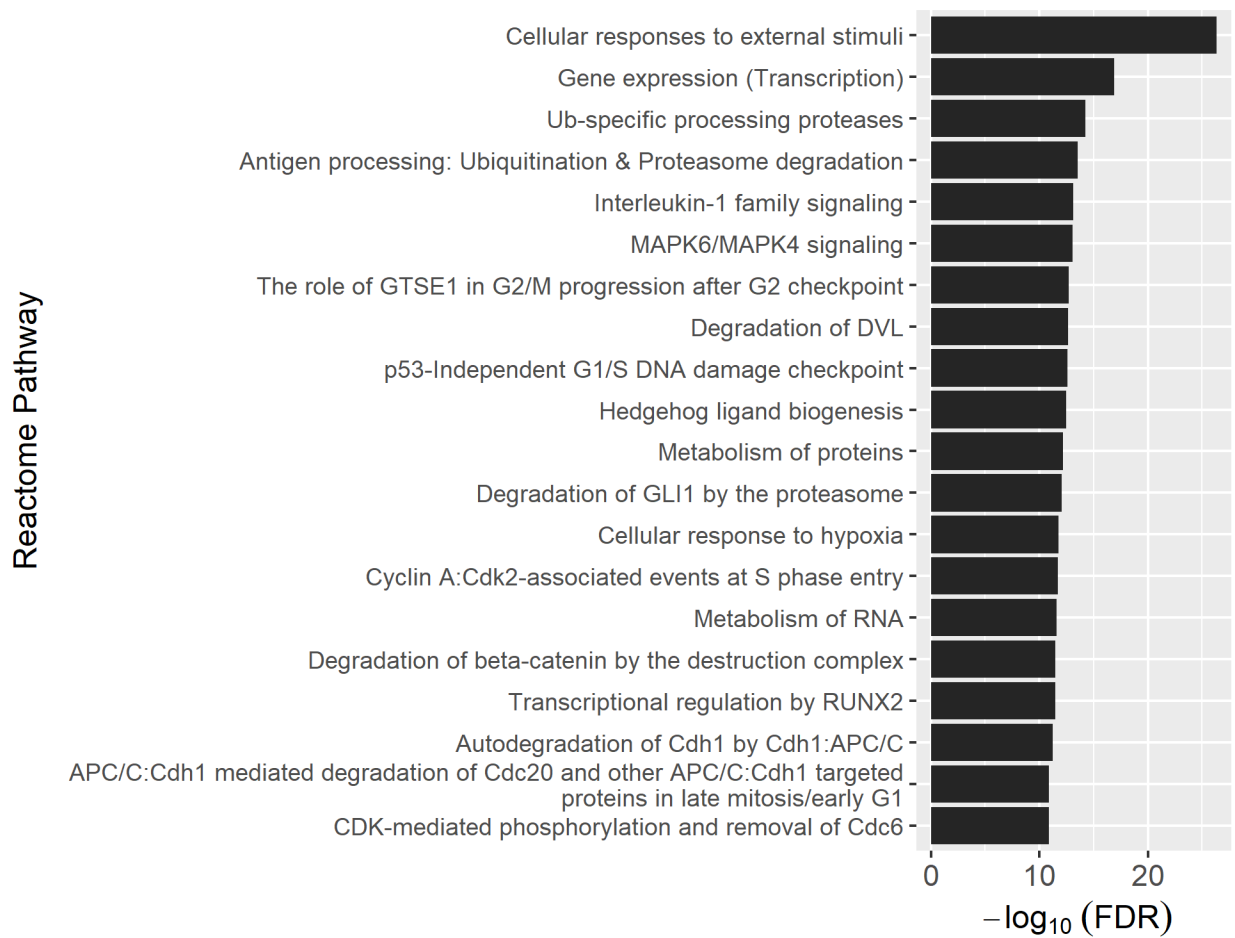


Figure 2-4: Top 20 Reactome pathways of the 1,284 genes upregulated with DEPe treatment. A $-\log_{10}(\text{FDR})$ value of at least 1.3 (equivalent to $\text{FDR} < 0.05$) is significant.

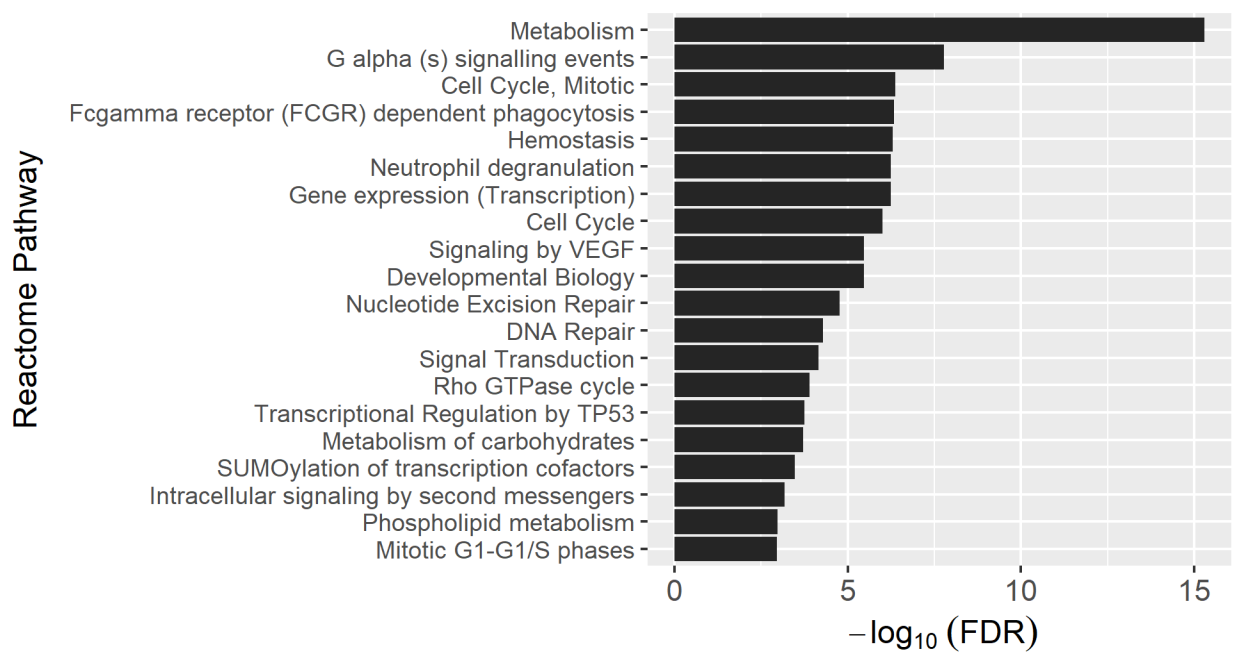


Figure 2-5: Top 20 Reactome pathways of the 1,428 genes downregulated with DEPe treatment. A $-\log_{10}(\text{FDR})$ value of at least 1.3 (equivalent to $\text{FDR} < 0.05$) is significant.

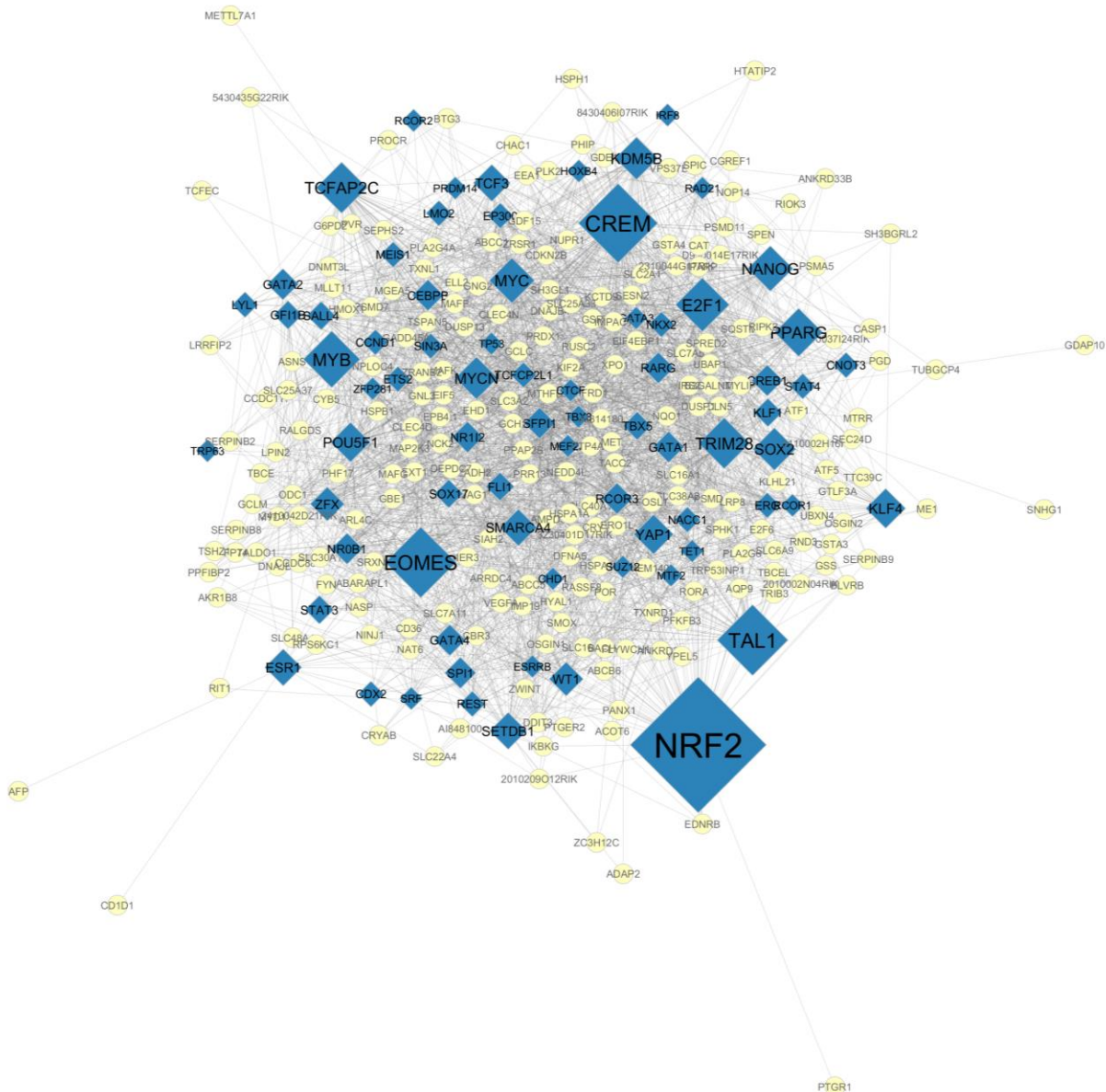
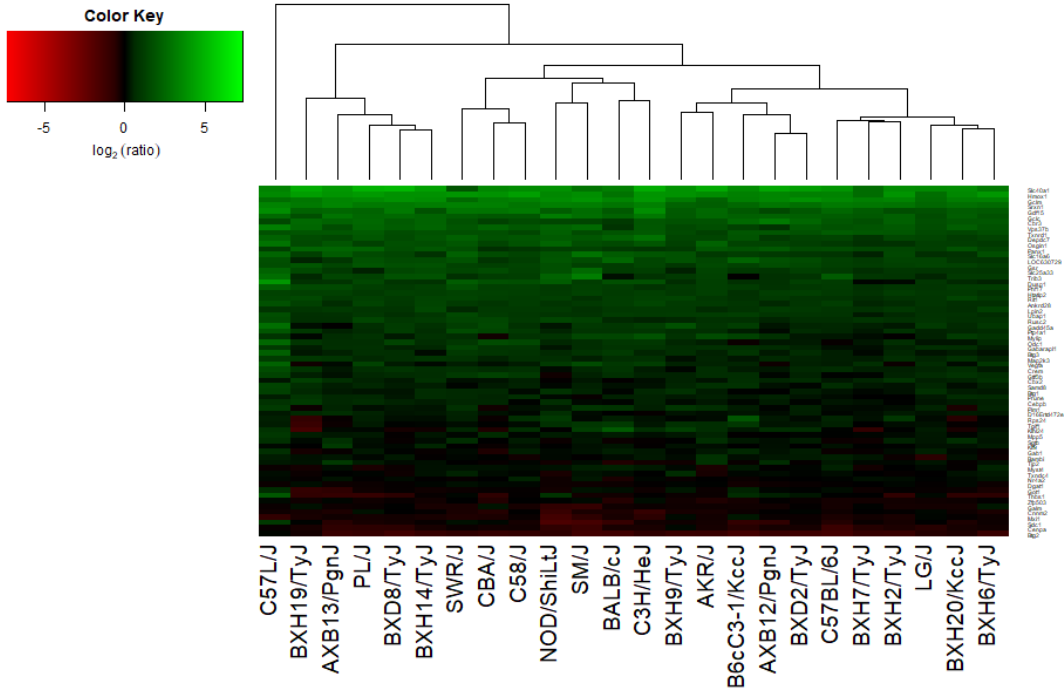
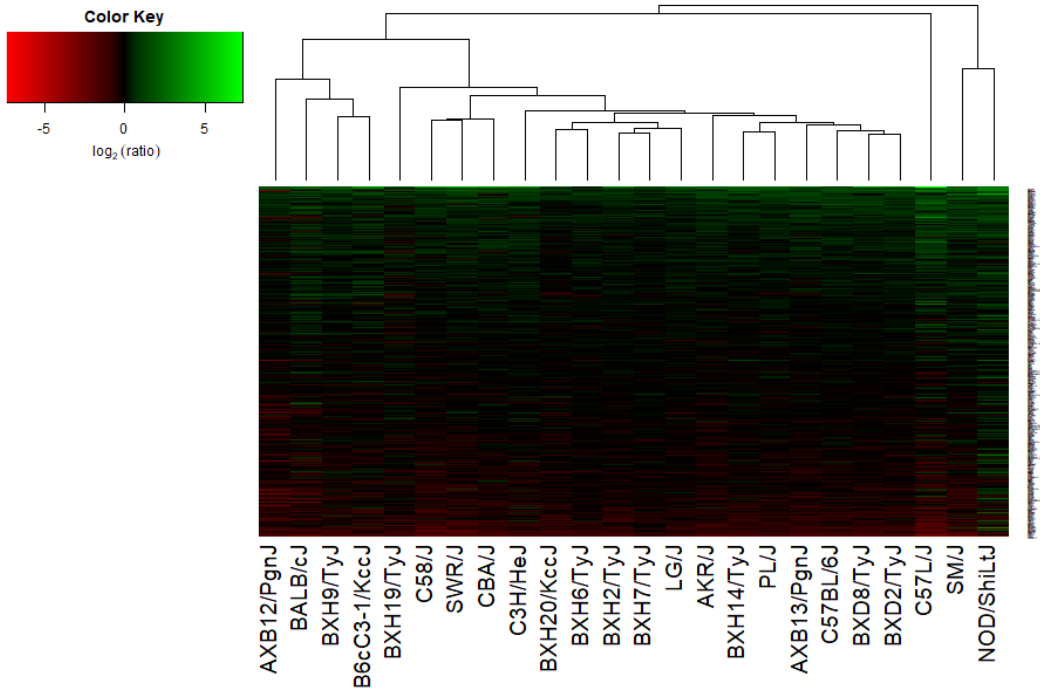


Figure 2-6: Transcription factor network of selected genes upregulated with DEPe. Genes that were significantly upregulated with $FDR < 0.05$ and had at least 1.5-fold change were inputted into the X2K software, which then predicted likely transcription factors. Inputted genes are represented as yellow circles, while blue diamonds represent the transcription factors. The size of the blue transcription factors corresponds to the p-value of the transcription factor enrichment analysis, with a larger size indicating a more significant (lower) p-value.

(a) Mox markers with DEPe treatment



(b) M1 markers with DEPe treatment



Continued on next page...

(c) M2 markers with DEPE treatment

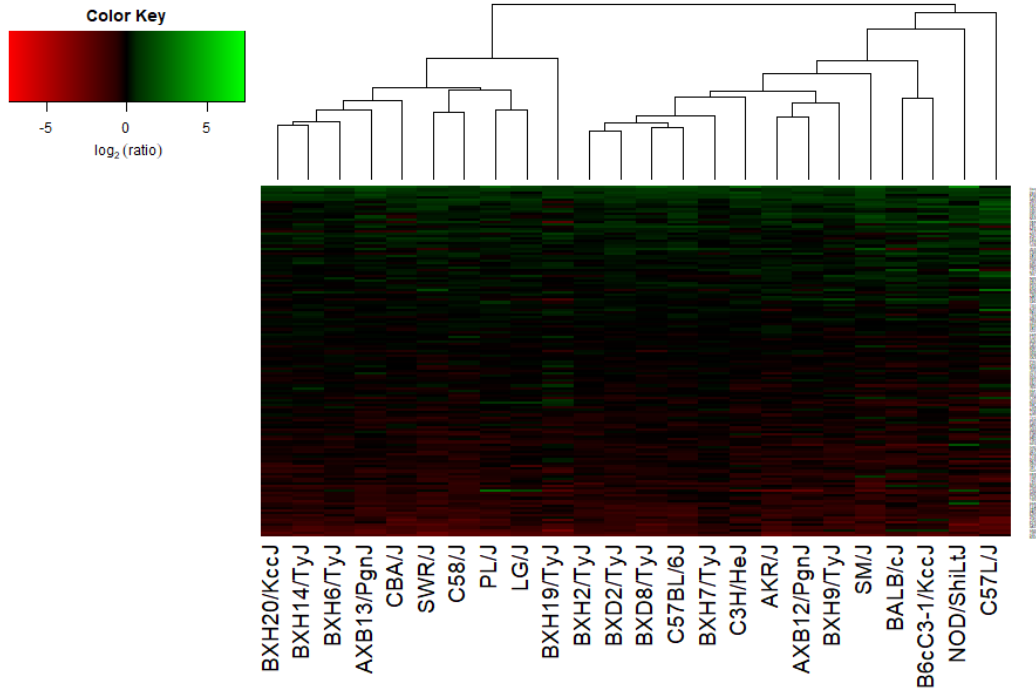


Figure 2-7: Gene expression of macrophage markers in peritoneal macrophages after DEPE exposure. The color key of the heat map represents $\log_2(\text{fold change})$ values. (a) Over half (53.1%) of the Mox marker genes were significantly upregulated at least 1.5-fold (equivalent to $\log_2(\text{fold change})$ of at least 0.585). A list of significantly differentially expressed Mox markers is in **Table 2-5**. Less than 5% of the (b) M1 and (c) M2 marker genes were significantly upregulated at least 1.5-fold with DEPE exposure. A list of the significantly differentially expressed M1 and M2 markers can be found in **Table 2-6** and **Table 2-7**, respectively.

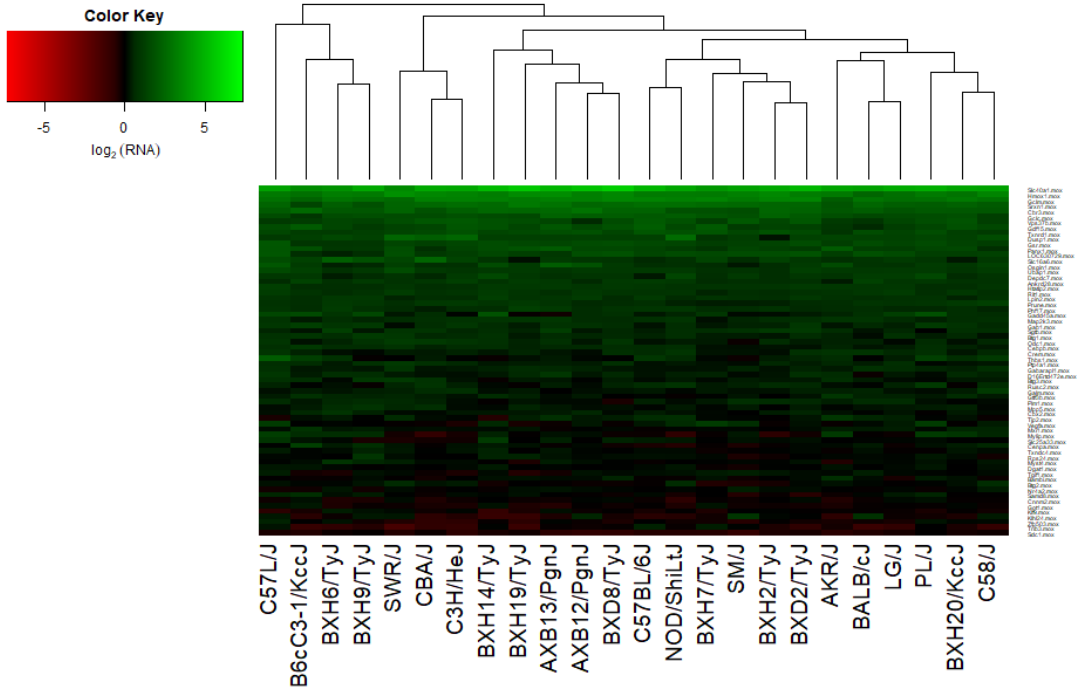
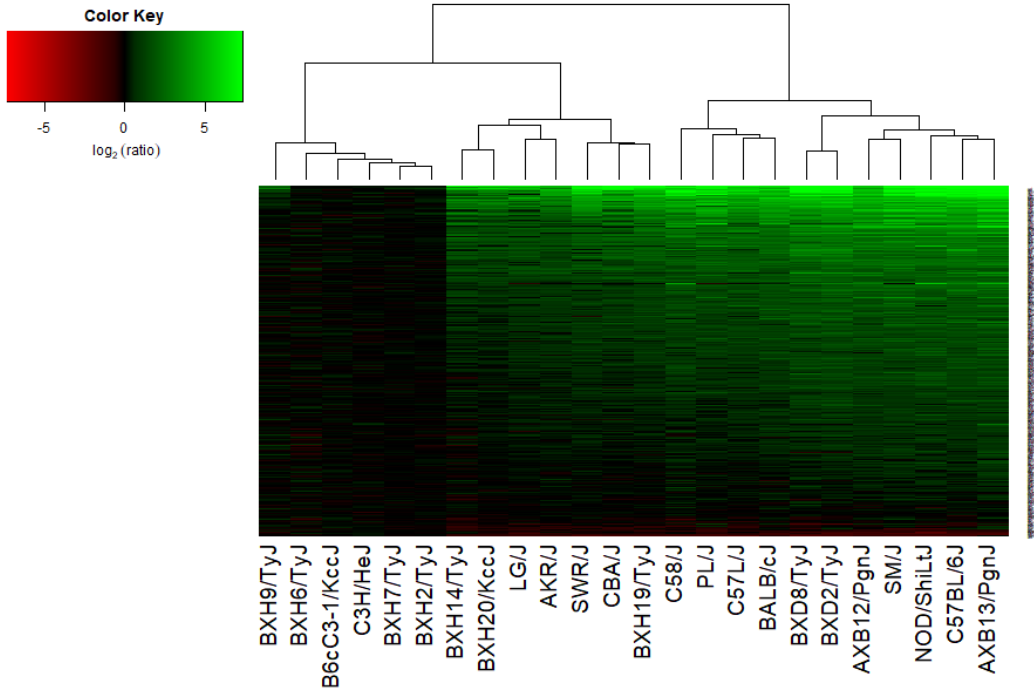


Figure 2-8: Expression of macrophage markers following OxPAPC treatment. The color key of the heat map represents $\log_2(\text{fold change})$ values. Nearly half (42.2%) of the Mox marker genes were significantly upregulated at least 1.5-fold (equivalent to $\log_2(\text{fold change})$ of at least 0.585) after OxPAPC treatment.

(a) M1 markers with LPS treatment



(b) All macrophage markers with LPS treatment

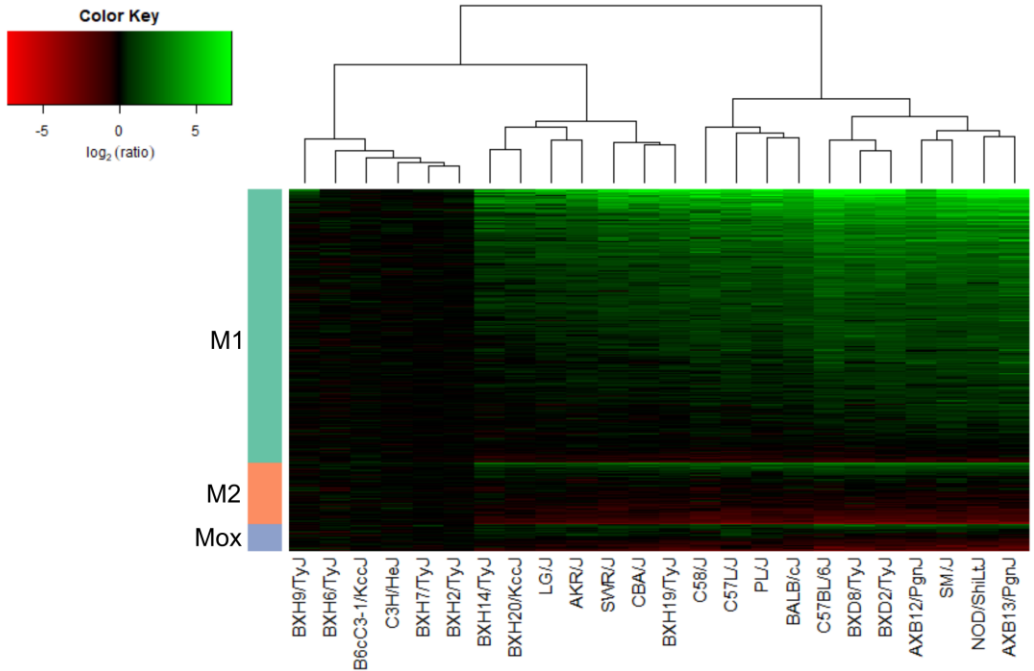


Figure 2-9: Expression of macrophage markers following LPS treatment. The color key of the heat map represents $\log_2(\text{fold change})$ values. (a) In peritoneal macrophages following LPS exposure, over half (57.1%) of the M1 marker genes were upregulated at least 1.5-fold (equivalent to $\log_2(\text{fold change})$ of at least 0.585). (b) Combination of the heat maps of M1, M2, and Mox markers with LPS treatment.

Tables

	Mouse Strain	Type of Inbred Strain	Number of Control-Treated Replicates	Number of DEPe-Treated Replicates
1	AKR/J	classic	1	1
2	AXB12/PgnJ	recombinant	2	3
3	AXB13/PgnJ	recombinant	2	2
4	B6cC3-1/KccJ	classic	2	2
5	BALB/cJ	classic	2	2
6	BXD2/TyJ	recombinant	2	2
7	BXD8/TyJ	recombinant	2	2
8	BXH2/TyJ	recombinant	2	2
9	BXH6/TyJ	recombinant	2	2
10	BXH7/TyJ	recombinant	2	2
11	BXH9/TyJ	recombinant	2	2
12	BXH14/TyJ	recombinant	2	2
13	BXH19/TyJ	recombinant	2	2
14	BXH20/KccJ	recombinant	3	4
15	C3H/HeJ	classic	2	2
16	C57BL/6J	classic	2	2
17	C57L/J	classic	2	2
18	C58/J	classic	1	3
19	CBA/J	classic	2	1
20	LG/J	classic	3	2
21	NOD/ShiLtJ	classic	3	2
22	PL/J	classic	2	2
23	SM/J	classic	2	2
24	SWR/J	classic	2	1

Table 2-1: Samples used for Affymetrix microarrays. In total, 98 microarrays were run on samples from 24 different strains of inbred mice (classic or recombinant), with each strain undergoing treatment with either media-only (Control) or DEPe. The recombinant strains were the result of crosses of either: A/J with C57BL/6J (resulting in the AXB recombinant strain), C57BL/6J with DBA/2J (resulting in the BXD recombinant strain), and C57BL/6J with C3H/HeJ (resulting in the BXH recombinant strain).

	Gene	Name	Fold Change	FDR
1	Hmox1	Heme oxygenase (decycling) 1	12.46	9.47E-33
2	Txnrd1	Thioredoxin reductase 1	3.50	1.59E-26
3	Srxn1	Sulfiredoxin 1 homolog (S. cerevisiae)	7.69	3.83E-23
4	Gclm	Glutamate-cysteine ligase, modifier subunit	9.82	7.61E-23
5	Ikbkg	Inhibitor of kappaB kinase γ	3.01	3.18E-21
6	Vps37b	Vacuolar protein sorting 37B (yeast)	3.89	2.06E-20
7	Htatip2	HIV-1 tat interactive protein 2, homolog (human)	2.19	2.06E-20
8	Slc40a1	Solute carrier family 40 (iron-regulated transporter), member 1	13.79	4.89E-20
9	Abcc1	ATP-binding cassette, sub-family C (CFTR/MRP), member 1	4.49	1.19E-19
10	Gclc	Glutamate-cysteine ligase, catalytic subunit	4.92	1.21E-19
11	Ptgr1	Prostaglandin reductase 1	3.64	2.94E-19
12	Chpf2	Chondroitin polymerizing factor 2	2.52	4.58E-19
13	Ier2	Immediate early response 2	0.43	5.72E-19
14	Gsr	Glutathione reductase	2.69	5.72E-19
15	Rit1	Ras-like without CAAX 1	2.15	6.27E-19
16	Pgd	Phosphogluconate dehydrogenase	2.17	6.42E-19
17	Slc7a11	Solute carrier family 7 (cationic amino acid transporter, y+ system), member 11	10.88	3.60E-18
18	Sqstm1	Sequestosome 1	1.94	4.40E-18
19	Kansl2	KAT8 regulatory NSL complex subunit 2	2.00	1.53E-17
20	Prr13	Proline rich 13	1.75	1.64E-17

Table 2-2: Top 20 genes differentially expressed with DEPe treatment in peritoneal macrophages. Genes are listed in descending order of the FDR. Nearly all the genes in the top 20 are upregulated (fold change > 1). Only *Ier2* was downregulated.

	Gene	Name	Fold Change	FDR
1	Hmox1	Heme oxygenase (decycling) 1	12.46	9.47E-33
2	Txnrd1	Thioredoxin reductase 1	3.50	1.59E-26
3	Srxn1	Sulfiredoxin 1 homolog (S. cerevisiae)	7.69	3.83E-23
4	Gclm	Glutamate-cysteine ligase, modifier subunit	9.82	7.61E-23
5	Ikbkg	Inhibitor of kappaB kinase γ	3.01	3.18E-21
6	Vps37b	Vacuolar protein sorting 37B (yeast)	3.89	2.06E-20
7	Htatip2	HIV-1 Tat interactive protein 2, homolog (human)	2.19	2.06E-20
8	Slc40a1	Solute carrier family 40 (iron-regulated transporter), member 1	13.79	4.89E-20
9	Abcc1	ATP-binding cassette, sub-family C (CFTR/MRP), member 1	4.49	1.19E-19
10	Gclc	Glutamate-cysteine ligase, catalytic subunit	4.92	1.21E-19
11	Ptgr1	Prostaglandin reductase 1	3.64	2.94E-19
12	Chpf2	Chondroitin polymerizing factor 2	2.52	4.58E-19
13	Gsr	Glutathione reductase	2.69	5.72E-19
14	Rit1	Ras-like without CAAX 1	2.15	6.27E-19
15	Pgd	Phosphogluconate dehydrogenase	2.17	6.42E-19
16	Slc7a11	Solute carrier family 7 (cationic amino acid transporter, y+ system), member 11	10.88	3.60E-18
17	Sqstm1	Sequestosome 1	1.94	4.40E-18
18	Kansl2	KAT8 regulatory NSL complex subunit 2	2.00	1.53E-17
19	Prr13	Proline rich 13	1.75	1.64E-17
20	E2f6	E2F transcription factor 6	2.39	2.51E-17
21	Cyb5a	cytochrome b5 type A (microsomal)	2.14	1.20E-16
22	Slc48a1	solute carrier family 48 (heme transporter), member 1	2.62	1.79E-16
23	Psm11	proteasome (prosome, macropain) 26S subunit, non-ATPase, 11	2.03	3.40E-16
24	Klhl21	kelch-like 21	2.35	3.74E-16
25	Prdx1	peroxiredoxin 1	1.55	3.88E-16
26	Mafg	v-maf musculoaponeurotic fibrosarcoma oncogene family, protein G (avian)	2.38	4.90E-16
27	Esd	esterase D/formylglutathione hydrolase	1.38	5.91E-16
28	Jade1	jade family PHD finger 1	2.26	7.10E-16
29	Bach1	BTB and CNC homology 1, basic leucine zipper transcription factor 1	1.58	7.40E-16
30	Zadh2	zinc binding alcohol dehydrogenase, domain containing 2	2.51	1.06E-15
31	Psm5	proteasome (prosome, macropain) 26S subunit, non-ATPase, 5	1.86	1.54E-15
32	Ninj1	ninjurin 1	1.67	1.87E-15
33	Ttc39c	tetratricopeptide repeat domain 39C	2.09	2.78E-15
34	Osgin1	oxidative stress induced growth inhibitor 1	2.94	3.44E-15
35	Tshz1	teashirt zinc finger family member 1	4.48	4.71E-15
36	Ypel5	yippee like 5	2.04	5.65E-15
37	Impact	impact, RWD domain protein	2.38	7.57E-15
38	Psm5	proteasome (prosome, macropain) subunit, alpha type 5	1.67	8.06E-15
39	Panx1	pannexin 1	2.90	1.05E-14
40	Ubap1	ubiquitin-associated protein 1	1.92	1.37E-14

Table 2-3: Top 40 genes upregulated with DEPe treatment. Genes are listed in descending order of the FDR.

	Gene	Name	Fold Change	FDR
1	Ier2	Immediate early response 2	0.43	5.72E-19
2	Lyl1	Lymphoblastic leukemia 1	0.28	1.91E-15
3	Itpkb	Inositol 1,4,5-trisphosphate 3-kinase B	0.30	3.98E-15
4	Fgd4	FYVE, RhoGEF and PH domain containing 4	0.57	7.99E-15
5	Ikbkg	UDP-GlcNAc: β Gal β -1,3-N-acetylglucosaminyltransferase 8	0.43	4.31E-14
6	Cnr2	Cannabinoid receptor 2 (macrophage)	0.48	1.08E-13
7	Frmd4b	FERM domain containing 4B	0.33	1.96E-13
8	Lcp1	Lymphocyte cytosolic protein 1	0.77	2.05E-13
9	Lfng	LFNG O-fucosylpeptide 3- β -N-acetylglucosaminyltransferase	0.56	3.34E-13
10	P2ry6	Pyrimidinergic receptor P2Y, G-protein coupled, 6	0.15	5.03E-13
11	Erp29	Endoplasmic reticulum protein 29	0.59	6.05E-13
12	Fes	Feline sarcoma oncogene	0.51	7.27E-13
13	Rgs2	Regulator of G-protein signaling 2	0.34	1.27E-12
14	Sash3	SAM and SH3 domain containing 3	0.44	1.41E-12
15	Ptpn6	Protein tyrosine phosphatase, non-receptor type 6	0.36	1.80E-12
16	Ppp1cc	Protein phosphatase 1 catalytic subunit γ	0.79	4.01E-12
17	Rai14	Retinoic acid induced 14	0.54	6.51E-12
18	Myo1e	Myosin IE	0.49	7.43E-12
19	Ikbke	Inhibitor of κ B kinase ϵ	0.37	8.89E-12
20	Enc1	Ectodermal-neural cortex 1	0.25	1.02E-11
21	Ptpro	protein tyrosine phosphatase, receptor type, O	0.34	2.01E-11
22	Arhgap45	Rho GTPase activating protein 45	0.47	2.09E-11
23	Metrnl	meteorin, glial cell differentiation regulator-like	0.71	2.39E-11
24	Sh3bp1	SH3-domain binding protein 1	0.59	5.88E-11
25	Rin2	Ras and Rab interactor 2	0.45	6.39E-11
26	Themis2	thymocyte selection associated family member 2	0.32	6.56E-11
27	Plxnb2	plexin B2	0.61	6.80E-11
28	Retreg1	reticulophagy regulator 1	0.65	7.37E-11
29	Coro1a	coronin, actin binding protein 1A	0.33	7.37E-11
30	Nab2	Ngfi-A binding protein 2	0.46	7.47E-11
31	Svil	supervillin	0.67	7.68E-11
32	Abcd1	ATP-binding cassette, sub-family D (ALD), member 1	0.52	8.79E-11
33	Mafb	v-maf musculoaponeurotic fibrosarcoma oncogene family, protein B (avian)	0.29	9.49E-11
34	Klf2	Kruppel-like factor 2 (lung)	0.37	1.06E-10
35	Apob48r	apolipoprotein B receptor	0.64	3.92E-10
36	Arhgef10l	Rho guanine nucleotide exchange factor (GEF) 10-like	0.53	6.40E-10
37	Mov10	Moloney leukemia virus 10	0.77	6.86E-10
38	Bcl6	B cell leukemia/lymphoma 6	0.58	8.38E-10
39	Sesn1	sestrin 1	0.45	9.10E-10
40	Arhgap9	Rho GTPase activating protein 9	0.56	1.08E-09

Table 2-4: Top 40 genes downregulated with DEPe treatment. Genes are listed in descending order of the FDR.

	Gene	Fold Change	FDR		Gene	Fold Change	FDR
1	Hmox1	12.46	9.47E-33	25	Slc16a6	2.80	6.47E-08
2	Txnrd1	3.50	1.59E-26	26	Ptp4a1	1.72	1.29E-07
3	Srxn1	7.69	3.83E-23	27	Btg3	1.56	1.92E-07
4	Gelm	9.82	7.61E-23	28	Gabarapl1	1.57	3.02E-07
5	Vps37b	3.89	2.06E-20	29	Trib3	2.35	1.35E-06
6	Htatip2	2.19	2.06E-20	30	Gdf15	5.26	1.56E-06
7	Slc40a1	13.79	4.89E-20	31	Dusp1	2.32	2.70E-06
8	Gclc	4.92	1.21E-19	32	Cbx2	1.38	3.51E-06
9	Gsr	2.69	5.72E-19	33	D16Erttd472e	1.23	9.16E-06
10	Rit1	2.15	6.27E-19	34	Odc1	1.66	2.81E-05
11	Phf17	2.26	7.10E-16	35	Gadd45a	1.83	3.68E-04
12	Osgin1	2.94	3.44E-15	36	Cebpb	1.31	4.27E-04
13	Panx1	2.90	1.05E-14	37	Btg1	1.35	5.64E-04
14	Ubap1	1.92	1.37E-14	38	Prune	1.32	1.07E-03
15	Cbr3	3.92	1.72E-14	39	Cnmm2	0.85	1.74E-03
16	Lpin2	1.92	5.80E-13	40	Cenpa	0.75	2.10E-03
17	LOC630729	2.77	6.05E-13	41	Gtlf3b	1.48	2.58E-03
18	Map2k3	1.54	1.85E-12	42	Mylip	1.68	8.69E-03
19	Rusc2	1.89	3.95E-12	43	Vegfa	1.51	9.23E-03
20	Slc25a33	2.36	4.08E-11	44	Samd8	1.35	1.18E-02
21	Crem	1.50	9.20E-11	45	Mxi1	0.81	1.61E-02
22	Depdc7	3.24	9.76E-11	46	Tgif1	1.23	2.61E-02
23	Ankrd28	2.01	5.20E-10	47	Mpp5	1.19	2.74E-02
24	Btg2	0.55	2.14E-08				

Table 2-5: Differentially expressed Mox marker genes with DEPe treatment. Out of 64 Mox marker genes analyzed, 47 had significantly different expression ($FDR < 0.05$) between DEPe and control. Genes are in descending order of the FDR across all 24 mouse strains; fold change values (DEPe over control) are also included.

	Gene	Fold Change	FDR		Gene	Fold Change	FDR		Gene	Fold Change	FDR
1	Abcc1	4.49	1.19E-19	51	Fbxl3	1.28	2.70E-05	101	Cdkn1a	1.45	1.03E-03
2	Sqstm1	1.94	4.40E-18	52	Slc16a1	1.50	2.75E-05	102	Dusp11	1.24	1.03E-03
3	Itpkb	0.30	3.98E-15	53	Dnaja1	1.35	3.42E-05	103	Eif6	1.14	1.07E-03
4	Map2k3	1.54	1.85E-12	54	Slc39a14	1.39	3.70E-05	104	Itga4	0.82	1.08E-03
5	Lrrfp2	1.69	2.17E-12	55	Usp16	1.24	3.91E-05	105	Gent2	0.72	1.14E-03
6	Ikbke	0.37	8.89E-12	56	Nup54	1.23	4.00E-05	106	Caml	1.18	1.18E-03
7	Txnl1	1.55	1.01E-11	57	Slc11a2	1.46	4.43E-05	107	Anxa7	1.17	1.20E-03
8	Rin2	0.45	6.39E-11	58	Hivep3	0.86	4.45E-05	108	Usb1	1.17	1.22E-03
9	Themis2	0.32	6.56E-11	59	Wdr43	1.17	5.03E-05	109	Snx10	1.16	1.39E-03
10	Met	3.36	2.90E-10	60	Rcsd1	0.64	7.57E-05	110	Rnf14	1.12	1.39E-03
11	Tiparp	1.55	3.00E-09	61	Parp12	0.69	8.29E-05	111	Rbpms	0.74	1.41E-03
12	Arrdc4	1.93	3.72E-09	62	Gch1	1.69	9.01E-05	112	Kctd12	0.63	1.43E-03
13	Slc2a1	1.82	7.40E-09	63	Ncoa5	1.25	9.26E-05	113	Arih2	1.21	1.63E-03
14	Zc3h12c	2.30	9.30E-09	64	Trex1	0.52	1.01E-04	114	Cacybp	1.25	1.72E-03
15	Ppp2r2a	1.33	1.35E-08	65	Rab22a	1.21	1.04E-04	115	Dgka	0.79	1.95E-03
16	Irf8	0.67	1.77E-08	66	D1Erttd622e	1.21	1.07E-04	116	Stag2	0.86	2.04E-03
17	Hspa1b	6.11	1.90E-08	67	Plscr1	0.85	1.14E-04	117	Samsn1	0.61	2.22E-03
18	Ii13ra1	0.69	2.73E-08	68	Nfkbib	1.25	1.17E-04	118	Rhob	0.68	2.44E-03
19	Irf5	0.49	3.32E-08	69	Sfrs3	0.83	1.17E-04	119	Klf7	0.69	2.57E-03
20	Nt5c3	1.28	9.14E-08	70	Ldlr	0.56	1.18E-04	120	Rock1	1.23	2.70E-03
21	Pvr	2.07	1.15E-07	71	Klf6	1.34	1.26E-04	121	Extl2	0.72	2.94E-03
22	Siah2	1.50	1.17E-07	72	Top1	1.27	1.65E-04	122	Clic4	1.22	3.01E-03
23	Sema4a	0.64	1.30E-07	73	Brd2	1.26	1.88E-04	123	Atad1	1.15	3.02E-03
24	Phip	1.72	1.48E-07	74	Tcf4	0.78	1.94E-04	124	Tmem39a	1.20	3.10E-03
25	Mapk6	1.34	2.05E-07	75	Pi4k2b	1.39	2.20E-04	125	Vasp	0.75	3.27E-03
26	Osgin2	1.95	2.56E-07	76	Cdyl	1.17	2.33E-04	126	Rnf4	1.17	3.30E-03
27	Crlf3	1.43	2.75E-07	77	Ppm1a	1.21	2.34E-04	127	Fbxo42	1.22	3.36E-03
28	Ube2f	1.40	3.06E-07	78	Hspa1a	2.83	2.46E-04	128	Ifih1	0.77	3.40E-03
29	Spred2	2.20	3.61E-07	79	Tlk2	1.17	2.46E-04	129	Rbl1	0.72	3.47E-03
30	Cd83	0.42	4.99E-07	80	Dram1	0.78	2.57E-04	130	Itga5	0.72	3.52E-03
31	Meep2	1.33	5.47E-07	81	Depdc6	0.74	2.99E-04	131	Gpr85	0.91	3.60E-03
32	Kpna4	1.42	8.76E-07	82	Myo1g	0.67	3.20E-04	132	Hat1	1.21	3.92E-03
33	Ets2	1.92	1.22E-06	83	Myo10	0.74	3.20E-04	133	Deun1d5	1.15	4.04E-03
34	Samhd1	0.57	1.53E-06	84	Gbp1	1.16	3.21E-04	134	Slc28a2	0.51	4.19E-03
35	Pxn	0.72	1.66E-06	85	Slc25a37	1.56	3.33E-04	135	Lrrc59	1.31	4.33E-03
36	Ell2	1.67	2.29E-06	86	Stard5	0.78	3.49E-04	136	Sertad2	1.36	4.34E-03
37	Ppap2b	1.66	2.80E-06	87	Nupr1	1.65	3.50E-04	137	Aftph	0.86	4.39E-03
38	Stx3	1.45	3.57E-06	88	Dnaja2	1.25	3.59E-04	138	Arih1	1.39	4.58E-03
39	Mafk	1.50	5.30E-06	89	Actn1	0.79	3.68E-04	139	Sbds	1.21	4.80E-03
40	Ankrd57	0.70	6.53E-06	90	Clef1	1.17	4.19E-04	140	Sh3bgrl2	1.50	4.84E-03
41	Rbm43	0.67	8.20E-06	91	Cerl2	0.64	4.20E-04	141	Ptpn23	1.33	4.95E-03
42	St3gal5	0.60	1.03E-05	92	Parp9	0.68	5.23E-04	142	Pspc1	0.78	5.30E-03
43	Ppp4r2	1.24	1.08E-05	93	Tmpo	0.78	5.28E-04	143	Vps37c	1.35	5.35E-03
44	Skil	0.60	1.14E-05	94	Rnf135	1.20	5.29E-04	144	Usp18	0.70	5.41E-03
45	Sptlc2	1.36	1.22E-05	95	Trim21	0.73	5.83E-04	145	Sgms1	1.24	5.76E-03
46	Ext1	1.52	1.28E-05	96	Stx6	0.85	6.51E-04	146	Rnd3	1.52	6.29E-03
47	Rasa2	1.39	1.39E-05	97	Appl1	1.15	7.18E-04	147	Znrf1	1.26	6.47E-03
48	Rbbp8	1.33	1.81E-05	98	Ints12	1.39	7.72E-04	148	Ankrd44	0.76	6.64E-03
49	Trim13	1.36	2.25E-05	99	Nr3c1	1.22	8.09E-04	149	Yrdc	1.19	6.79E-03
50	Lancl2	0.74	2.46E-05	100	Ehd1	1.90	9.43E-04	150	Pvrl2	0.76	6.82E-03

Continued on next page...

...continued from previous page.

Gene	Fold Change	FDR	Gene	Fold Change	FDR	Gene	Fold Change	FDR			
151	Slfn2	0.77	6.82E-03	179	Rabgef1	1.19	1.86E-02	207	Pofut2	1.13	3.17E-02
152	Arl4a	1.16	6.88E-03	180	Gramd1a	0.83	1.87E-02	208	Hmgb2	1.12	3.26E-02
153	Gdap10	1.87	6.94E-03	181	Ints8	1.14	1.89E-02	209	Gas7	0.83	3.30E-02
154	Sf1	1.19	7.01E-03	182	Zyx	1.24	1.91E-02	210	Pip5k1a	1.16	3.35E-02
155	Gspt1	1.26	7.01E-03	183	Ktn1	1.22	2.00E-02	211	Rnpc3	1.18	3.40E-02
156	Azi2	1.17	7.25E-03	184	Spred1	1.23	2.04E-02	212	Gca	1.11	3.45E-02
157	Ugeg	1.29	7.31E-03	185	Ktelc1	0.85	2.05E-02	213	Car13	1.28	3.46E-02
158	Apobec3	0.87	7.54E-03	186	Tbc1d1	0.84	2.08E-02	214	Ankib1	1.07	3.52E-02
159	Gabpb1	1.22	7.77E-03	187	Stom	0.85	2.10E-02	215	Daxx	0.84	3.57E-02
160	Cdk5r1	1.12	8.02E-03	188	Adar	0.85	2.18E-02	216	Acbd3	1.28	3.65E-02
161	Larp1	1.16	8.32E-03	189	Thr7	0.83	2.20E-02	217	Stip1	1.14	3.74E-02
162	Cul3	1.16	8.52E-03	190	Isg20	1.18	2.45E-02	218	Chd1	1.23	3.82E-02
163	Errf1	1.47	8.97E-03	191	Mthfr	1.24	2.48E-02	219	Foxp1	0.78	3.83E-02
164	4930453N24Rik	1.13	9.02E-03	192	Marcks	0.79	2.48E-02	220	Lrrc8c	0.82	3.94E-02
165	Hck	0.69	9.62E-03	193	Cd80	0.84	2.48E-02	221	Larp2	1.21	3.96E-02
166	Tnip1	0.85	9.62E-03	194	Mmp14	0.62	2.51E-02	222	Psat1	1.47	4.05E-02
167	Lmo4	1.32	1.02E-02	195	Slc23a2	1.16	2.62E-02	223	Ptpn2	1.09	4.12E-02
168	Rap2c	0.86	1.03E-02	196	Slc44a1	0.79	2.62E-02	224	Thr3	0.87	4.19E-02
169	Cpeb4	1.23	1.31E-02	197	Eif1a	1.16	2.74E-02	225	Sh3bp4	1.10	4.19E-02
170	Fam133b	1.17	1.38E-02	198	Mpp5	1.19	2.74E-02	226	Traf6	1.19	4.28E-02
171	Kif1b	1.16	1.39E-02	199	Cdc42ep4	0.76	2.79E-02	227	Cpd	0.87	4.55E-02
172	E2f8	0.83	1.43E-02	200	Clec5a	0.66	2.79E-02	228	Ccdc50	1.29	4.64E-02
173	Rffl	1.23	1.55E-02	201	Stk4	0.85	2.81E-02	229	Nras	0.87	4.71E-02
174	Ppm1b	1.11	1.59E-02	202	Mitf	0.83	2.90E-02	230	Frmd6	1.35	4.72E-02
175	Itgav	0.81	1.61E-02	203	Rnf2	1.15	2.95E-02	231	Src	0.88	4.73E-02
176	Dusp16	1.31	1.65E-02	204	Kbtbd2	1.13	3.07E-02	232	Phldb1	0.88	4.79E-02
177	Cflar	1.24	1.78E-02	205	Pgs1	1.15	3.08E-02	233	St3gal3	0.84	4.86E-02
178	Atp11b	1.15	1.84E-02	206	Denr	0.93	3.09E-02	234	Ppp1r11	1.18	4.89E-02

Table 2-6: Differentially expressed M1 marker genes with DEPe treatment. Out of the 644 M1 marker genes analyzed, 234 had significantly different expression (FDR < 0.05) between DEPe and control. Genes are listed in descending order of the FDR across all 24 mouse strains; fold change values (DEPe over control) are also included.

	Gene	Fold Change	FDR		Gene	Fold Change	FDR
1	Rps6kc1	1.83	3.34E-14	29	Cltc	1.15	1.26E-03
2	Cnr2	0.48	1.08E-13	30	Bcl2l11	0.62	1.74E-03
3	Mafb	0.29	9.49E-11	31	Fbxo33	1.25	1.82E-03
4	Sla	0.34	9.01E-09	32	Bmp2	0.74	1.82E-03
5	Zrsr1	1.56	3.10E-08	33	Rbbp6	1.27	1.97E-03
6	Ralgds	2.97	3.54E-08	34	Tlr4	0.73	3.55E-03
7	Tspyl4	0.80	6.65E-08	35	Plekhf1	0.86	3.82E-03
8	Fyn	1.64	1.68E-07	36	B3galt4	0.80	4.21E-03
9	Map3k12	0.80	2.57E-07	37	Clen3	1.16	4.24E-03
10	Gpr155	0.62	2.58E-07	38	St6gal1	0.79	6.65E-03
11	Ppargc1b	0.53	2.60E-07	39	Ugcg	1.29	7.31E-03
12	Tiam1	0.77	3.83E-06	40	Itsn2	1.17	8.24E-03
13	Abcd2	0.52	3.99E-06	41	Dab2	0.71	1.16E-02
14	Tmem51	0.60	4.40E-06	42	Plekha3	1.11	1.41E-02
15	Ptpre	0.62	1.75E-05	43	Ak2	0.80	1.53E-02
16	Casp6	0.74	2.79E-05	44	Ncoa3	0.80	1.84E-02
17	Snx16	1.34	1.92E-04	45	Sulf2	0.78	2.00E-02
18	Tlr8	0.48	2.10E-04	46	Id1	0.79	2.01E-02
19	Hnrpll	0.77	2.70E-04	47	Clk4	1.32	2.31E-02
20	Tnfaip8	0.71	2.73E-04	48	Gatm	0.69	2.79E-02
21	Znrf2	1.15	2.96E-04	49	Dck	1.28	3.44E-02
22	Slc39a6	1.28	3.39E-04	50	Dmxl1	1.11	3.76E-02
23	Pdgfc	0.72	4.02E-04	51	Egr2	0.84	3.81E-02
24	Zfp36l1	0.61	5.09E-04	52	Foxj3	1.18	4.05E-02
25	Tbc1d14	0.76	5.44E-04	53	Ctdp1	1.19	4.18E-02
26	Ski	0.79	6.51E-04	54	Tcf7l2	0.88	4.44E-02
27	Tsr1	1.21	7.18E-04	55	Etv3	1.20	4.50E-02
28	P2ry1	0.55	1.15E-03	56	Arl4c	1.62	4.89E-02

Table 2-7: Differentially expressed M2 marker genes with DEPe treatment. Out of 143 M2 marker genes analyzed, 56 had significantly different expression (FDR < 0.05) between DEPe and control. Genes are in descending order of the FDR across all 24 mouse strains; fold change values (DEPe over control) are also included.

	DEPe (%)	LPS (%)	OxPAPC (%)
M1 (644 genes)	4.66	57.14	3.11
M2 (143 genes)	3.50	11.19	2.10
Mox (64 genes)	53.13	12.50	42.19

Table 2-8: Summary of macrophage polarization by treatment. Numbers represent the percentage of significantly upregulated (FDR < 0.05 and fold change > 1.5) macrophage marker genes for peritoneal macrophages undergoing that particular treatment (DEPe, LPS, or OxPAPC). The total number of macrophage marker genes used in the analyses are also indicated for each subtype.

References

Affymetrix (2007). Data Sheet: GeneChip Mouse Genome Arrays. Santa Clara, CA, Affymetrix.

Affymetrix (2009). [HT_MG-430A] Affymetrix HT Mouse Genome 430A Array. I. Affymetrix. Gene Expression Omnibus.

Aoki, Y., H. Sato, N. Nishimura, S. Takahashi, K. Itoh and M. Yamamoto (2001). "Accelerated DNA adduct formation in the lung of the Nrf2 knockout mouse exposed to diesel exhaust." Toxicol Appl Pharmacol **173**(3): 154-160.

Araujo, J. A. (2010). "Particulate air pollution, systemic oxidative stress, inflammation, and atherosclerosis." Air Qual Atmos Health **4**(1): 79-93.

Ashburner, M., C. A. Ball, J. A. Blake, D. Botstein, H. Butler, J. M. Cherry, A. P. Davis, K. Dolinski, S. S. Dwight, J. T. Eppig, M. A. Harris, D. P. Hill, L. Issel-Tarver, A. Kasarskis, S. Lewis, J. C. Matese, J. E. Richardson, M. Ringwald, G. M. Rubin and G. Sherlock (2000). "Gene ontology: tool for the unification of biology. The Gene Ontology Consortium." Nat Genet **25**(1): 25-29.

Becker, S., J. M. Soukup and J. E. Gallagher (2002). "Differential particulate air pollution induced oxidant stress in human granulocytes, monocytes and alveolar macrophages." Toxicol In Vitro **16**(3): 209-218.

Bennett, B. J., R. C. Davis, M. Civelek, L. Orozco, J. Wu, H. Qi, C. Pan, R. R. Packard, E. Eskin, M. Yan, T. Kirchgessner, Z. Wang, X. Li, J. C. Gregory, S. L. Hazen, P. S. Gargalovic and A. J. Lusis (2015). "Genetic Architecture of Atherosclerosis in Mice: A Systems Genetics Analysis of Common Inbred Strains." PLoS Genet **11**(12): e1005711.

Bennett, B. J., C. R. Farber, L. Orozco, H. M. Kang, A. Ghazalpour, N. Siemers, M. Neubauer, I. Neuhaus, R. Yordanova, B. Guan, A. Truong, W. P. Yang, A. He, P. Kayne, P. Gargalovic, T. Kirchgessner, C. Pan, L. W. Castellani, E. Kostem, N. Furlotte, T. A. Drake, E. Eskin and A. J. Lusis (2010). "A high-resolution association mapping panel for the dissection of complex traits in mice." Genome Res **20**(2): 281-290.

Chen, E. Y., H. Xu, S. Gordonov, M. P. Lim, M. H. Perkins and A. Ma'ayan (2012). "Expression2Kinases: mRNA profiling linked to multiple upstream regulatory layers." Bioinformatics **28**(1): 105-111.

Farber, C. R., B. J. Bennett, L. Orozco, W. Zou, A. Lira, E. Kostem, H. M. Kang, N. Furlotte, A. Berberyan, A. Ghazalpour, J. Suwanwela, T. A. Drake, E. Eskin, Q. T. Wang, S. L. Teitelbaum and A. J. Lusis (2011). "Mouse genome-wide association and systems genetics identify *Asx12* as a regulator of bone mineral density and osteoclastogenesis." PLoS Genet **7**(4): e1002038.

Farina, F., G. Sancini, C. Battaglia, V. Tinaglia, P. Mantecca, M. Camatini and P. Palestini (2013). "Milano summer particulate matter (PM10) triggers lung inflammation and extra pulmonary adverse events in mice." PLoS One **8**(2): e56636.

Finch, G. L., C. H. Hobbs, L. F. Blair, E. B. Barr, F. F. Hahn, R. J. Jaramillo, J. E. Kubatko, T. H. March, R. K. White, J. R. Krone, M. G. Menache, K. J. Nikula, J. L. Mauderly, J. Van Gerpen, M. D. Merceica, B. Zielinska, L. Stankowski, K. Burling and S. Howell (2002). "Effects of subchronic inhalation exposure of rats to emissions from a diesel engine burning soybean oil-derived biodiesel fuel." Inhal Toxicol **14**(10): 1017-1048.

Ghazalpour, A., C. D. Rau, C. R. Farber, B. J. Bennett, L. D. Orozco, A. van Nas, C. Pan, H. Allayee, S. W. Beaven, M. Civelek, R. C. Davis, T. A. Drake, R. A. Friedman, N. Furlotte, S. T. Hui, J. D. Jentsch, E. Kostem, H. M. Kang, E. Y. Kang, J. W. Joo, V. A. Korshunov, R. E. Laughlin, L. J. Martin, J. D. Ohmen, B. W. Parks, M. Pellegrini, K. Reue, D. J. Smith, S. Tetradis, J. Wang, Y. Wang, J. N. Weiss, T. Kirchgessner, P. S. Gargalovic, E. Eskin, A. J. Lusis and R. C. LeBoeuf (2012). "Hybrid mouse diversity panel: a panel of inbred mouse strains suitable for analysis of complex genetic traits." Mamm Genome **23**(9-10): 680-692.

Gordon, S. (2003). "Alternative activation of macrophages." Nat Rev Immunol **3**(1): 23-35.

Hiura, T. S., M. P. Kaszubowski, N. Li and A. E. Nel (1999). "Chemicals in diesel exhaust particles generate reactive oxygen radicals and induce apoptosis in macrophages." J Immunol **163**(10): 5582-5591.

Hoover, D. L. and C. A. Nacy (1984). "Macrophage activation to kill *Leishmania tropica*: defective intracellular killing of amastigotes by macrophages elicited with sterile inflammatory agents." J Immunol **132**(3): 1487-1493.

Irizarry, R. A., B. Hobbs, F. Collin, Y. D. Beazer-Barclay, K. J. Antonellis, U. Scherf and T. P. Speed (2003). "Exploration, normalization, and summaries of high density oligonucleotide array probe level data." Biostatistics **4**(2): 249-264.

Kadl, A., A. K. Meher, P. R. Sharma, M. Y. Lee, A. C. Doran, S. R. Johnstone, M. R. Elliott, F. Gruber, J. Han, W. Chen, T. Kensler, K. S. Ravichandran, B. E. Isakson, B. R. Wamhoff and N. Leitinger (2010). "Identification of a novel macrophage phenotype that develops in response to atherogenic phospholipids via Nrf2." Circ Res **107**(6): 737-746.

Kensler, T. W., N. Wakabayashi and S. Biswal (2007). "Cell survival responses to environmental stresses via the Keap1-Nrf2-ARE pathway." Annu Rev Pharmacol Toxicol **47**: 89-116.

Koike, E., S. Hirano, N. Shimojo and T. Kobayashi (2002). "cDNA microarray analysis of gene expression in rat alveolar macrophages in response to organic extract of diesel exhaust particles." Toxicol Sci **67**(2): 241-246.

Kulkarni, N., N. Pierse, L. Rushton and J. Grigg (2006). "Carbon in airway macrophages and lung function in children." N Engl J Med **355**(1): 21-30.

Lam, D., D. Harris and Z. Qin (2013). "Inflammatory mediator profiling reveals immune properties of chemotactic gradients and macrophage mediator production inhibition during thioglycollate elicited peritoneal inflammation." Mediators Inflamm **2013**: 931562.

- Li, N., J. Alam, M. I. Venkatesan, A. Eiguren-Fernandez, D. Schmitz, E. Di Stefano, N. Slaughter, E. Killeen, X. Wang, A. Huang, M. Wang, A. H. Miguel, A. Cho, C. Sioutas and A. E. Nel (2004). "Nrf2 is a key transcription factor that regulates antioxidant defense in macrophages and epithelial cells: protecting against the proinflammatory and oxidizing effects of diesel exhaust chemicals." J Immunol **173**(5): 3467-3481.
- Li, N., S. Kim, M. Wang, J. Froines, C. Sioutas and A. Nel (2002). "Use of a stratified oxidative stress model to study the biological effects of ambient concentrated and diesel exhaust particulate matter." Inhal Toxicol **14**(5): 459-486.
- Li, N., M. Wang, T. D. Oberley, J. M. Sempf and A. E. Nel (2002). "Comparison of the pro-oxidative and proinflammatory effects of organic diesel exhaust particle chemicals in bronchial epithelial cells and macrophages." J Immunol **169**(8): 4531-4541.
- Lusis, A. J., M. M. Seldin, H. Allayee, B. J. Bennett, M. Civelek, R. C. Davis, E. Eskin, C. R. Farber, S. Hui, M. Mehrabian, F. Norheim, C. Pan, B. Parks, C. D. Rau, D. J. Smith, T. Vallim, Y. Wang and J. Wang (2016). "The Hybrid Mouse Diversity Panel: a resource for systems genetics analyses of metabolic and cardiovascular traits." J Lipid Res **57**(6): 925-942.
- Marano, F., S. Boland, V. Bonvallot, A. Baulig and A. Baeza-Squiban (2002). "Human airway epithelial cells in culture for studying the molecular mechanisms of the inflammatory response triggered by diesel exhaust particles." Cell Biol Toxicol **18**(5): 315-320.
- Martinez, F. O. and S. Gordon (2014). "The M1 and M2 paradigm of macrophage activation: time for reassessment." F1000Prime Rep **6**: 13.
- Misharin, A. V., R. Saber and H. Perlman (2012). "Eosinophil contamination of thioglycollate-elicited peritoneal macrophage cultures skews the functional readouts of in vitro assays." J Leukoc Biol **92**(2): 325-331.
- Nguyen, T., P. Nioi and C. B. Pickett (2009). "The Nrf2-antioxidant response element signaling pathway and its activation by oxidative stress." J Biol Chem **284**(20): 13291-13295.
- Org, E., B. W. Parks, J. W. Joo, B. Emert, W. Schwartzman, E. Y. Kang, M. Mehrabian, C. Pan, R. Knight, R. Gunsalus, T. A. Drake, E. Eskin and A. J. Lusis (2015). "Genetic and environmental control of host-gut microbiota interactions." Genome Res **25**(10): 1558-1569.
- Orozco, L. D., B. J. Bennett, C. R. Farber, A. Ghazalpour, C. Pan, N. Che, P. Wen, H. X. Qi, A. Mutukulu, N. Siemers, I. Neuhaus, R. Yordanova, P. Gargalovic, M. Pellegrini, T. Kirchgessner and A. J. Lusis (2012). "Unraveling inflammatory responses using systems genetics and gene-environment interactions in macrophages." Cell **151**(3): 658-670.
- Rizzo, A. M., P. A. Corsetto, F. Farina, G. Montorfano, G. Pani, C. Battaglia, G. Sancini and P. Palestini (2014). "Repeated intratracheal instillation of PM10 induces lipid reshaping in lung parenchyma and in extra-pulmonary tissues." PLoS One **9**(9): e106855.

- Roy, S., S. Khanna, K. Bentley, P. Beffrey and C. K. Sen (2002). Functional Genomics: High-Density Oligonucleotide Arrays. USA, Elsevier Science.
- Sagai, M., H. Saito, T. Ichinose, M. Kodama and Y. Mori (1993). "Biological effects of diesel exhaust particles. I. In vitro production of superoxide and in vivo toxicity in mouse." Free Radic Biol Med **14**(1): 37-47.
- Shannon, P., A. Markiel, O. Ozier, N. S. Baliga, J. T. Wang, D. Ramage, N. Amin, B. Schwikowski and T. Ideker (2003). "Cytoscape: a software environment for integrated models of biomolecular interaction networks." Genome Res **13**(11): 2498-2504.
- Smyth, G. K., M. Ritchie, N. Thorne, J. Wettenhall, W. Shi and Y. Hu (2018). limma: Linear Models for Microarray and RNA-Seq Data: User's Guide, The Walter and Eliza Hall Institute of Medical Research, Melbourne, Australia.
- Strom, K. A., B. D. Garg, J. T. Johnson, J. B. D'Arcy and K. L. Smiler (1990). "Inhaled particle retention in rats receiving low exposures of diesel exhaust." J Toxicol Environ Health **29**(4): 377-398.
- Suwa, T., J. C. Hogg, K. B. Quinlan, A. Ohgami, R. Vincent and S. F. van Eeden (2002). "Particulate air pollution induces progression of atherosclerosis." J Am Coll Cardiol **39**(6): 935-942.
- Takano, H., T. Yoshikawa, T. Ichinose, Y. Miyabara, K. Imaoka and M. Sagai (1997). "Diesel exhaust particles enhance antigen-induced airway inflammation and local cytokine expression in mice." Am J Respir Crit Care Med **156**(1): 36-42.
- The Gene Ontology Consortium (2017). "Expansion of the Gene Ontology knowledgebase and resources." Nucleic Acids Res **45**(D1): D331-d338.
- The Jackson Laboratory. "B6cC3-1/KccJ." Retrieved September 30, 2018, 2018, from <https://www.jax.org/strain/003787>.
- Vogel, S. N., D. Johnson, P. Y. Perera, A. Medvedev, L. Lariviere, S. T. Qureshi and D. Malo (1999). "Cutting edge: functional characterization of the effect of the C3H/HeJ defect in mice that lack an Lpsn gene: in vivo evidence for a dominant negative mutation." J Immunol **162**(10): 5666-5670.
- Wittkopp, S., N. Staimer, T. Tjoa, T. Stinchcombe, N. Daher, J. J. Schauer, M. M. Shafer, C. Sioutas, D. L. Gillen and R. J. Delfino (2016). "Nrf2-related gene expression and exposure to traffic-related air pollution in elderly subjects with cardiovascular disease: An exploratory panel study." J Expo Sci Environ Epidemiol **26**(2): 141-149.
- Xiao, G. G., M. Wang, N. Li, J. A. Loo and A. E. Nel (2003). "Use of proteomics to demonstrate a hierarchical oxidative stress response to diesel exhaust particle chemicals in a macrophage cell line." J Biol Chem **278**(50): 50781-50790.

Yanamala, N., M. K. Hatfield, M. T. Farcas, D. Schwegler-Berry, J. A. Hummer, M. R. Shurin, M. E. Birch, D. W. Gutkin, E. Kisin, V. E. Kagan, A. D. Bugarski and A. A. Shvedova (2013). "Biodiesel versus diesel exposure: enhanced pulmonary inflammation, oxidative stress, and differential morphological changes in the mouse lung." Toxicol Appl Pharmacol **272**(2): 373-383.

Yitshak Sade, M., I. Kloog, I. F. Liberty, J. Schwartz and V. Novack (2016). "The Association Between Air Pollution Exposure and Glucose and Lipids Levels." J Clin Endocrinol Metab **101**(6): 2460-2467.

Zhang, X., R. Goncalves and D. M. Mosser (2008). "The isolation and characterization of murine macrophages." Curr Protoc Immunol **Chapter 14**: Unit 14.11.

CHAPTER 3 –
DELETION OF NRF2 IN MYELOID CELLS INDUCES ABNORMAL
CARDIOPULMONARY RESPONSES

Abstract

Exposure to air pollutants is known to result in oxidative stress. Many of the genes that become dysregulated in response to this stress include those coding for antioxidant factors regulated by the transcription factor NRF2. Myeloid cells are a key family of cells responsive to inhaled pollutants and include macrophages and granulocytes. Thus, we developed myeloid-specific Nrf2 (mNrf2) KO mice using Cre-Lox technology to test the response of these mice to acute exposures to diesel exhaust particles. The KO mice suffered worsened cardiopulmonary responses as compared to controls, including changes in antioxidant defense and ventricular relaxation. Additionally, single-cell RNA sequencing expression profiles demonstrated that KO and control cells respond differently to DEP, especially in terms of immune-related pathways.

Introduction

Air pollution is a dense source of compounds that can induce prooxidative effects. Numerous studies have implicated the role of oxidative stress on the health effects induced by air pollution exposure (Risom et al. 2005). In Chapter 2, we demonstrated that responses to external stimuli including stress were the top upregulated pathways in peritoneal macrophages treated with diesel exhaust particles extract (DEPe). The transcription of many of the top upregulated genes in these cells were regulated by the antioxidant transcription factor NRF2 (nuclear factor (erythroid-derived 2)-like 2). Furthermore, these peritoneal macrophages demonstrated a Mox-

like expression profile, with the Mox macrophage subtype having been identified for its overexpression of *Nrf2*-regulated genes (Kadl et al. 2010). Under stressed conditions, NRF2 is released from its repressor KEAP1 and becomes activated to promote the transcription of a variety of antioxidant genes and phase II detoxifying enzymes that contain the antioxidant response element (ARE) in their promoter regions in order to counteract the stress (Kensler et al. 2007). These enzymes include heme oxygenase 1 (HMOX1), glutathione S-transferases (GSTs) and UDP glucuronosyltransferases (UGTs), among many others (Kensler et al. 2007).

Studies on cells and animal models have demonstrated an increased *Nrf2*-regulated response to pollutants. For instance, RAW 264.7 macrophages and Sprague Dawley alveolar macrophages that were cultured with the organic extract of diesel exhaust particles, a model air pollutant, had increased expression of genes for several *Nrf2*-regulated antioxidants and Phase II enzymes, including Hmox1, GST-Ya and UGT-1a6 (Koike et al. 2002, Li et al. 2004). Another study suggests that the effects of air pollution exposure can be more far-reaching beyond the lungs. In ApoE KO mice exposed to ultrafine particles, their livers had significant upregulation of *Nrf2* and its downstream genes, including catalase, NAD(P)H quinone dehydrogenase 1 (Nqo1), and GST-Ya. (Araujo et al. 2008).

In this study, we developed myeloid-specific *Nrf2* (mNrf2) KO mice to test the importance of myeloid expression of *Nrf2* in the cardiopulmonary responses triggered by acute exposure to air pollutants, such as diesel exhaust particles (DEP).

Materials and Methods

Mice

C57BL/6J mice were acquired from either the UCLA Division of Laboratory Animal Medicine (DLAM) or The Jackson Laboratory (JAX). Myeloid-specific knockout mice were developed using Cre-Lox technology, by crossing floxed *Nrf2* mice (*Nrf2^{fl/fl}*) with *LysM-Cre* mice.

Nrf2^{fl/fl} mice were generously provided by Jingbo Pi, Ph.D., who developed the mice at The Hamner Institutes for Health Sciences, Research Triangle Park, NC (www.informatics.jax.org/allele/MGI:5566912) (Xue et al. 2013). In *Mus musculus*, the *Nrf2* gene has 5 exons and is found on chromosome 2 (NCBI Gene ID: 18024). The *Nrf2^{fl/fl}* mice have loxP sites inserted at locations flanked around exon 5, the largest exon of the *Nrf2* gene (**Figure 3-1**).

LysM-Cre mice were generously provided by Min Zhang, M.D., Ph.D., an investigator in our laboratory (Zhang et al. 2018). These mice express the enzyme Cre recombinase under the control of the lysozyme M promoter (Clausen et al. 1999). The lysozyme M gene (*Lyz2*; formerly known as M lysozyme, or *Lysm*) contains four exons and is located on chromosome 10 in *Mus musculus* (NCBI Gene ID: 17105). The Cre gene has specifically been inserted at the ATG translational start site and within exon 1 of the *Lyz2* gene, so that the expression of Cre is dependent on the *Lyz2* promoter element (Clausen et al. 1999). *Lyz2* is specifically expressed in myeloid cells, which includes macrophages, dendritic cells, granulocytes (neutrophils, eosinophils, and basophils), and mast cells (Cross et al. 1990, Murphy et al. 2008).

With Cre/Lox breeding, exon 5 is excised out when the Cre recombinase, under control of the myeloid-specific *Lyz2* promoter, acts on the flanking loxP sites; this excision of exon 5

renders the NRF2 protein non-functional (Xue et al. 2013), thus “knocking out” NRF2 in myeloid cells (**Figure 3-1**). These mice will be hereafter referred to as mNrf2 KO mice, or more concisely, KO mice. All mice were housed in the UCLA’s Division of Laboratory Animal Medicine in accordance with Institutional Animal Care and Use Committee (IACUC) guidelines.

Isolation of macrophages for characterization of KO mice

Both alveolar and peritoneal macrophages were harvested. Bronchoalveolar lavage fluid was collected by flushing the mouse lungs three times with 1 mL of PBS containing 5 mM EDTA. Peritoneal lavage fluid was collected by injecting 10 mL of ice-cold PBS into the peritoneal cavity of the mouse, agitating the cavity, and then retrieving as much fluid as possible. The cells from the bronchoalveolar lavage fluid and the peritoneal cavity were plated in DMEM at 37°C and washed with PBS to remove non-adherent cells, leaving alveolar macrophages and peritoneal macrophages, respectively. The macrophages were later harvested for RNA using either the RNeasy Mini Kit (cat. no. 74104, QIAGEN, Germantown, MD) or the Direct-zol RNA MiniPrep (cat. no. R2052, Zymo Research, Irvine, CA).

To detect NRF2 protein levels, peritoneal macrophages were additionally plated and treated with 100 µg/mL DEPe for 4 hours. (The cells were treated with DEPe because in our experience, untreated peritoneal macrophages from control mice had such low NRF2 protein levels to be undetectable by Western blot with our antibody.) Cells were then lysed for protein isolation for Western blot using Reducing SDS Loading Buffer (cat. no. 56036 and 14265, Cell Signaling Technology, Danvers, MA). Protein samples were run in a polyacrylamide gel (cat. no. 4561094, Bio-Rad Laboratories, Inc., Hercules, CA) for approximately 1.5 hours and transferred to a nitrocellulose membrane (cat. no. 926-31090, LI-COR, Lincoln, NE) for 1 hour. Primary

antibodies used were mouse monoclonal β -actin (8H10D10, Cell Signaling Technology, Danvers, MA) and rabbit polyclonal Nrf2 (ab137550, Abcam, Cambridge, MA). Secondary antibodies used were IRDye 800CW goat anti-mouse (925-32210, LI-COR, Lincoln, NE) and IRDye 680RD goat anti-rabbit (925-68071, LI-COR, Lincoln, NE). Blocking, and primary and secondary antibody incubations were done in 5% milk in TBST. The blot was visualized using the Odyssey® imager (LI-COR, Lincoln, NE) and Image Studio™ software (LI-COR, Lincoln, NE).

Diesel exhaust particles (DEP) and exposures via oropharyngeal aspiration

DEP was produced from an ultra-low sulfur highway-grade number 2 diesel fuel by an automobile single cylinder diesel engine from the Yanmar America Corporation (Yin et al. 2013). Particles were resuspended in phosphate-buffered saline (PBS) at a concentration of 10 mg DEP per 5 mL PBS. To break the DEP up into smaller, more soluble particles, the DEP/PBS solution was sonicated for several minutes on ice. Aliquots were made and stored at -80°C.

For the exposures, mice were instilled with either 200 μ g DEP in 100 μ L PBS or 100 μ L PBS only (vehicle control) via oropharyngeal aspiration. In this procedure, the mice were anesthetized with 5% isoflurane (with 1 L of oxygen flow) and then placed on a stand with its two incisors perched on a metal wire to keep the mouth propped open to allow access to the oral cavity. A pair of forceps was then used to pull the tongue out, and the nose was plugged while the 100 μ L of the treatment (PBS or DEP) was pipetted into the back of the throat, where the solution would reach the lungs upon gasping. Mice (males, 3-5.5 months of age) were divided into four exposure groups:

1. Wild-type Nrf2 mice (Control), treated with PBS,
2. Wild-type Nrf2 mice (Control), treated with DEP,
3. mNrf2 KO mice (KO), treated with PBS,
4. mNrf2 KO mice (KO), treated with DEP,

The number of mice per group varied depending on the measured endpoint; the *n* is indicated accordingly in the caption of each figure. The mice that were used as "Controls" included C57BL/6J and LysM-Cre mice. The LysM-Cre mice were included as Controls as recommended by the Jackson Laboratory since the presence of Cre recombinase may lead to a phenotype if the enzyme acts upon "loxP-like" sequences outside of the normal loxP sites (The Jackson Laboratory 2013). For 13 out of 14 of the post-exposure functional measurements analyzed, there were no significant differences between the C57BL/6J mice and LysM-Cre mice (**Table 3-1**).

Echocardiography

Cardiac function was measured using the Vevo 770 High-Resolution In Vivo Micro-Imaging System (FUJIFILM VisualSonics Inc., Toronto, Ontario, Canada). Mice were anesthetized with 4-5% isoflurane and placed on the imaging platform. The isoflurane level was then reduced to 1.5-2.5% during the echocardiography. The chest hair was removed, and ultrasound transmission gel was placed on the chest. ECG measurements were taken, and the transducer recorded B-mode and M-mode images of the heart, as well as Doppler images of the pulmonary artery. Recordings were analyzed using the Vevo LAB software (FUJIFILM VisualSonics Inc., Toronto, Ontario, Canada). Pulmonary acceleration time (PAT) and mean

pulmonary arterial pressure (MPAP) were calculated from Doppler images, using averaged values of ten pulses per sample.

Cardiac catheterization

After echocardiography, mice underwent cardiac catheterization, after which they were euthanized. For cardiac catheterization, mice were initially anesthetized with 4-5% isoflurane, and then placed on a warming pad, where the mice were ventilated and remained anesthetized with 2% isoflurane. A thoracotomy was performed to expose the heart, and the SPR-671 Mikro-Tip® mouse pressure catheter (Millar Inc., Houston, TX) was inserted in the right or left ventricles. Ventricular pressures from both sides of the heart were recorded and analyzed using the LabChart software (ADInstruments Inc., Colorado Springs, CO). Ten beats towards the end of right and left ventricular catheterization recordings were used to calculate average ventricular pressures and developed pressures (dP/dt) to ensure enough time for measurements to stabilize. Ventricular maximum developed pressure (dP/dt max) is an index of contractility, and is especially useful for detecting acute changes in systolic function (Hoit 1998). Ventricular minimum developed pressure (dP/dt min) serves as an index of relaxation (diastole) (Hoit 1998); it may also be referred to as the maximum rate of fall of left ventricular pressure (Gleason et al. 1962). Mathematically, dP/dt max is the largest slope (most positive) of the upstroke of left ventricular pressure, corresponding to the pressure buildup during contraction, while dP/dt min is the largest slope (most negative) of the downstroke of this curve, corresponding to the pressure release as the ventricle is filling up with blood. Following cardiac catheterization, mice were immediately euthanized with isoflurane overdose.

Collection and analysis of bronchoalveolar lavage fluid (BALF) cells

BALF was collected by flushing the mouse lungs three times with 1 mL of PBS containing 5 mM EDTA each flush. The fluid was pooled to give approximately 3 mL total lavage. The cells were counted using a hemacytometer to acquire cell concentrations. A 100 μ L aliquot of the cells was taken for cytocentrifugation at 600 rpm for 5 minutes to make cytospin slides. The slides were later analyzed for cell differentials following staining with the Fisher HealthCare PROTOCOL Hema 3 Manual Staining System and Stat Pack (cat. no. 22-122911, Fisher Scientific, Hampton, NH). Pictures of the stained slides were taken using the Axio Observer Z.1 Inverted Microscope and the accompanying AxioVision software (Carl Zeiss MicroImaging GmbH, Jena, Germany). Two hundred cells were counted on the cytospin slides to determine relative number of macrophages, lymphocytes, and granulocytes for cell differentials. The remaining BALF cells were plated in DMEM at 37°C for 1 hour, after which the cells were washed with PBS and kept frozen at -80°C for later RNA harvesting.

Plasma collection and assessment of paraoxonase 1 (PON1) activity

Blood from the mice was collected via cardiac puncture into tubes containing sodium heparin. The samples were kept on ice until centrifugation at 1600 g for 15 minutes. The top plasma layer was then kept frozen at -80°C for later measurement of paraoxonase 1 (PON1) activity. PON1 is an enzyme that has been negatively associated with cardiovascular disease. From each sample, 5 μ L of plasma was added with paraoxon in PON1 assay buffer in a 96-well plate. PON1 activity of each of the plasma samples was measured in duplicate. The kinetics of the degradation of paraoxon by the PON1 enzyme into diethyl phosphate and *p*-nitrophenol was measured immediately for four minutes using the Synergy plate reader (BioTek Instruments,

Inc., Winooski, VT). The measurements were based on the fact that the *p*-nitrophenol degradation product emits a yellow color, and thus the compound's absorbance can be measured at the 405 nm wavelength. The values were then converted into nmol of *p*-nitrophenol formed per minute per mL.

Tissue collections

To remove blood from the tissues prior to collection, systemic and pulmonary perfusions were performed by inserting an 18g needle into the heart, through which PBS was flowed via gravity from a hanging IV bag. Perfusion was determined to be completed once the lungs and the liver became pale. The lungs were first collected and weighed, with the right lobes separately frozen in liquid nitrogen while the left lobe was kept in 4% paraformaldehyde, then transferred to a sucrose/PB buffer solution the following day, and then finally transferred to an OCT block the day after for histology. Liver, spleen, heart, and kidneys were also weighed and frozen in liquid nitrogen. All tissue samples were then kept at -80°C until analysis.

Quantitative real-time PCR

RNA was isolated from cells and tissues using either the RNeasy Mini Kit (cat. no. 74104, QIAGEN, Germantown, MD) or the Direct-zol RNA MiniPrep kit (cat. no. R2052, Zymo Research, Irvine, CA), according to manufacturers' directions, and the RNA was quantified using the Synergy 2 Microplate Reader (BioTek, Instruments, Inc., Winooski, VT). A portion of the lungs, liver, spleen, and heart were taken for RNA isolation. RNA was then converted to cDNA using the High Capacity cDNA Reverse Transcription Kit (cat. no. 4368814, Applied Biosystems, Foster City, CA). Primers were purchased from Integrated DNA Technologies

(Skokie, IL) and corresponding probes were purchased from Roche Molecular Systems, Inc. (Pleasanton, CA) from their Universal ProbeLibrary System. The list of primers and probes used can be found in **Table 3-2**. Gene expression was measured by quantitative real-time PCR using the LightCycler 480 Instrument (Roche Molecular Systems, Inc., Pleasanton, CA), with the results normalized to *β-actin* expression levels.

Lung Cell Isolation for Single-Cell RNA Sequencing (scRNA-seq)

The right lobes (superior, middle, inferior, and post-caval lobes) of the mouse lung were taken for single cell dissociation. The lobes were kept in PBS on ice and then ground with the plunger end of a 10 mL syringe. The tissue was transferred into a tube and then centrifuged at 300 g for ten minutes at 4°C. The supernatant was removed and then the pellet was resuspended in the dissociation media (DMEM media, containing 10% FBS, 40 mg/mL of bovine serum albumin (BSA), and 1 mg/mL of collagenase I). Collagenase I (cat. no. LS004194, Worthington Biochemical Corporation, Lakewood, NJ) was chosen based on its recommendation by the vendor for digestion of lungs. The solution was incubated at 37°C for 1 hour. During the hour, the tissue was pipetted gently up and down every five minutes to allow for aeration and to minimize settling of the tissue. Afterwards, the dissociated cells were passed through a 70 μm cell strainer and centrifuged at 300 g for ten minutes at 4°C (Alphonse et al. 2015). The supernatant was removed, and the cell pellet was resuspended in PBS containing 2 mM EDTA. The cells were then passed through a 40 μm cell strainer and centrifuged at 300 g for ten minutes at 4°C. The supernatant was removed once more, and the cell pellet was resuspended in PBS containing 0.01% BSA. The cells were counted, and the concentration was adjusted to 1 x 10⁵ cells/mL.

The Drop-seq method used for scRNA-seq has been described previously (Macosko et al. 2015) and in an updated protocol provided by those authors (Protocol Version 3.1, <http://mccarrolllab.com/dropseq/>) Briefly, lung cell samples were run through a microfluidics device where single cells were combined with barcoded beads and lysis buffer into droplets; within those droplets, the cells underwent lysis and reverse transcription (Macosko et al. 2015). Library preparations were performed, and cDNA concentrations were measured using the Agilent TapeStation system as a quality control check.

Analysis of clusters and differentially expressed genes from scRNA-seq data

Clustering of the cells that were identified through scRNA-seq was done using the Seurat package in R (Butler et al. 2018). This package, aptly named for the Pointillism painter Georges Seurat, utilizes t-distributed stochastic neighbor embedding (t-SNE) to calculate distances between datapoints and map them into spatial patterns (van der Maaten et al. 2008, Macosko et al. 2015, Satija et al. 2015). The Immunological Genome Project resource (Heng et al. 2008) and the Mouse Cell Atlas (Han et al. 2018) were used for classifying cells into their likely cell types. In our clustering, endothelial cells have a few subtypes, identified by having high expression of kinase insert domain protein receptor (*Kdr*), transmembrane protein 100 (*Tmem100*), and Von Willebrand factor (*Vwf*) (Han et al. 2018). Differentially expressed genes (DEGs) were identified also using the Seurat package in R (Butler et al. 2018).

Statistical analyses

For comparisons between two groups, the statistical significance was calculated with a two-tailed Student's t-test. For comparisons between multiple groups, a two-way analysis of

variance (ANOVA) was performed to determine any significant interactions. Post-hoc tests for multiple comparisons were done using pairwise t-tests with a Benjamini-Hochberg correction. For all analyses, a p-value of <0.05 was considered significant, and specific levels of significance in the figures are indicated with asterisks: *p < 0.05, **p < 0.01, and ***p < 0.001. Statistical analysis for data obtained from single-cell RNA sequencing was done as indicated previously, using the Seurat package in R (Butler et al. 2018).

Results

Characterization of mNrf2 KO mice

Alveolar and peritoneal macrophages from the KO mice clearly show no or almost undetectable mRNA expression of *Nrf2*, indicative of successful deletion of the *Nrf2* gene (**Figure 3-2**). NRF2 protein levels also were undetectable from DEPE-treated KO peritoneal macrophages (**Figure 3-2**). As a transcription factor, NRF2 regulates the expression of multiple target genes, including antioxidant and detoxifying Phase II enzymes. Indeed, selected *Nrf2* target genes – *Gclm*, *Hmox1*, and *Srxn1* – also demonstrated significantly reduced expression in both alveolar and peritoneal macrophages, confirming the deletion of *Nrf2* (**Figure 3-2**).

The lungs, liver, spleen, and heart were also analyzed for gene expression to characterize the mRNA levels of *Nrf2* and its target genes in whole tissue. None of the genes tested in the lungs, liver, and spleen had a significant reduction in expression levels, although there were trends toward significance for reduced expression of *Nrf2* and *Hmox1* in lungs and spleen in KO mice (**Figure 3-3**). In the heart, while *Nrf2*, *Hmox1*, and *Srxn1* showed no differences between KO and control mice, surprisingly, *Gclm* had significantly increased expression in the KO mice (**Figure 3-3**).

Macroscopic observations of mice following DEP exposure

In testing the gene-environment interactions between DEP and the *Nrf2* gene, we divided the mice into four groups: (1) PBS-treated control mice, (2) DEP-treated control mice, (3) PBS-treated KO mice, and (4) DEP-treated KO mice. The oropharyngeal aspiration efficiently delivered the particles to the lungs. Within hours after treatment, the lungs of the mice exposed to DEP were speckled with the black particles (**Figure 3-4**).

After administration of the DEP, we noted some physical appearances of poor health with a subset of the experimental mice. Specifically, some DEP-treated KO mice were noted to be breathing quicker, having ruffled fur, being hunched, and showing little activity (**Figure 3-5**). We therefore pursued additional physiologic and molecular studies to elucidate the cause for those health effects.

Pulmonary responses to DEP

The appearance of particles was present in multiple macrophages in both DEP-treated groups (**Figure 3-6**). There was also a significant influx of granulocytes in the BALF due to DEP exposure in both the control and KO mice (**Figure 3-7**), with no significant difference in BALF cell concentrations and in lymphocyte and macrophage numbers. While the *mNrf2* KO mice visibly appeared to have different respiratory patterns compared to the other groups as described earlier, we did not detect any cellular differences in the BALF between genotypes as the distribution of cell types only differed between DEP vs. PBS, with $p < 0.05$ with the effect of treatment only according to two-way ANOVA analysis (**Figure 3-7**). Histological analysis of lung sections also appeared to show similar results, with potentially more nuclei in DEP-treated

groups compared to the PBS-treated groups, and with no obvious differences between genotypes noted (**Figure 3-8**).

At the molecular level, consistent with baseline levels (**Figure 3-2**), analysis of the lung alveolar macrophages continued to show reductions in macrophage antioxidant capacities in the KO mice compared with control, with decreased expression of *Nrf2*, *Hmox1*, and *Srxn1* (**Figure 3-9a**). The control mice, on the other hand, had increased expression of *Hmox1* and *Srxn1* in response to DEP (**Figure 3-9a**). The inflammatory genes *Il6* and *Mip2* appeared to be increased in the KO mice compared to both PBS- and DEP-treated control groups, although these values did not reach statistical significance (**Figure 3-9b**). Cytokine levels of TNF- α in the BALF were also measured but did not show differences (**Figure 3-9c**).

Cardiovascular responses to DEP

We performed echocardiographies and cardiac catheterizations on mice post-exposure to determine whether DEP-induced effects on the cardiovascular system could explain the phenotype observed in the KO mice. DEP did elicit a reduction in the heart rate in both control and KO mice, as measured by echocardiography (**Figure 3-10**). Additionally, the PBS-treated KO mice also had a higher heart rate compared with the PBS-treated control. DEP treatment also affected cardiac output, although these changes only differed between DEP vs. PBS, with $p < 0.05$ with the effect of treatment only according to two-way ANOVA analysis (**Figure 3-10**). However, despite the differences in the heart rates and cardiac output, this did not lead to changes in the ejection fraction, fractional shortening, and stroke volume (**Figure 3-10**).

For cardiac catheterization, mice were intubated and mechanically ventilated under general anesthesia. There were no differences in heart rates of the mice (**Figure 3-11**), nor in

right and left ventricular pressures (**Figure 3-12**), as measured by cardiac catheterization. However, the curves of the left ventricular pressure did show some distinct reflected peaks in the KO mice, with the appearance more prominent in the DEP-treated KO mice (**Figure 3-13**). Specifically, the abnormality occurred in diastole, likely related to left ventricular relaxation (Pasipoularides 2018). Further analysis of the rate of pressure development (dP/dt) confirmed this finding. While the left ventricular maximum developed pressure (dP/dt max) did not differ across all groups (**Figure 3-14**), DEP-treated mNrf2 KO mice did have a lower left ventricular minimum developed pressure (dP/dt min), indicating impaired relaxation (diastolic dysfunction) (**Figure 3-14**). On the right ventricular side, there were no differences in dP/dt max and dP/dt min, suggesting no difference in contractility nor relaxation in this ventricle, respectively (**Figure 3-14**).

Inhaled particulates such as cigarette smoke and DEP have been thought to potentially lead to pulmonary hypertension (Grunig et al. 2014, Liu et al. 2018), thus we also analyzed effects on pulmonary pressure. Mean pulmonary arterial pressure (MPAP) did not demonstrate differences between the groups (**Figure 3-15**).

In addition to the physiologic measurements, we also assayed the activity of paraoxonase 1 (PON1) in the plasma, in order to gauge the level of protection against systemic oxidative stress. Knocking out *Nrf2* expression in myeloid cells of our KO mice manifested in reductions in plasma PON1 activity, demonstrating not only a reduction in antioxidant capacity at the myeloid level, but also at the systemic level (**Figure 3-16**).

The differences in PON1 and dP/dt min may help explain the symptoms the DEP-treated KO mice showed, but these findings still cannot fully explain the mechanisms behind the health

effects observed in the sick mice. With such a hyperacute exposure period, the DEP is unlikely to itself directly affect the cardiovascular system.

scRNA-seq analysis of lung cells

To better characterize the responses in the lungs and dissect cellular responses and pathways responsible for the DEP-induced health effects in KO mice, right lung lobes of two mice from each group were taken for scRNA-seq to identify gene expression patterns of specific cell types in each genotype and treatment group. Altogether, there were 19,279 lung cells that were captured in the Drop-seq protocol, and these were classified into 20 types of cells (**Table 3-3**). Several cells (alveolar macrophages, endothelial cells, monocytes, and stromal cells) were separated as subtypes 1, 2, or 3 because while these cells formed distinct clusters, they remain identified as being the same general type of cell (**Figure 3-17a**). All cell types were represented in all four experimental groups (**Table 3-3; Figure 3-17b**), with some cells more highly represented in a particular experimental group, such as endothelial cells (Tmem100 marker) in DEP-treated control mice, and neutrophils in DEP-treated KO mice (**Figure 3-17c-f**). For each of the four groups, the cells most represented in the Drop-seq analyses were endothelial cells (combining subtypes 1, 2, 3, Kdr, Tmem100, and Vwf), neutrophils, and alveolar macrophages (combining subtypes 1 and 2) (**Figure 3-18**). The expression of *Nrf2* across multiple lung cell types was also analyzed and confirmed the deletion of this gene in alveolar macrophages in the KO mouse groups (**Figure 3-19**). The *Nrf2* levels of several other cell types such as endothelial and T cells also showed that control cells had low expression similar to KO cells (**Figure 3-19**). The DEP-treated KO neutrophils also demonstrated deletion of *Nrf2* as expected, but surprisingly, expression was present in the PBS-treated neutrophils, although lower than in the

PBS- and DEP-treated control cells (**Figure 3-19**). The presence of *Nrf2* expression here could be due to the clustering method pulling some non-myeloid cells into these myeloid populations. Also, it was not apparent to us what portion of the *Nrf2* sequence was used for detection and quantification of the *Nrf2* gene; our mNrf2 KO mice have exon 5 of the *Nrf2* gene knocked out, so the other exons remained present (**Figure 3-1**) and could have been detected as false positives.

scRNA-seq analysis demonstrated that DEP treatment affected the gene expression of many cell types. It was mentioned earlier that alveolar macrophages, endothelial cells, and neutrophils were the most abundant cell types in our samples (**Figure 3-18**). These three cell types (involving specifically the alveolar macrophages 1 and endothelial cells [Tmem100 marker] subtypes) also accounted for the top dysregulated cell types across various comparisons, including DEP- vs. PBS-treated control (**Table 3-4**), DEP- vs. PBS-treated KO (**Table 3-5**), and DEP-treated KO vs. DEP-treated control (**Table 3-7**). One exception was for PBS-treated KO vs. PBS-treated control, in which endothelial cells (Tmem100 marker) was bumped to the fourth most dysregulated cell type after monocytes 2 (**Table 3-6**).

In control mice, immune-related processes were prominently affected with DEP exposure in alveolar macrophages and neutrophils, such as pathways related to the immune system, toll-like receptors, antimicrobial proteins, and neutrophil degranulation (**Table 3-4**). In KO mice, DEP exposure did not appear to affect as many pathways, although antimicrobial processes were still dysregulated (**Table 3-5**). When comparing PBS-treated KO vs. PBS-treated control mice (**Table 3-6**) and DEP-treated KO vs. DEP-treated control mice (**Table 3-7**), immune-related pathways were frequently listed for several cell types, demonstrating that at the genotypic level, there were fundamental differences in the level of immune activation.

From these tables, it can be noted that there were many differentially expressed genes (DEGs) that could be categorized as either unique to one cell, or common across many cells. For the unique DEGs, once again, alveolar macrophages, neutrophils, and endothelial cells (Tmem100 marker) consistently made up the top three cells in this regard (**Figure 3-20**). However, it is also apparent that a distinct expression pattern from endothelial cells may have been primarily regulating the response of KO mice to DEP treatment, as endothelial cells clearly had the highest number of unique DEGs in the DEP- vs. PBS-treated KO comparison and the DEP-treated KO vs. DEP-treated control (**Figure 3-20**).

Multiple genes were also dysregulated across multiple cell types, mostly in the same direction across those cells (**Figure 3-21**). These common DEGs represent genes with especially robust responses, not necessarily just in myeloid cells, and therefore could be strong candidates for a mechanistic role in linking the poor respiratory patterns in our DEP-treated KO mice with the abnormal cardiovascular responses described earlier. Among these genes, there were a few genes that were especially common between the four comparisons we looked at: *S100a8* (S100 calcium binding protein A8 [calgranulin A]), *S100a9* (calgranulin B), and *mt-Rnr2* (16S rRNA, mitochondrial). These three genes even showed the opposite expression patterns in control vs. KO mice when comparing DEP vs. PBS treatment (**Figure 3-21a-b**).

Among PBS-treated groups, the lung cells in the control mice compared with the KO mice already clearly exhibited different genetic signatures, even in the non-myeloid cells. For instance, while macrophages, monocytes, and neutrophils had many dysregulated genes, the endothelial cells (Tmem100 marker) were also a very prominently affected cell type, especially in comparisons involving the DEP-treated KO group (**Figure 3-20**). And, as expected, comparing the DEP-treated KO with the DEP-treated control mice also confirmed the presence

of multiple differentially expressed genes and cell types, with a few identified as behaving in the opposite directions in control vs. KO mice (**Figure 3-21a-b**).

Because immune-related processes were a major dysregulated pathway, we were also interested in determining whether any macrophage subtype was prominent under these in vivo conditions like the macrophage marker patterns we saw under our in vitro conditions in Chapter 2. Two genes that were significantly upregulated in alveolar macrophages 1 in DEP-treated KO mice compared with each of the other groups were two pro-inflammatory genes, *Ly6c1* (lymphocyte antigen 6 complex, locus C1) and *S100a6* (S100 calcium binding protein A6 [calcylin]) (**Figure 3-22a-b**). In addition, looking at M1, M2, and Mox marker genes in our alveolar macrophages provided some evidence that these cells may have been more activated in the KO mice. An M1 marker, *Cxcl10* (chemokine (C-X-C motif) ligand 10) was significantly higher in the KO groups compared to each of the control groups, although the expression of this inflammatory gene was not different between the PBS- and DEP-treated KO mice (**Figure 3-22c**). An M2 marker, *Fcgr2b* (Fc receptor, IgG, low affinity Iib), also behaved similarly, in addition to its expression being higher in the DEP-treated KO compared with the PBS-treated KO (**Figure 3-22d**). And, like we saw in Chapter 2, the expression of a Mox marker, *Txnrd1*, was higher in the DEP-treated control vs. the PBS-treated control, and both control groups were significantly upregulated in comparison with both KO groups (**Figure 3-22e**). Although these selected macrophage markers (*Cxcl10*, *Fcgr2b*, and *Txnrd1*) demonstrated significant expression patterns among the groups, overall only 5.1% of M1, 4.5% of M2, and 11.1% of Mox marker genes were differentially expressed in any paired comparison.

Discussion

In this chapter, we successfully developed myeloid-specific Nrf2 KO mice and demonstrated that they exhibit abnormal responses to DEP compared to its genotype and treatment controls. These responses included a sickly appearance, diastolic dysfunction, and reduced antioxidant activity both in macrophages and in serum. Also, scRNA-seq data showed differences in responses at the cellular and genetic levels, indicating a more robust immune response in DEP-treated KO mice.

The successful development of myeloid-specific Nrf2 KO mice was demonstrated by deletion of the *Nrf2* gene in alveolar and peritoneal macrophages (**Figure 3-2**). As described in Chapter 2, NRF2 is an important transcription factor that regulates the expression of multiple antioxidant and Phase II detoxifying genes. And indeed, the *Nrf2*-regulated genes *Gclm*, *Hmox1*, and *Srxn1* showed significantly reduced expression in the macrophages from our KO mice (**Figure 3-2**). In whole tissue homogenates of the lung, liver, spleen, and heart, mRNA expression of *Nrf2* and its regulated genes generally did not show significantly different expression in KO vs. control mice, likely due to continued expression of these genes in other, non-myeloid cell types in the KO mice (**Figure 3-3**). For instance, a majority of the cells in the liver is made of hepatocytes, estimated to be approximately 60-80%, while the rest are mostly endothelial cells, followed by lymphocytes, Kupffer cells (macrophages), biliary cells, and stellate cells (Mannaa et al. 2016). Although we didn't assess *Nrf2* expression in Kupffer cells, it is likely *Nrf2* was deleted here, but they only represent less than half of all total cells in the liver (Mannaa et al. 2016). The lungs and the spleen did have somewhat reduced levels of *Nrf2* and *Hmox1* in KO mice (**Figure 3-3**), likely because both tissues have a sizeable subpopulation of

myeloid cells, as illustrated by our lung scRNA-seq data (**Figure 3-18**) and as has been noted for the spleen (Cesta 2006).

The only significant exception was increased *Gclm* in the KO heart (**Figure 3-3**). One possible reason is that non-myeloid cell types may be compensating for the lack of *Nrf2* in the myeloid cells in the heart. The percentage of cardiomyocytes in the heart reported in the literature have ranged from 25% to 56%, with the other cell types (non-myocytes) primarily being endothelial cells and fibroblasts (Banerjee et al. 2007, Pinto et al. 2016, Zhou et al. 2016). It is estimated then that just a small proportion of cardiac cells are hematopoietic-derived (Pinto et al. 2016). Another possible reason is that other members of the *Nrf2* family may be compensating. For instance, another Cap'n'Collar (CNC) transcription factor, *Nrf1* (Nfe2l1, nuclear factor, erythroid derived 2,-like 1), may be present at especially high levels in the heart (Biswas et al. 2010), and *Nrf1* can regulate *Gclm* expression (Leung et al. 2003). Additionally, the levels of *Gclm* may be especially important to maintain in this particular organ since it has been shown that the *Gclm* KO mice have heightened risks of cardiac injury and death following ischemia-reperfusion (Kobayashi et al. 2010).

As we showed in Chapter 2, DEPe treatment led peritoneal macrophages to overexpress *Nrf2*-regulated genes. Thus, we were interested in determining the in vivo responses of mice lacking *Nrf2* in macrophages and other myeloid cells. Signs of sickness were visibly apparent after DEP treatment particularly in the KO mice, such as an unkempt and hunched appearance and quiet attitude (**Figure 3-5**). Healthy mice normally are well-groomed and are curious and active when their cages are opened (Foltz et al. 1999). Our DEP-treated KO mice also had quick and shallow breathing, also known as tachypnea, which may occur due to direct abnormalities of the cardiovascular and/or respiratory system (Long 2012). Similar physical symptoms

("exhausted appearance characterized by shallow rapid breathing, ruffled fur, and hunched postures") were also noted previously by Chan and Kan (1999) in their systemic Nrf2 KO and control mice that were fed butylated hydroxytoluene (BHT), a respiratory phenolic toxin; in fact, their systemic Nrf2 KO group developed worsening disease over time, with 80% dying nearly two weeks later (Chan et al. 1999). In our study, we looked both at pulmonary and cardiovascular measurements to further dissect health effects induced by DEP in our KO mice.

Respiratory distress can be due to pulmonary inflammation (Bhatia et al. 2004). Therefore, we analyzed the inflammatory status of our mouse lungs at the cellular and genetic levels. Both our DEP-treated KO and control groups had increased granulocytic infiltration, including neutrophils, in the lungs. This is consistent with other studies. For our study, we used a dose of 200 μg DEP in 100 μL PBS. In our lab, we have seen that a 200 $\mu\text{g}/\text{mL}$ dose of the standard reference diesel particulate SRM 2975 (National Institute of Standards and Technology) can elicit pulmonary inflammation, with increased total cells and increased neutrophils after 48 hours (not published). A similar concentrated ambient particles (CAPs) inhaled dose of $176.7 \pm 95.9 \mu\text{g}$ (calculated from concentrations of $105.1 \pm 583 \mu\text{g}/\text{m}^3$ in the exposure chamber) in humans led to some acute cardiopulmonary changes within a day after exposure, including significant increases in neutrophil infiltration in the lungs and reductions in heart rate variability per $10 \mu\text{g}/\text{m}^3$ CAPs increase (Graff et al. 2009). However, we didn't see differences in granulocyte numbers between DEP-treated KO vs. DEP-treated control (**Figure 3-7**). Our scRNA-seq data appeared to show that neutrophils made up the highest proportion of cells in the lungs from the DEP-treated KO group (14%) compared with all others (2-7%), although this data only had an $n=2$ (**Figure 3-18**), and thus no statistical tests could be conducted here.

Tachypnea can also occur in patients with pulmonary hypertension (Widlitz et al. 2003), and inhaled particulates have been shown to induce pulmonary hypertension (Grunig et al. 2014). However, we did not observe differences in pulmonary arterial pressure (**Figure 3-15**). Thus, pulmonary hypertension is unlikely to describe our DEP-treated KO mice.

Tachypnea could be due to ventricular dysfunction and congestive heart failure (Bryant et al. 1998), thus we performed echocardiographies and cardiac catheterizations to evaluate right and left ventricular function. Some measures of cardiac function (ejection fraction, fractional shortening, stroke volume, and cardiac output) were not significantly different across the four groups. This is not unusual as heart disease patients may still show values in the normal ranges for these parameters even while sick. For instance, those with heart failure can still have normal ejection fraction (Zile et al. 2001, Petrie et al. 2002), fractional shortening (Petrie et al. 2002), and cardiac output (Reddy et al. 2016). Some ischemic cardiomyopathy patients may also have normal stroke volume (Adhyapak et al. 2014). For a future direction, it may be useful to conduct scRNA-seq on whole hearts, similarly to what we did for the lungs, in order to potentially measure the expression of genetic markers of hypertrophic cardiomyopathy and other abnormal cardiac conditions.

One cardiovascular measurement that did show some differences between the groups was heart rate. In both the KO and control groups, DEP treatment led to a significant reduction in the heart rate as measured by echocardiography (**Figure 3-10**). Studies measuring heart rate following air pollution exposure have been mixed. For example, while some previous studies on adult humans have shown that higher air pollution exposure led to increased heart rates (Peters et al. 1999, Pope et al. 1999, Chuang et al. 2005), studies on other populations and models, such as our data here, have shown the opposite behavior. For instance, premature and low-birth weight

newborns with higher air pollution exposure had more bradycardia (slow heart rate) events (Peel et al. 2011). And, ApoE^{-/-} mice exposed to concentrated ambient particles (CAPs) for 5 months also had lowered heart rate (Chen et al. 2005). However, what has been consistently demonstrated in many studies is that air pollution does decrease heart rate variability (Pope et al. 1999, Devlin et al. 2003, Park et al. 2005), which we didn't assess in the current study but would be a worthwhile endpoint to study in our mice in the future. Our data also indicated that perhaps DEP elicited a stronger response in the KO as compared with the control because with PBS treatment, the heart rate was higher in the KO as compared with the control group, although after DEP exposure, this difference between the genotypes was no longer apparent (**Figure 3-10**). Additionally, it is also worth noting that under echocardiography, but not cardiac catheterization, the heart rates differed between the groups. This is likely because of the different conditions of the mouse during each procedure since closed-chest (echocardiography) vs. open-chest (catheterization) procedures have been shown to result in different cardiac measurements (Hoit et al. 1997).

That said, the most noteworthy cardiovascular observation was that several of the PBS- and DEP-treated mNrf2 KO mice had reflected peaks in the left ventricular pressure curves, resulting in a second positive peak in the pressure derivative (dP/dt) curves (**Figure 3-13**), which are characteristic of hypertrophic cardiomyopathy patients (Pasipoularides 2018). Additionally, the dP/dt min values in our DEP-treated KO mice were significantly less in magnitude than the other groups (**Figure 3-14**), further indicating impaired relaxation. In a previous study looking at systemic Nrf2 KO mice, Erkens et al. (2015) showed that lack of *Nrf2* in the whole body resulted in these animals having hypertrophy and diastolic dysfunction in the left ventricle. Strom et al. (2017) also showed that systemic Nrf2 KO mice have hypertrophy that led to heart failure

(Strom et al. 2017). Although our KO mice had *Nrf2* specifically knocked out in just myeloid cells, it is remarkable that our animals similarly demonstrated symptoms of the cardiac abnormalities seen in systemic *Nrf2* KO mice, underscoring the importance of myeloid cells in cardiovascular health. Even knowing this, though, there still remains a question as to what the mechanistic link is between exposures and the obvious sickness seen in our mice.

As mentioned earlier, the distribution of cell types did not differ between the DEP-treated KO vs. the DEP-treated control mice based on our cell differential counts and observations of the lung histology. Even so, the gene expression profiles for many of the cell types did, based on our scRNA-seq data. Across all four group comparisons that were conducted, neutrophils was among the top three cell types in terms of the number of differentially expressed genes (**Figure 3-20**). At the DEP level, the KO and control neutrophils had differential expression of genes related to the immune system, neutrophil degranulation, and keratinization (**Table 3-7**), indicating that the neutrophils in the DEP-treated KO mice may be more active than those in the DEP-treated control group. Indeed, increases in both neutrophilic influx and granule release occur in acute lung injury (Strieter et al. 1994, Grommes et al. 2011).

As expected, alveolar macrophages 1 was also one of the cell types with the most DEGs across all comparisons (**Figure 3-20**). Two out of three genes involved in the detoxification of reactive oxygen species predictably had reduced expression in the KO (**Table 3-7**), confirming a reduced antioxidant capacity in these mice. Like neutrophils, genes of the immune system and neutrophil degranulation pathways also showed different expression patterns in KO vs. control alveolar macrophages 1 (**Table 3-7**). Another pathway on the list, regulation of TLR (toll-like receptors), has also been implicated in lung injury since therapeutic inhibition of TLR7 has been shown to reduce lung injury (Pawar et al. 2007). And cardiovascular processes (hemostasis and

cell surface interactions at the vascular wall) were affected in DEP-treated KO vs. control (**Table 3-7**), which could be a potential link explaining the cardiovascular dysfunctions described earlier, although this would require further confirmation.

Another major cell type that showed different responses to DEP in KO vs. control mice is the endothelial (Tmem100 marker) cell. In fact, this cell type had the greatest number of DEGs in this comparison (**Table 3-7**). Here, the immune system and neutrophil degranulation also were prominent pathways that were differentially regulated in KO vs. control endothelial (Tmem100) cells following DEP treatment. Genes involved in cell signaling and cell death were also differentially expressed, although it is unclear whether one of these pathways was more active in the KO or in the control as several genes were both upregulated and downregulated in KO vs. control (**Table 3-7**). Like neutrophils, though, pro-inflammatory endothelial cells have been shown to be present in lung injury (Asimakopoulos et al. 1999).

In addition to those major cell types, it is worth discussing select genes that were expressed in the opposite directions with DEP in KO mice vs. control mice. Genes that were upregulated in KO but downregulated in control mice in response to DEP may help explain why the DEP-treated KO mice appeared much sicker. Two genes in particular very clearly followed this trend in more than one cell type – *S100a8* (S100 calcium binding protein A8 [calgranulin A]) and *S100a9* (calgranulin B). These two proteins may be present as homodimers but may also be found together as a heterodimer called calprotectin, which is secreted by neutrophils and has been shown to be involved in pro-inflammatory processes (Gebhardt et al. 2006, Jonasson et al. 2017). Both of these genes have also been shown to be upregulated in mice with acute lung injury (Harada et al. 2011), and circulating levels of S100A8 are also elevated in certain heart failure patients (Raphael et al. 2016).

On the other hand, some genes that were downregulated in KO but upregulated in control mice following DEP treatment, have protective functions. The gene that was differentially expressed across most cell types in both control mice and KO mice following DEP treatment was a mitochondrial gene, *mt-Rnr2* (16S rRNA, mitochondrial) (**Figure 3-21**). In control mice, *mt-Rnr2* was upregulated with DEP treatment but was downregulated in DEP-treated KO mice. This gene encodes for humanin, a circulating anti-apoptotic peptide that has been shown to be protective against stress-induced cardiac dysfunction (Bodzioch et al. 2009). However, although we did not evaluate apoptosis in the current study, it has been shown that *Nrf2* deletion can promote cell death; for instance, the hepatocytes of *Nrf2* KO mice had greater risk for undergoing apoptosis upon injury to the liver compared to controls (Beyer et al. 2008).

Inflammation is often an inevitable consequence of oxidative stress. For instance, in response to a prooxidative environment, many transcription factors can promote the expression of inflammatory molecules (Wilson et al. 2001). Indeed, mice that lack *Nrf2* are more susceptible to toxins, such as being more likely to develop pulmonary DNA adducts (increasing their risk for developing cancer) (Aoki et al. 2001) and an asthma-like condition (Li et al. 2008), both after DEP inhalation. Similarly, cigarette smoke-exposed *Nrf2* KO mice have an increased risk of developing emphysema (Rangasamy et al. 2004, Sussan et al. 2009). *Nrf2* KO mice are also more susceptible to lung damage due to hyperoxia (Cho et al. 2002). Even cell-specific *Nrf2* KO mice can have distinct phenotypes from control mice. For instance, animals lacking the gene in lung Clara cells still have a greater degree of hyperoxic-lung injury than their genotypic controls (Reddy et al. 2011).

Our m*Nrf2* KO demonstrate reduced antioxidant capacity both at the cellular and systemic levels. We demonstrated in Chapter 2 that several *Nrf2*-regulated genes were

upregulated with DEP exposure. With our KO, the expressions of selected *Nrf2*-regulated genes were predictably decreased, including *Hmox1* and *Srxn1* (**Figure 3-9**). Additionally, the KO mice also had lowered serum PON1 activity. PON1 is an important antioxidant enzyme present in the plasma. In association with high-density lipoprotein (HDL), PON1 reduces oxidized phospholipids on low-density lipoproteins (LDL) (Watson et al. 1995). Thus, low levels of PON1 activity have been demonstrated to be associated with increased risk for cardiovascular disease (Mackness et al. 2004). Because of the enzyme's role as an antioxidant and because of the association between air pollution and cardiovascular disease, PON1 has also been suggested as a potential biomarker of air pollution exposures (Delfino et al. 2011). However, it is not known whether decreased PON1 activity could modulate cardiopulmonary responses in an acute manner.

In Chapter 2, we evaluated the prevalence of macrophage subtypes in DEP-treated peritoneal macrophages from various HMDP mice, and we showed in that study that it was likely these cells were polarized to the Mox subtype. Thus, in this study we were also interested in looking at macrophage marker patterns in the scRNA-seq data from the alveolar macrophage 1 cluster. There was some evidence that these cells may have been more activated in the KO. The M1 marker, *Cxcl10*, was significantly upregulated in the KO mice compared to either control group (**Figure 3-22c**); it has been shown previously that chronic PM_{2.5} exposure in mice can lead to increased levels of this pro-inflammatory cytokine, helping to promote a Th1 immune response in the lungs (Deiuliis et al. 2012). On the other hand, an M2 marker, *Fcgr2b*, also showed a similar pattern (**Figure 3-22d**); this gene is also involved in immunity as it interacts with IgG (Wu et al. 2014) and is upregulated in mouse asthma models (Di Valentin et al. 2009). A Mox macrophage marker and *Nrf2*-regulated gene, *Txnrd1*, showed the opposite response

from *Cxcl10* and *Fcgr2b* as expected, being upregulated in DEP-treated control mice vs. PBS-treated control mice, but being downregulated in KO mice compared to control mice (**Figure 3-22e**). Despite the significant expression patterns of these selected macrophage marker genes, as well as the pro-inflammatory genes *Ly6c1* and *S100a6* (**Figure 3-22a-b**), there was not a prominent macrophage subtype characterizing the alveolar macrophage 1 cluster, with just 4.5-11.1% of the M1, M2, and Mox macrophage markers being differentially expressed. However, this is likely due to the heterogeneity of our alveolar macrophage population. For instance, while clearly some cells came into contact with particles and phagocytosed them, others did not (**Figure 3-6**). Additionally, there may well be a mix of macrophage subtypes in the KO mouse lungs, with some cells potentially being pro-inflammatory while others could be anti-inflammatory to counteract the former cells' responses in this hyperacute exposure condition. Therefore, future analysis will involve determining whether the alveolar macrophage 1 cluster could be further subclustered into M1, M2, and Mox subtypes.

In this chapter, we have demonstrated an interplay between myeloid-specific *Nrf2* expression, inflammatory status, cellular activation, and cardiopulmonary disease. In the literature, *Nrf2* has been noted as having both health-promoting and disease-promoting properties, under specific conditions. In the human population, there are multiple polymorphisms of *NRF2* (Yamamoto et al. 2004). Individuals with a less functional form of the protein have a greater likelihood for developing trauma-induced acute lung injury (Marzec et al. 2007). On the other hand, this same polymorphism in cancer patients makes their tumors more responsive to treatment (Ishikawa 2014). In our mNrf2 KO mice, we demonstrate that the KO mice fare worse than their controls in response to DEP, indicating that myeloid expression of *Nrf2* is important in this situation.

DEP-treated KO lungs thus may be more susceptible to air pollution due to a combination of increased pro-inflammatory and reduced protective responses beginning in the lungs and affecting cardiac function via secreted factors, such as calprotectin. Despite the lack of difference in the number of inflammatory cells in DEP-treated KO vs. DEP-treated control groups, the genetic profiles of these and other cells in the lung microenvironment were different. Thus, lack of the *Nrf2* antioxidant transcription factor in myeloid cells affected many cell types beyond myeloid cells and many processes beyond those related to oxidative stress. It appears to be a multitude of genes and processes that act in concert to promote the apparent sickness in the DEP-treated KO mice. In order to better elucidate a specific mechanism, though, it will be necessary to pursue further characterization of the presence of circulating factors, such as S100A8/9, humanin, and other cytokines that were indicated as dysregulated by our scRNA-seq data. In our study, we only looked at plasma levels of the antioxidant enzyme PON1 and the cytokine TNF- α . It will also be necessary to quantify the respiratory functions of these mice. It would be informative to measure oxygen levels and perform whole body plethysmography to assess respiratory status in order to better compare the mouse groups and determine whether hypoxia could be a cause for the tachypnea observed in our mice.

Some limitations in our study must also be discussed. It has been estimated that the lungs are comprised of about 40 types of cells, including macrophages, Clara cells, and epithelial cells, among others (*Franks et al. 2008*). Although 20 cell types were identified with scRNA-seq, it is important to note that some prominent lung cell types were unfortunately not detected in our analyses, including pneumocytes and Clara cells. It is possible that our dissociation method using Collagenase I was perhaps too harsh on the undetected cells, or perhaps the method was more favorable at dissociating the cells we did detect. Nevertheless, at least the major immune cells

that have historically been shown to be responsive to DEP exposures in other studies were still able to be thoroughly analyzed in our dataset. Additionally, as can be seen in **Figure 3-4**, the DEP particles did not disperse evenly over the whole lungs. Therefore, it was beneficial for us to digest whole lung lobes for scRNA-seq to best analyze gene expression profiles in this tissue.

With the scRNA-seq of whole lung tissues, we did not see the type of antioxidant responses that were prominently observed in the microarrays of DEP-treated peritoneal macrophages in culture in Chapter 2. This may be likely due to a few differences between in vivo and in vitro conditions. For one, we can say with high likelihood that not all cells, including alveolar macrophages, in the lungs are going to be exposed to the instilled DEP, as opposed to in cell culture conditions. Additionally, the type of toxin for the in vivo exposures here are the particles themselves, as opposed to the organic extract form used in the in vitro experiments, and accordingly, the doses are different as well. And lastly, the duration of exposure for the in vivo experiments may not have been long enough to elicit macrophage polarization as we had seen with the cultured macrophages in Chapter 2. In this current chapter, we were most interested in capturing the cells at a timepoint that had manifested in visible responses to DEP, including difficulty breathing and a quiet attitude. In a previous study using systemic Nrf2 KO mice treated with BHT, these animals' health worsened over time, leading to death in 80% of the mice by day 12; it therefore would be of interest from a physiological standpoint to also monitor the health of our mNrf2 KO mice over a longer period than the several hours used in this study.

Figures

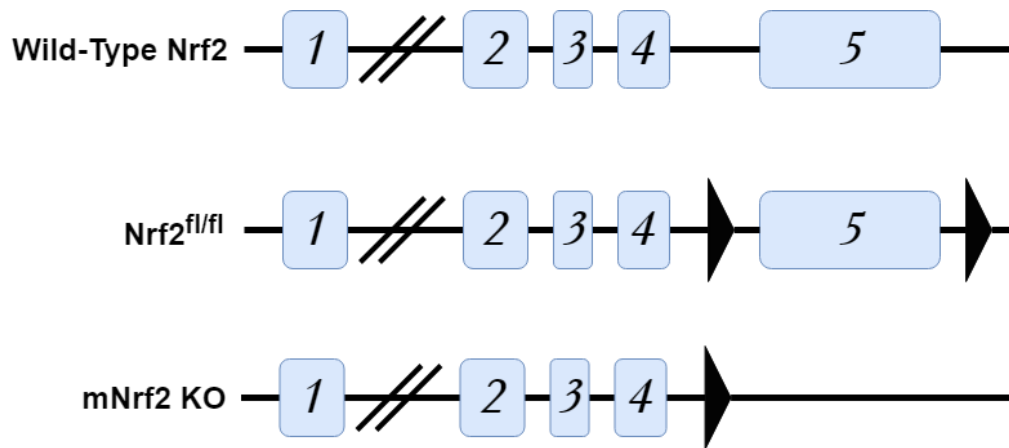
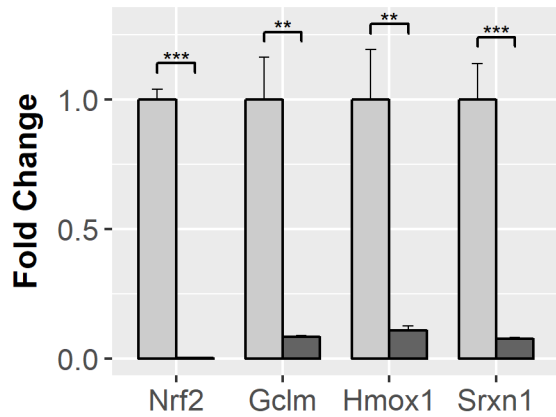
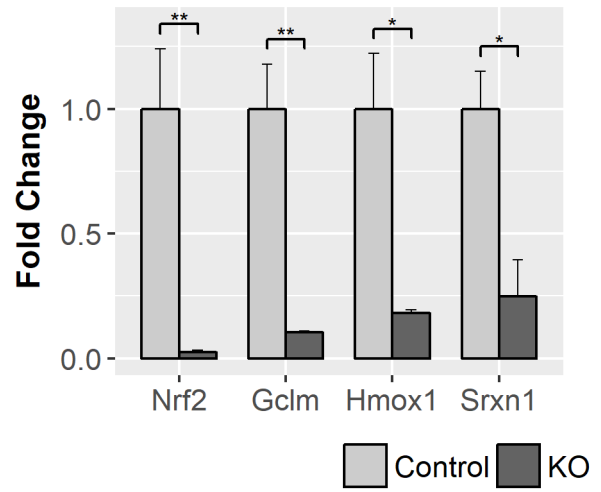


Figure 3-1: Nrf2 and its constructs. (a) The wild-type *Nrf2* gene has 5 exons. Exon 1 has 278 base pairs (bp), exon 2 has 267 bp, exon 3 has 90 bp, exon 4 has 168 bp, and exon 5 has 1,672 bp (not drawn to scale) (Ensembl 2018). The two dashed lines represent the especially large intron space between exons 1 and 2 which could not be depicted to scale. (b) *Nrf2^{fl/fl}* has loxP sites (triangles) flanking exon 5. (c) Upon breeding *Nrf2^{fl/fl}* mice with LysM-Cre mice, exon 5 is excised out, resulting in a myeloid-specific *Nrf2* KO mouse (mNrf2 KO). Figure adapted from Xue et al. (2013).

(a) mRNA of alveolar macrophages



(b) mRNA of peritoneal macrophages



(c) Protein of peritoneal macrophages

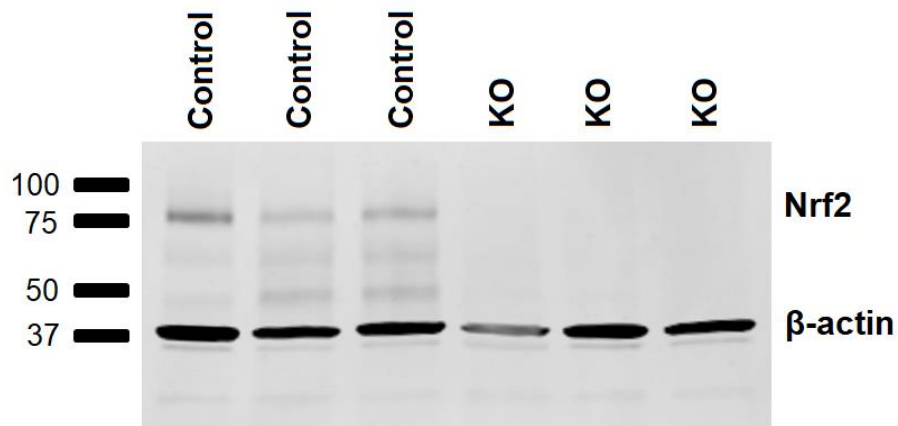


Figure 3-2: Alveolar and peritoneal macrophages mRNA and protein expression. mRNA expression of *Nrf2* and select *Nrf2*-regulated genes in (a) alveolar and (b) peritoneal macrophages of control mice vs. mNrf2 KO mice (n=4). Bars represent mean \pm SEM. *p<0.05, **p<0.01, ***p<0.001. (c) NRF2 protein expression of DEPe-treated peritoneal macrophages from control mice vs. mNrf2 KO mice (n=3).

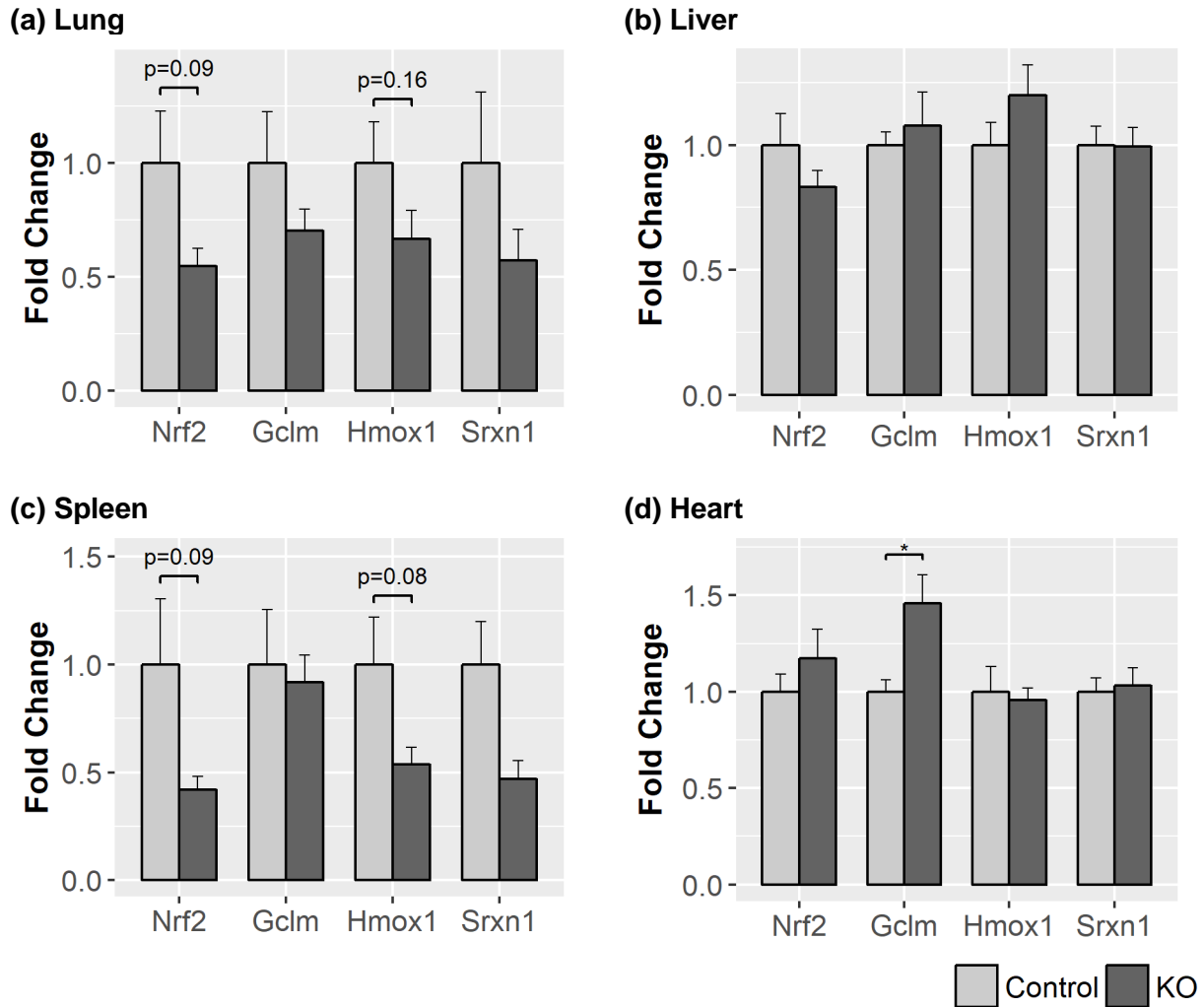


Figure 3-3: Whole tissue gene expression. Expression of *Nrf2* and select *Nrf2*-regulated genes in (a) lung, (b) liver, (c) spleen, and (d) heart of control mice vs. m*Nrf2* KO mice (n=6). Bars represent mean \pm SEM. * $p < 0.05$

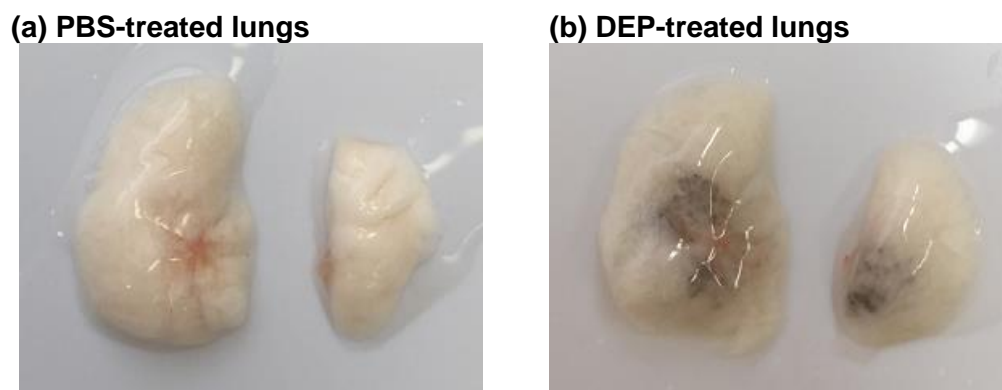
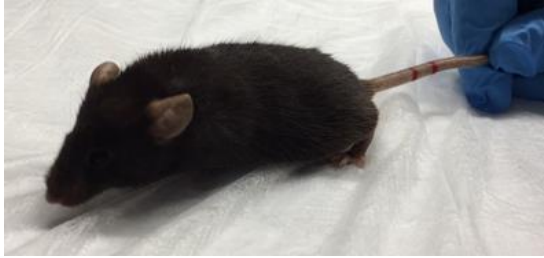


Figure 3-4: Appearance of perfused lungs following exposures. Representative lungs are from (a) a PBS-treated mouse, and (b) a DEP-treated mouse, approximately 5-6 hours following oropharyngeal aspiration. Black particles were apparent in the latter. The appearances of the PBS- and DEP-exposed lungs did not differ macroscopically between control and KO mice.

(a) DEP-treated control



(b) DEP-treated KO

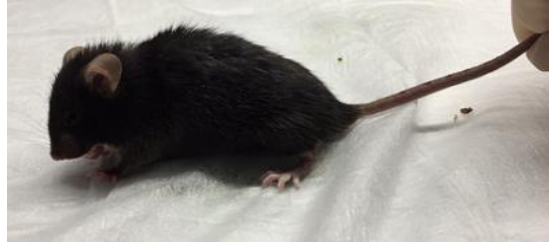
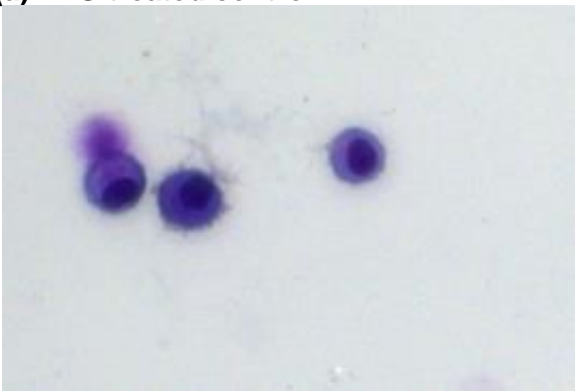
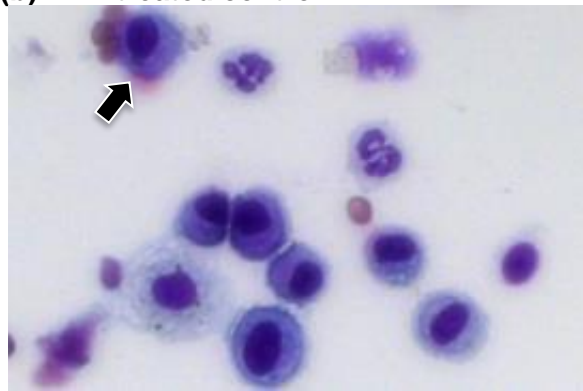


Figure 3-5: Appearance of mice following oropharyngeal aspiration of DEP. (a) Control mice that were exposed to DEP did not appear to be in severe ill health like the (b) mNrf2 KO mice that were exposed to the particles, with visible characteristics of sickness such as being hunched and having ruffled fur. Videos of these mice are available as supplemental files to this dissertation.

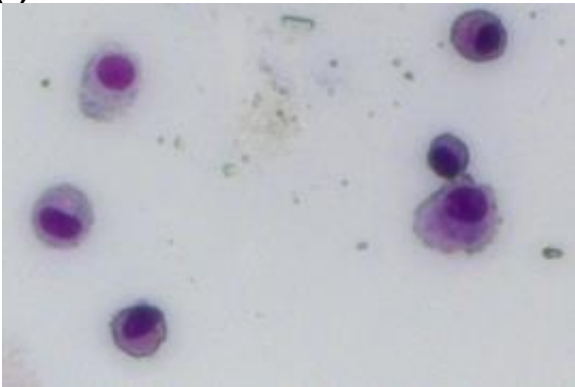
(a) PBS-treated control



(b) DEP-treated control



(c) PBS-treated KO



(d) DEP-treated KO

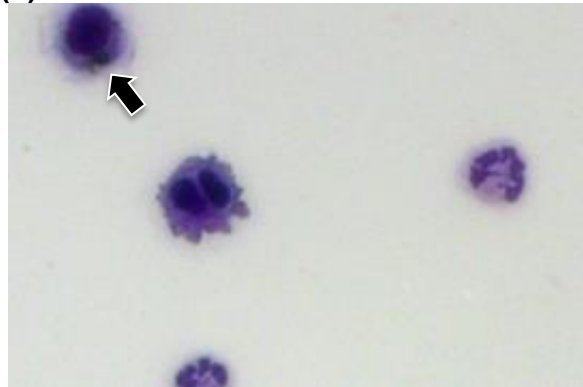
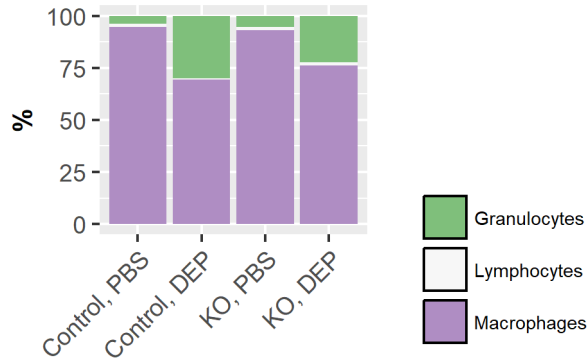
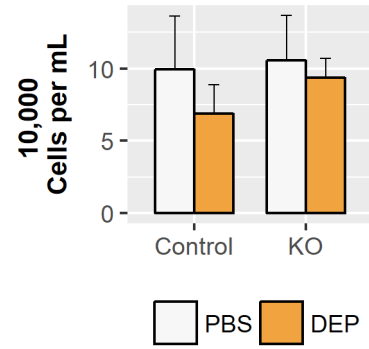


Figure 3-6: Cytopsin slides of bronchoalveolar lavage cells Representative pictures of Hema 3-stained cytopsin slides from (a) a PBS-treated control mouse, (b) a DEP-treated control mouse, (c) a PBS-treated KO mouse, and (d) a DEP-treated KO mouse. Magnification 20x. Arrows represent particulates taken up by macrophages.

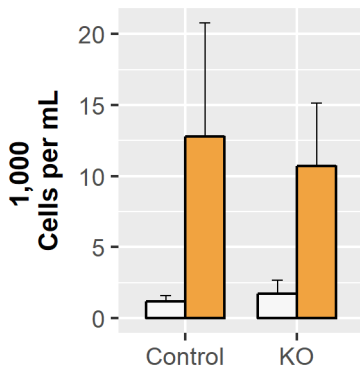
(a) Cell differentials



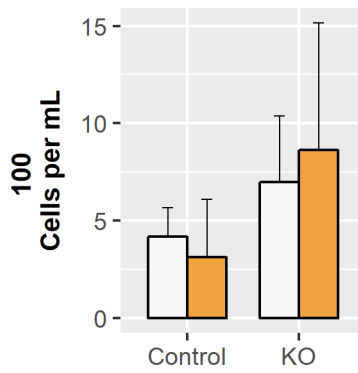
(b) Cell concentrations



(c) Granulocytes



(d) Lymphocytes



(e) Macrophages

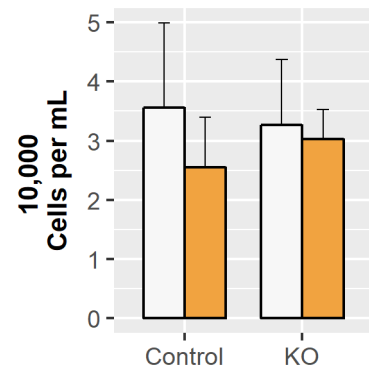
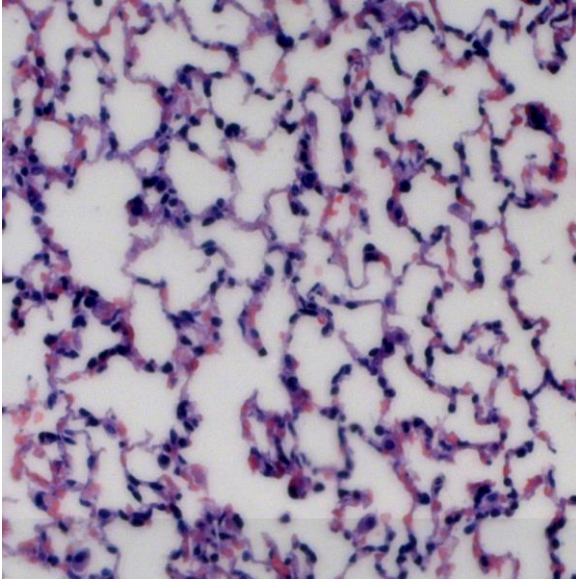
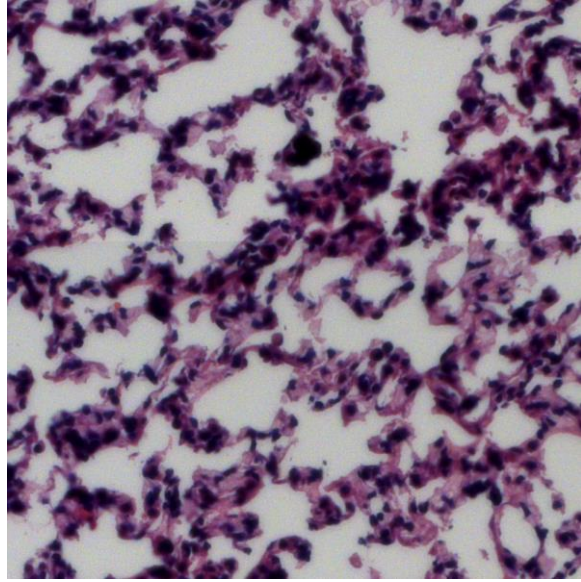


Figure 3-7: Bronchoalveolar lavage numbers following exposures. (a) Percentage distributions of cell types and (b) total cell concentrations in the BALF (n=4-6). Numbers of (c) granulocytes, (d) lymphocytes, and (e) macrophages, as estimated from total cell concentrations and percentage distributions (n=4-6). For granulocytes, a two-way ANOVA analysis indicated a significant effect of treatment on cell numbers, with $p < 0.05$.

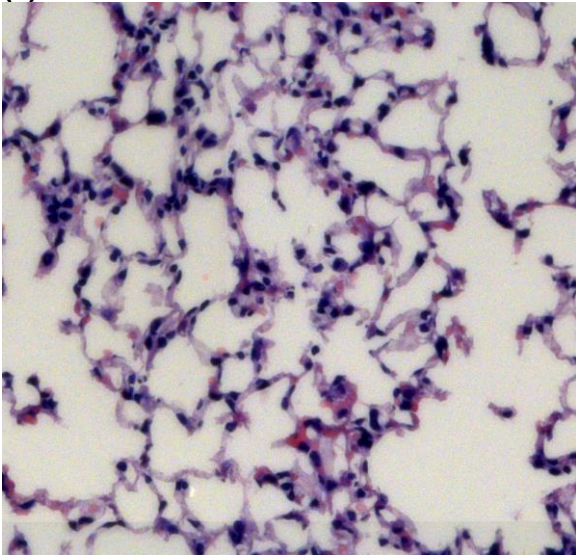
(a) PBS-treated control



(b) DEP-treated control



(c) PBS-treated KO



(d) DEP-treated KO

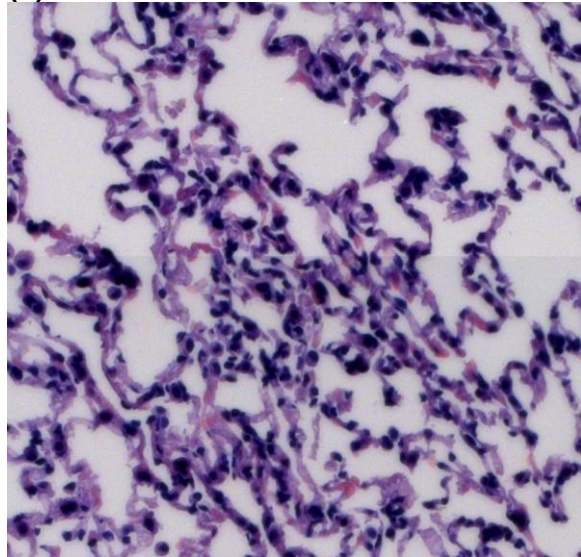
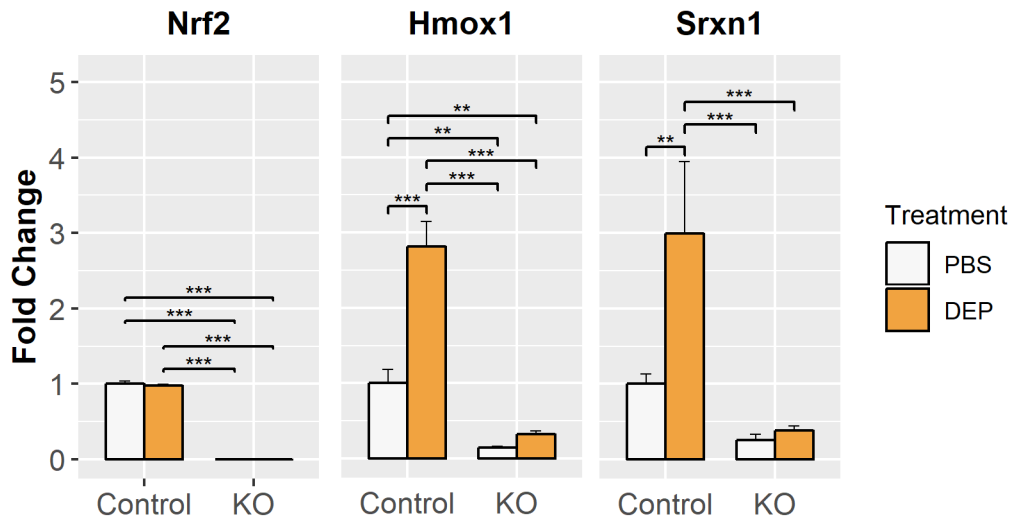
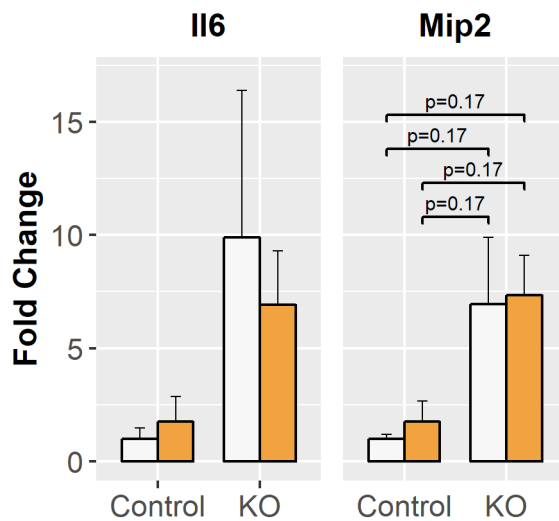


Figure 3-8: H&E-stained lung sections following exposures. Representative pictures of H&E-stained lung sections from (a) a PBS-treated control mouse, (b) a DEP-treated control mouse, (c) a PBS-treated KO mouse, and (d) a DEP-treated KO mouse. Magnification 20x.

(a) Nrf2 and antioxidant genes



(b) Inflammatory genes



(c) TNF- α concentration

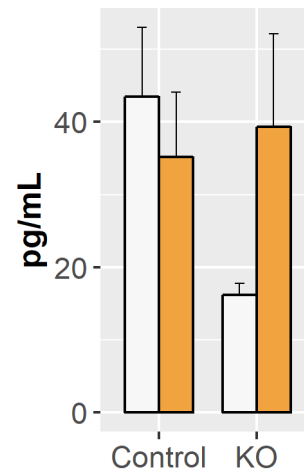


Figure 3-9: Alveolar macrophage gene expression and BALF cytokine concentration after exposures. mRNA levels of (a) *Nrf2* and select *Nrf2* target genes demonstrated deletion of *Nrf2* in KO mice. While the control mice had increased *Hmox1* and *Srxn1* expression, the mRNA levels for these two genes remained low in KO mice. mRNA levels of (b) select inflammatory genes, *Il6* and *Mip2*. Neither of these two genes reached statistical significance, although for *Mip2*, a two-way ANOVA analysis demonstrated significant effects of genotype on the expression of this gene. (c) There were no differences in TNF- α concentration in the BALF between the groups. n=4-6. **p<0.01 and ***p<0.001.

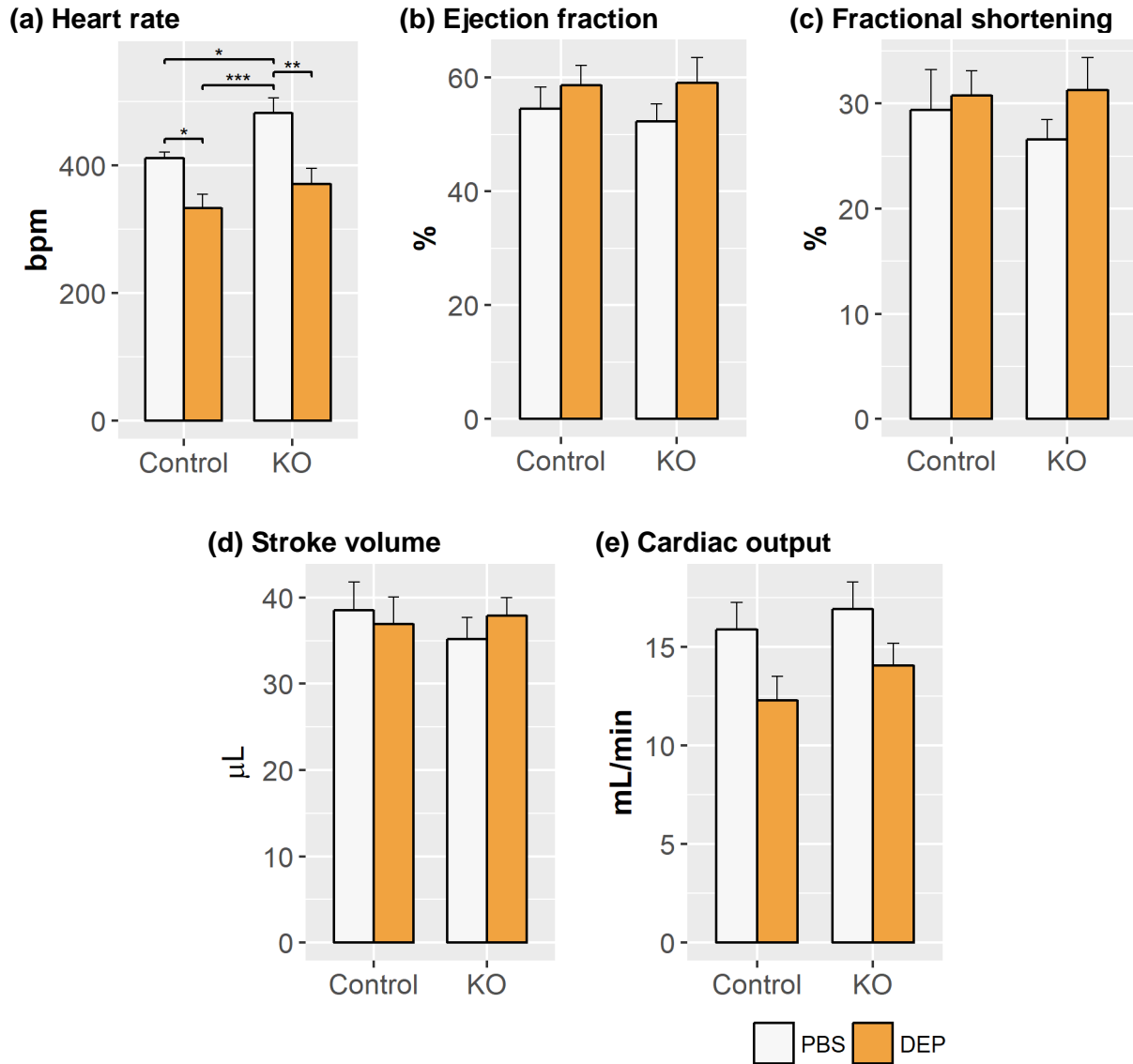
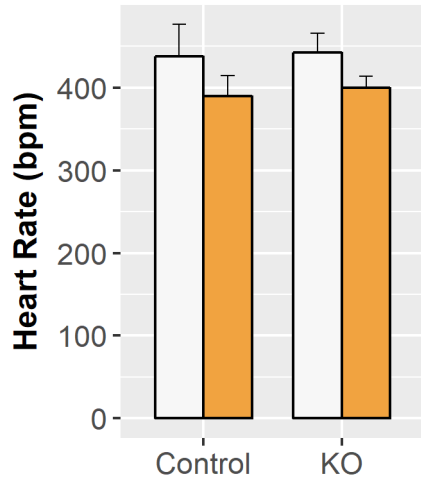


Figure 3-10: Echocardiography left ventricular measurements. Left ventricular M-mode measurements were used to calculate (a) heart rate, (b) ejection fraction, (c) fractional shortening, (d) stroke volume, and (e) cardiac output (n=6). For cardiac output, while there were no significant differences among the four groups, there was a significant treatment effect, according to a two-way ANOVA analysis ($p < 0.05$). * $p < 0.05$, ** $p < 0.01$, and *** $p < 0.001$.

(a) Right ventricle



(b) Left ventricle

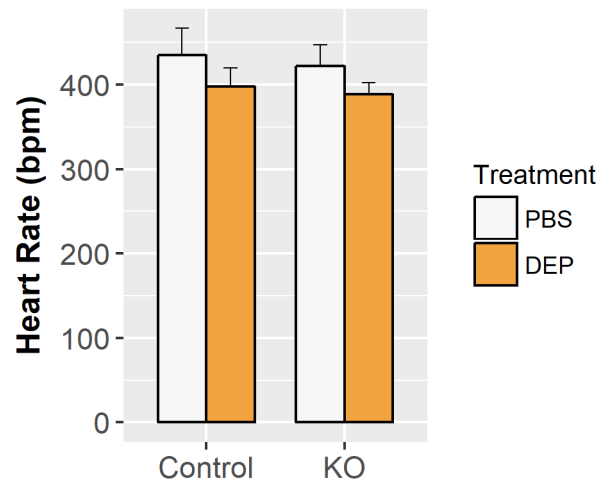
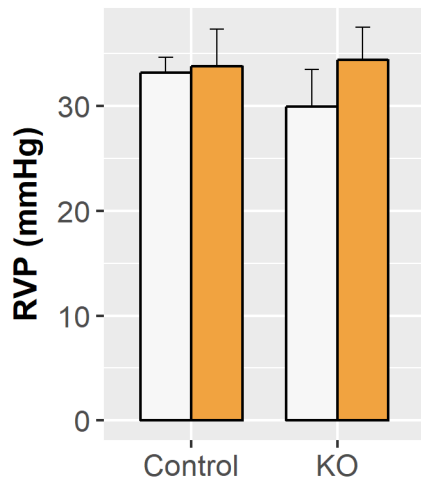


Figure 3-11: Heart rates as measured by cardiac catheterization. There were no differences in heart rates between the four groups in either the (a) right ventricle or the (b) left ventricle (n=6). The heart rate values for each group also did not differ between the right and left ventricles.

(a) Right ventricle



(b) Left ventricle

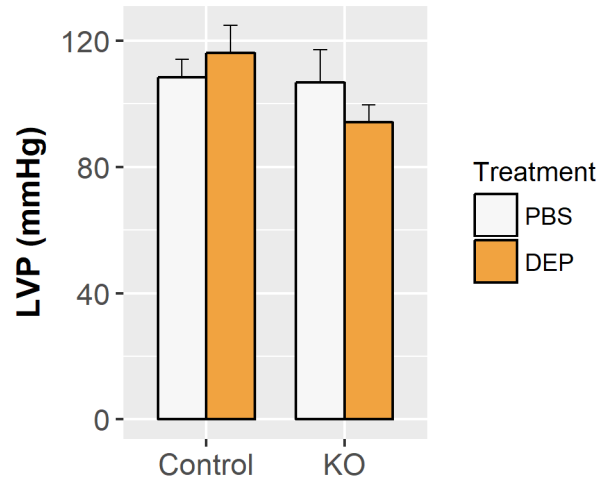
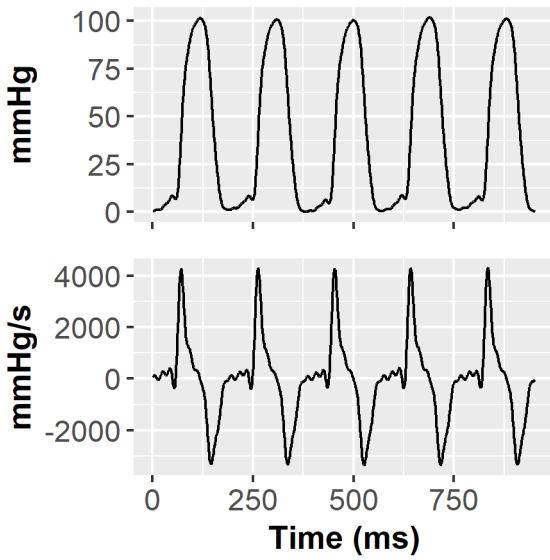
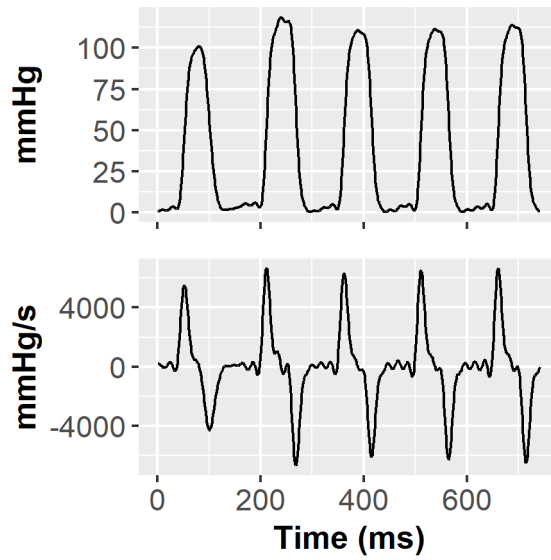
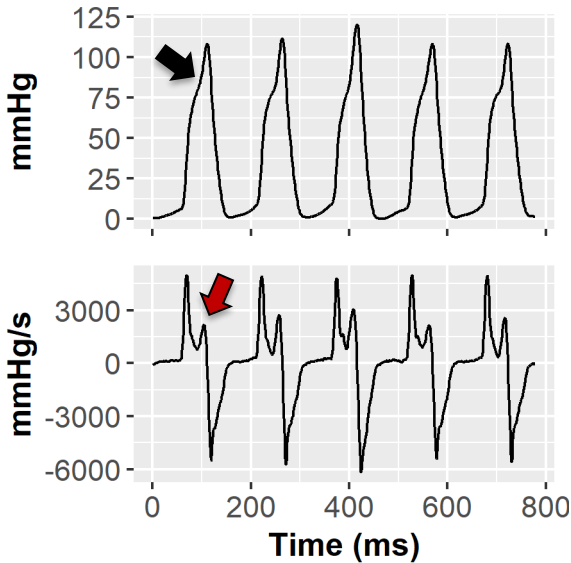
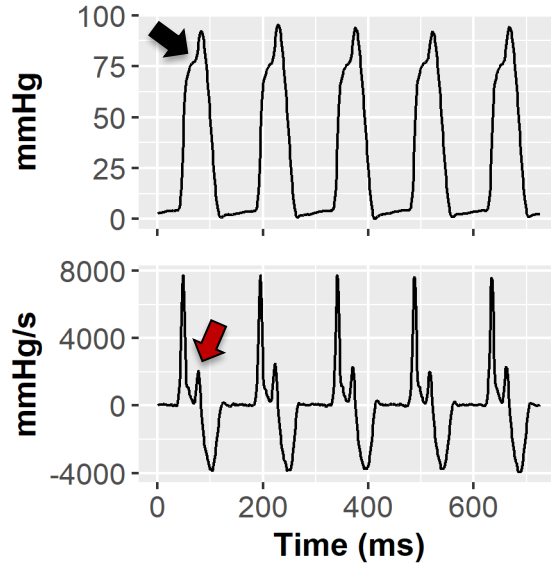


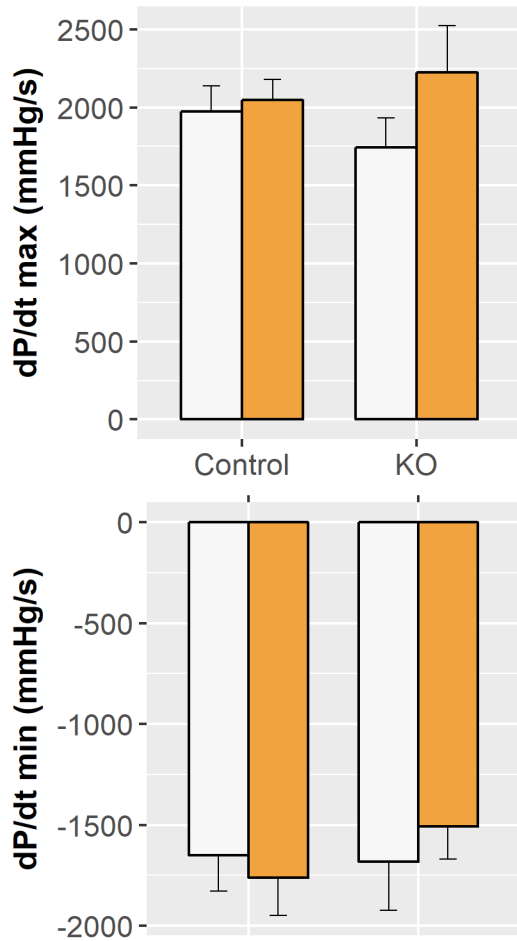
Figure 3-12: Ventricular pressures. There were no differences in (a) right and (b) left ventricular pressures across all four groups (n=6) as measured by cardiac catheterization.

(a) PBS-treated control**(b) DEP-treated control****(c) PBS-treated KO****(d) DEP-treated KO****(e) Summary table**

	PBS-Treated Control Mice	DEP-Treated Control Mice	PBS-Treated KO Mice	DEP-Treated KO Mice
Abnormal peaks	0/6 samples	0/6 samples	2/6 samples	4/6 samples

Figure 3-13: Cardiac catheterization pressure curves of the left ventricles. (a-d) Five beats from representative mice from each group are illustrated. In several KO mice, from both the PBS-treated and the DEP-treated groups, there were prominent reflected peaks (black arrows) in the left ventricular pressure curves (mmHg), which resulted in a second positive peak (red arrows) for each beat in the pressure derivative (dP/dt) curves (mmHg/s). (e) The number of samples with these reflected peaks are summarized (n=6). These prominent peaks were not seen in the control mice. A chi-square test determined a significant p-value of 0.02 for the table.

(a) Right ventricle



(b) Left ventricle

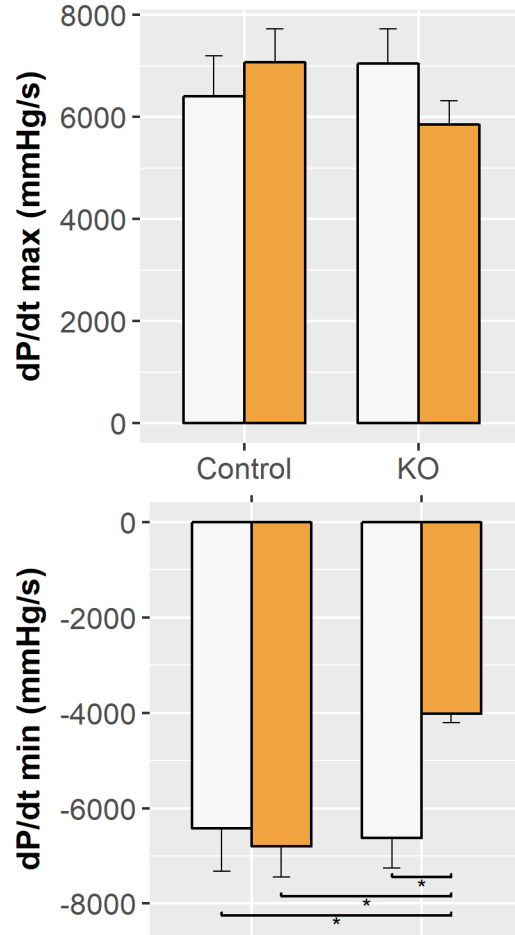


Figure 3-14: Ventricular developed pressures. (a) In the right ventricle, there were no differences in dP/dt maximum and dP/dt minimum (n=6). (b) In the left ventricle, there were no differences in dP/dt maximum between the four groups, suggesting no difference in contractility (n=6). However, for left ventricular dP/dt minimum, a two-way ANOVA analysis demonstrated a significant interaction effect of genotype and treatment (*p<0.05).

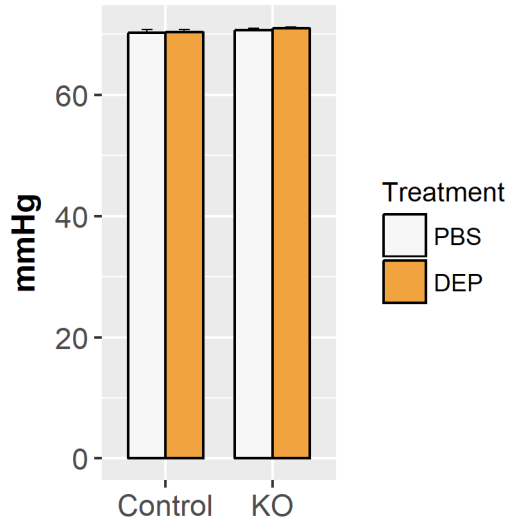


Figure 3-15: Mean pulmonary arterial pressure (MPAP). There were no differences in MPAP between the groups (n=6). Bars represent mean \pm SEM.

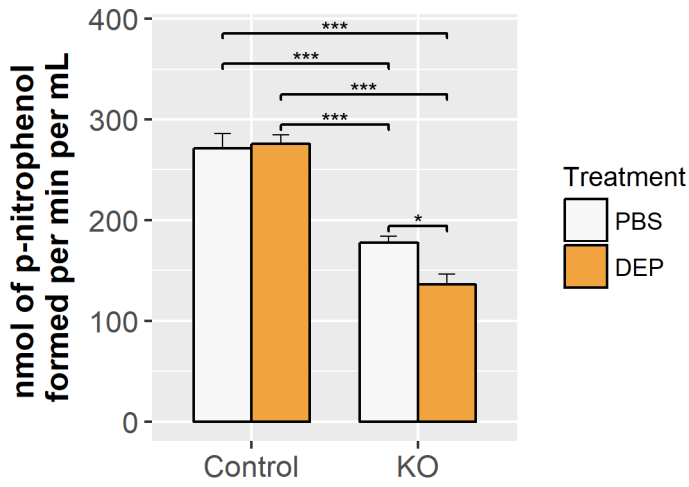
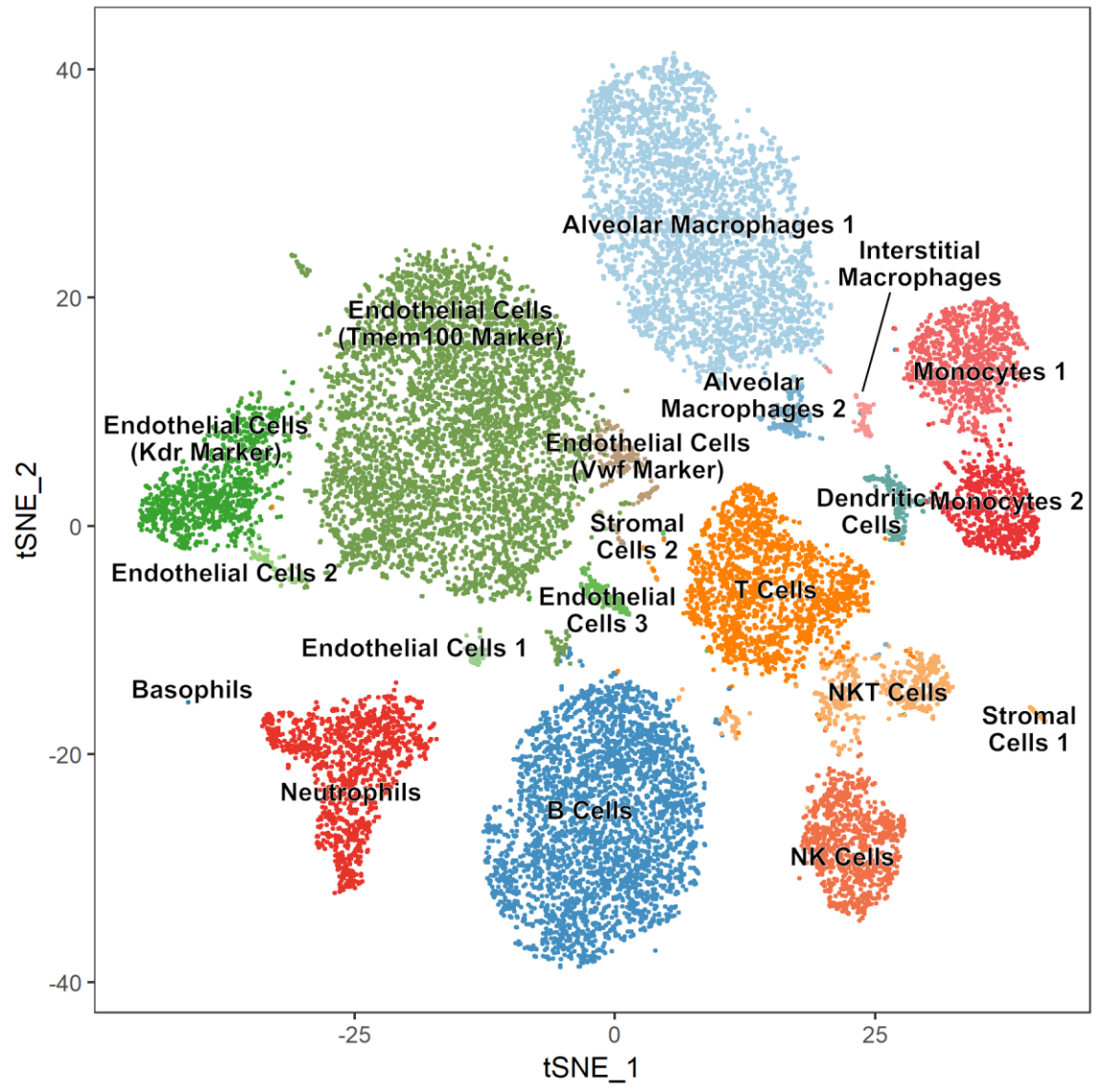


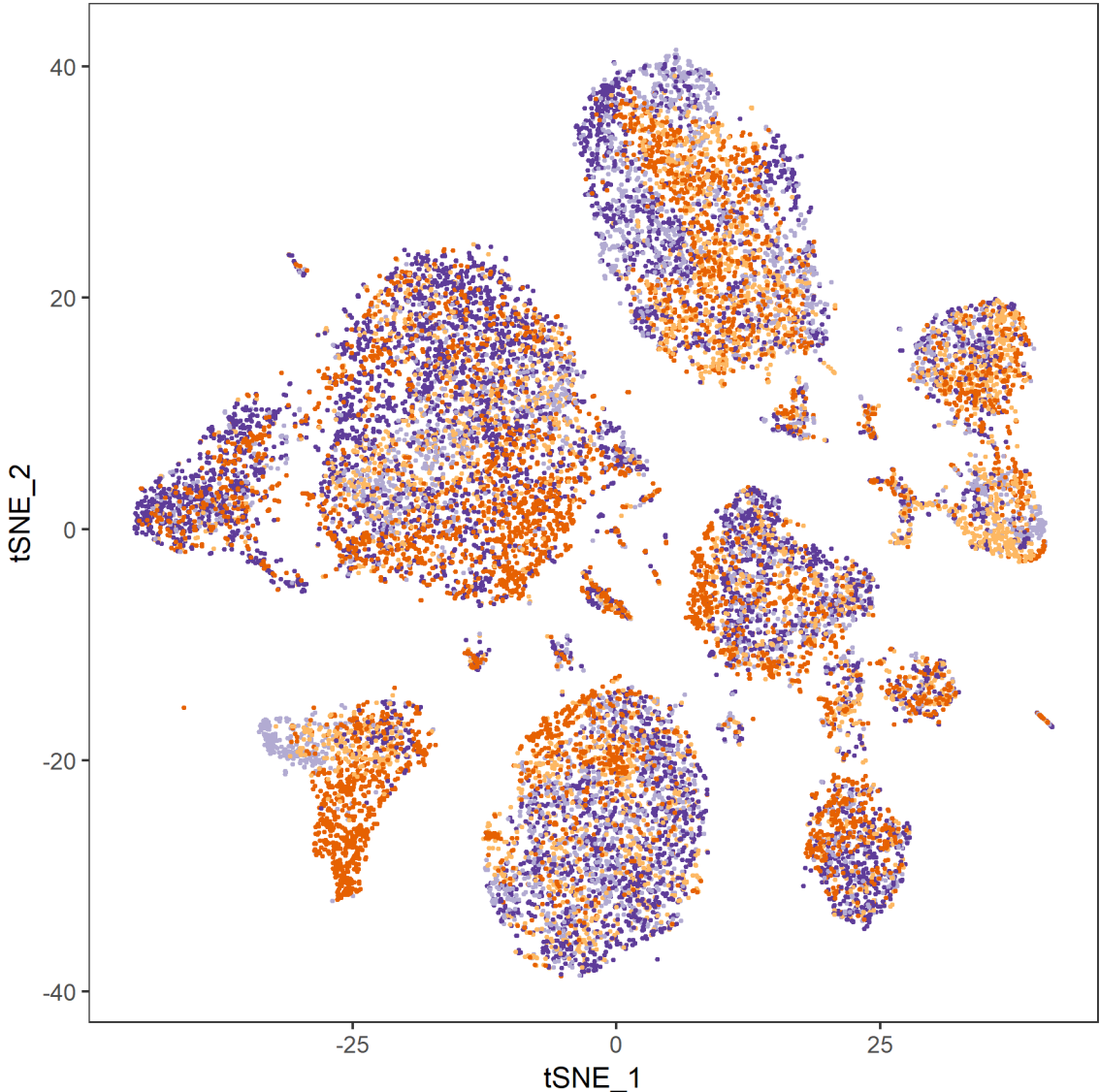
Figure 3-16: Plasma PON1 activity. PON1 activity is less in KO mice compared to control mice (n=6) and is further reduced following DEP exposure. Bars represent mean \pm SEM. *p<0.05, ***p<0.001.

(a) All groups, colored by cell cluster



Continued on next page...

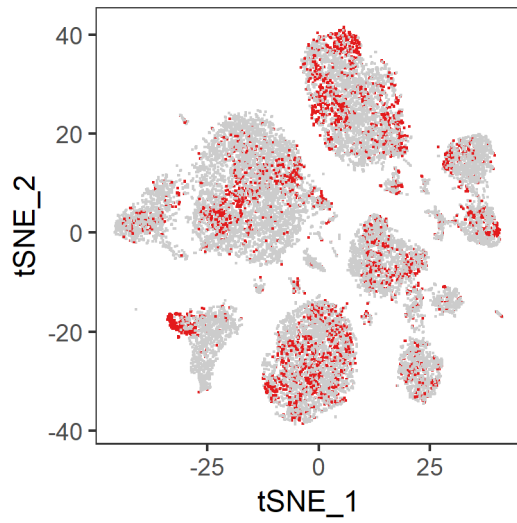
(b) All groups, colored by group



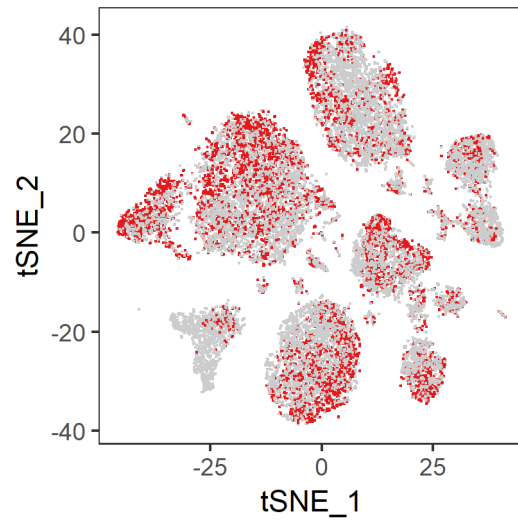
- PBS-treated control
- PBS-treated KO
- DEP-treated control
- DEP-treated KO

Continued on next page...

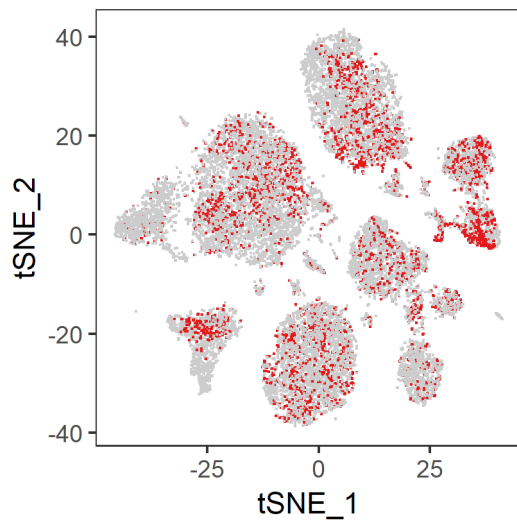
(c) PBS-treated control



(d) DEP-treated control



(e) PBS-treated KO



(f) DEP-treated KO

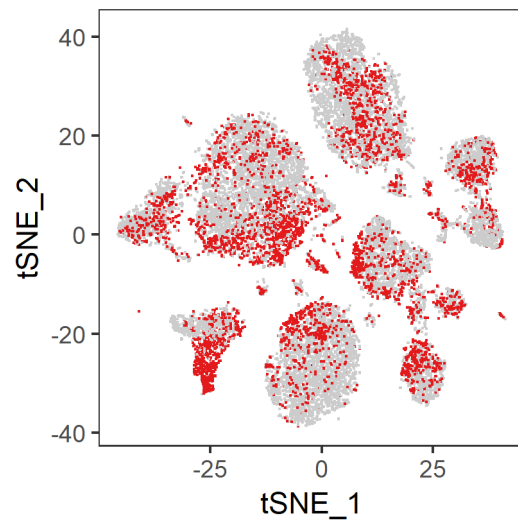
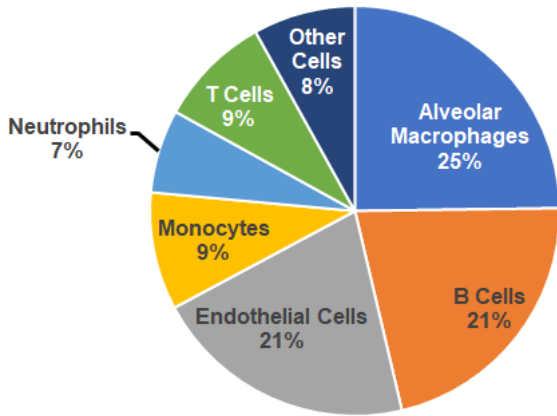
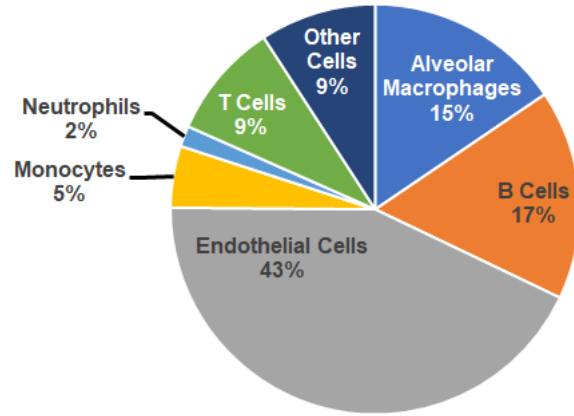


Figure 3-17: Clustering of cells analyzed in scRNA-seq. (a) Twenty lung cell types were identified through t-SNE analysis. The distribution of cell types by group was also plotted for (b) all groups, and separately for (c) PBS-treated control mice, (d) DEP-treated control mice, (e) PBS-treated KO mice, and (f) DEP-treated KO mice. The cell types of the clusters in (b-f) correspond to those in (a).

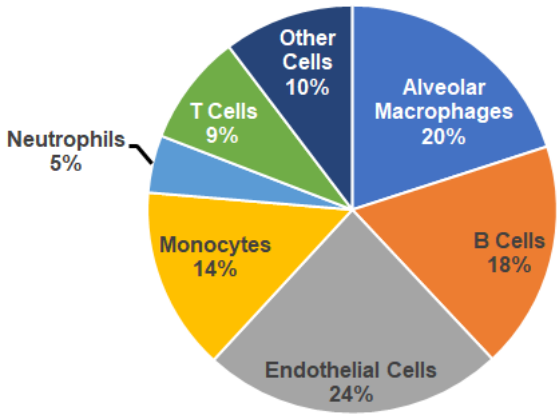
(a) PBS-treated control



(b) DEP-treated control



(c) PBS-treated KO



(d) DEP-treated KO

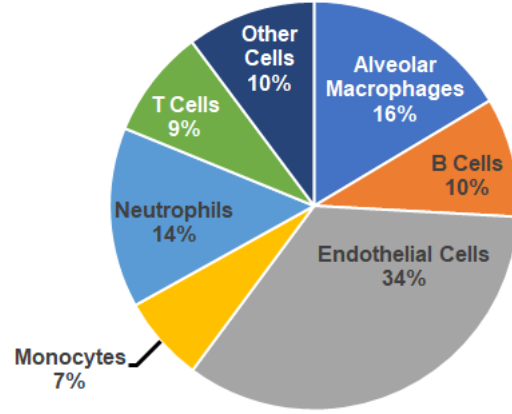
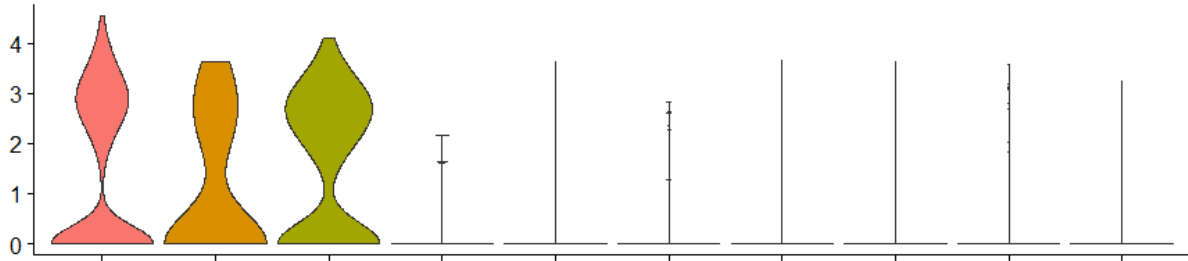
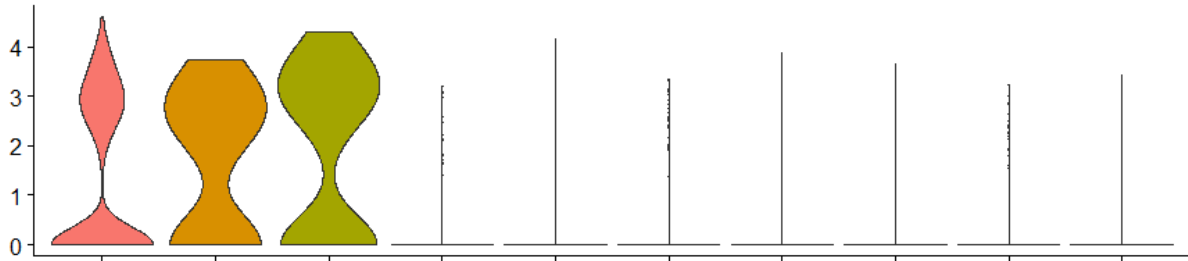


Figure 3-18: Distribution of general lung cell types for scRNA-seq. Cells of similar type were grouped together in the same slice in the pie chart when appropriate: "Alveolar macrophages" includes the alveolar macrophage subtypes 1 and 2; "Endothelial cells" includes the endothelial cell subtypes 1, 2, 3, Kdr marker, Tmem100 marker, and Vwf marker; and "Monocytes" includes the monocyte subtypes 1 and 2.

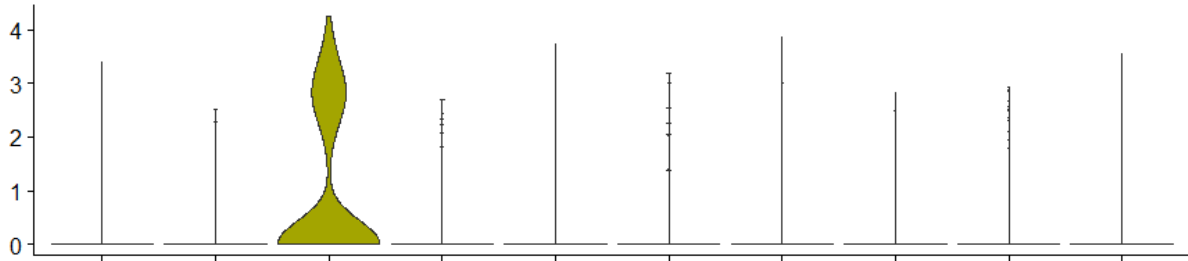
(a) PBS-treated control



(b) DEP-treated control



(c) PBS-treated KO



(d) DEP-treated KO

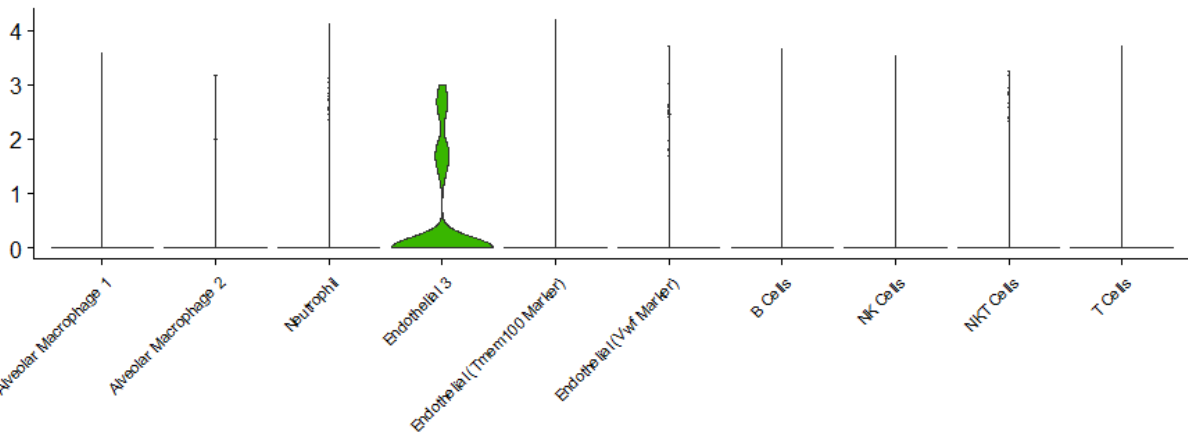
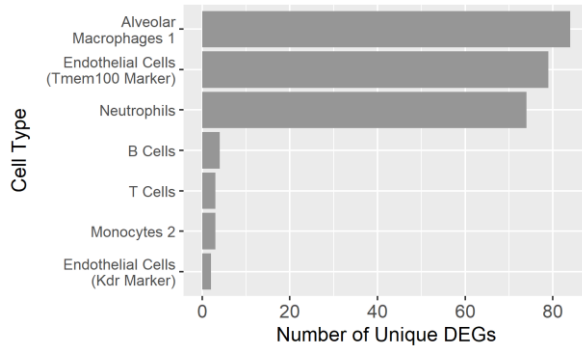
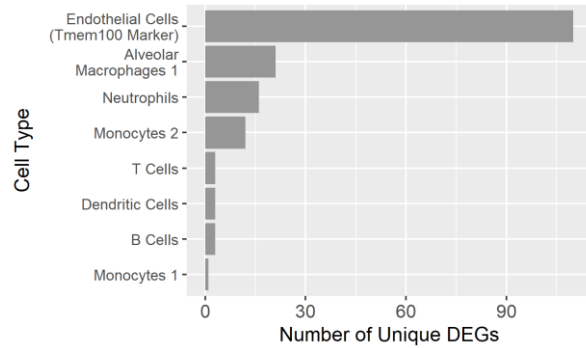


Figure 3-19: Violin plots of *Nrf2* expression. *Nrf2* expression for 10 identified lung cells were plotted for each group: (a) PBS-treated control mice, (b) DEP-treated control mice, (c) PBS-treated KO mice, and (d) DEP-treated KO mice. *Nrf2* expression was confirmed to be knocked out in KO mice in alveolar macrophages compared to control mice. The y-axis is the normalized expression level, which is in units of $\ln(\text{normalized UMI counts} + 1)$, where UMI refers to Unique Molecular Identifiers, and the normalized UMI counts refer to $10000 * (\text{counts}) / (\text{total transcripts per cell})$.

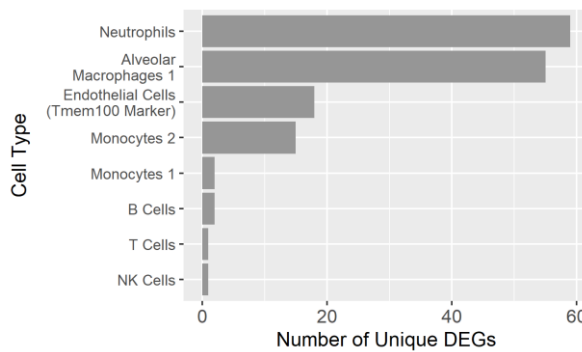
(a) DEP-treated vs. PBS-treated control



(B) DEP-treated vs. PBS-treated KO



(C) PBS-treated KO vs. PBS-treated control



(d) DEP-treated KO vs. DEP-treated control

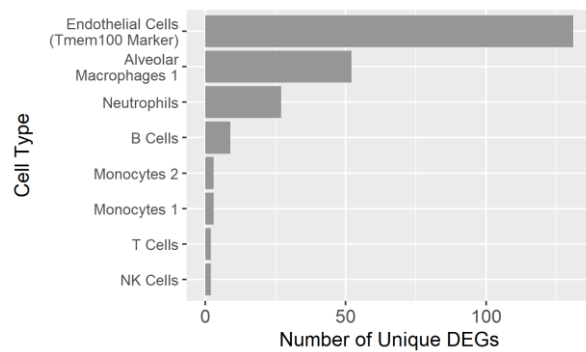


Figure 3-20: Number of unique differentially expressed genes (DEGs) by cell type. (a) In DEP- vs. PBS-treated control mice, seven cell types had unique DEGs. In total, 249 unique genes were differentially expressed in only one cell type, with alveolar macrophages 1, endothelial cells (Tmem100 marker), and neutrophils clearly having the highest number. (b) In DEP- vs. PBS-treated KO mice, eight cell types had unique DEGs. In total, 169 unique genes were differentially expressed in only one cell type, with endothelial cells (Tmem100 marker) by far having the highest number. (c) In PBS-treated KO vs. PBS-treated control mice, eight cell types had unique DEGs. In total, 153 unique genes were differentially expressed in only one cell type, with neutrophils and alveolar macrophages 1 having the highest number. (d) In DEP-treated KO vs. DEP-treated control mice, eight cell types had unique DEGs. In total, 233 unique genes were differentially expressed in only one cell type, with endothelial cells (Tmem100 marker) clearly having the highest number.

(a) DEP- vs. PBS-treated control



(b) DEP- vs. PBS-treated KO



For figures (a) and (b):



Upregulated in DEP-treated



Downregulated in DEP-treated

Continued on next page...

(c) PBS-treated KO vs. PBS-treated control



(d) DEP-treated KO vs. DEP-treated control

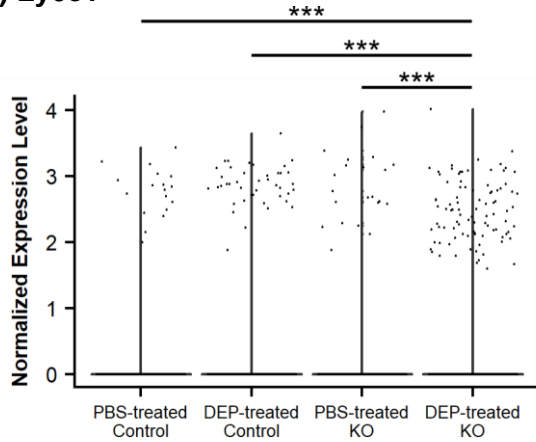


For figures (c) and (d):

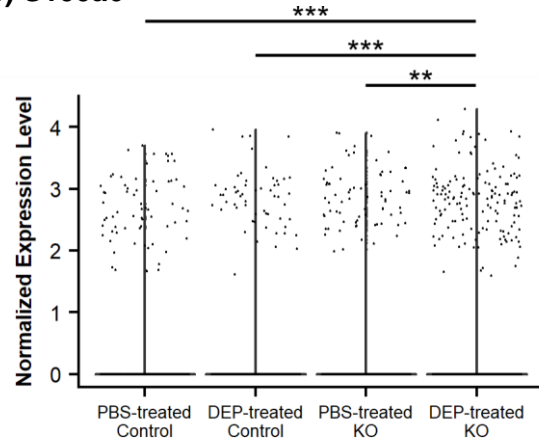
■ Upregulated in KO ■ Downregulated in KO

Figure 3-21: Common DEGs across three or more cell types in DEP- vs. PBS-treated control. DEGs are illustrated as either being upregulated (green square) or downregulated (red square) for each comparison. Genes are listed across the top in decreasing order of occurrence in the cells, while cells are listed in descending order (top to bottom) of the number of DEGs. (a) There were 11 DEGs that were found across three or more lung cell types in DEP- vs. PBS-treated control, (b) 9 DEGs in the DEP- vs. PBS-treated KO comparison, (c) 11 DEGs in the PBS-treated KO vs. PBS-treated control comparison, and (d) 16 DEGs in the DEP-treated KO vs. DEP-treated control.

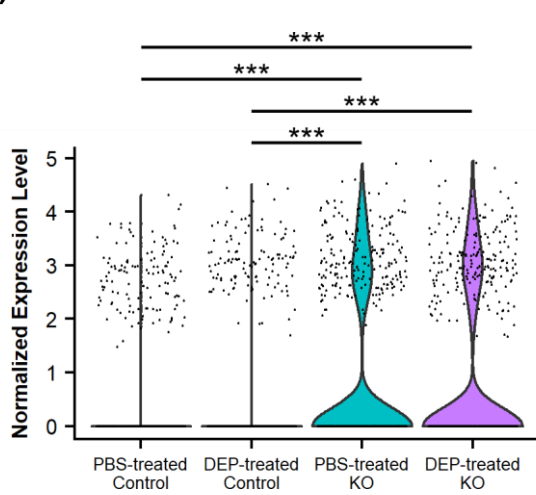
(a) *Ly6c1*



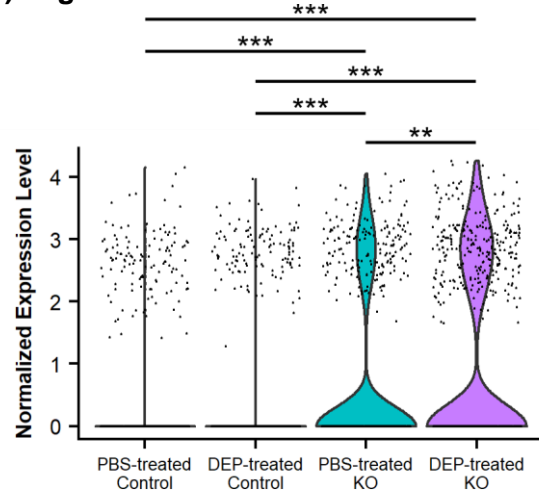
(b) *S100a6*



(c) *Cxcl10*



(d) *Fcgr2b*



(e) *Txnrd1*

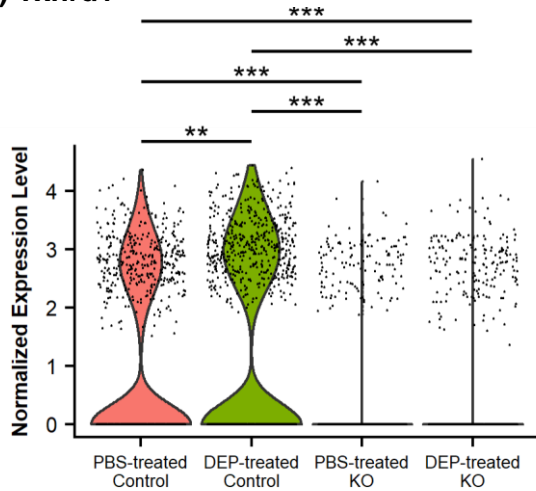


Figure 3-22: Violin plots of selected genes for the alveolar macrophages 1 cluster. (a) *Ly6c1* and (b) *S100a6* are both pro-inflammatory genes. Macrophage marker genes were also plotted, including (c) *Cxcl10* (M1 marker), (d) *Fcgr2b* (M2 marker), and (e) *Txnrd1* (Mox marker). ** $p < 0.01$, and *** $p < 0.001$. The normalized expression level on the y-axis is $\ln(\text{normalized UMI counts} + 1)$, where UMI refers to Unique Molecular Identifiers, and the normalized UMI counts refer to $10000 \cdot (\text{counts}) / (\text{total transcripts per cell})$.

Tables

		PBS-treated-C57Bl/6J vs. PBS-treated-LysM-Cre (p-value)	DEP-treated-C57Bl/6J vs. DEP-treated-LysM-Cre (p-value)
Echocardiography	Heart Rate (bpm)	0.73	0.34
	Ejection Fraction (%)	0.81	0.50
	Fractional Shortening (%)	0.58	0.58
	Stroke Volume (μ L)	0.99	0.99
	Cardiac Output (mL/min)	0.82	0.70
	Pulmonary Acceleration Time, PAT (ms)	0.31	0.20
Cardiac Catheterization	Right Ventricle Heart Rate (bpm)	0.25	0.48
	Left Ventricle Heart Rate (bpm)	0.67	0.54
	Right Ventricle Pressure (mmHg)	0.47	0.14
	Left Ventricle Pressure (mmHg)	0.99	0.60
	Right Ventricle dP/dt Max (mmHg/s)	0.71	0.71
	Left Ventricle dP/dt Max (mmHg/s)	0.40	0.65
	Right Ventricle dP/dt Min (mmHg/s)	0.68	0.46
	Left Ventricle dP/dt Min (mmHg/s)	0.03	0.41

Table 3-1: C57BL/6J vs. LysM-Cre measurements. 13 out of 14 measurements were not different between the two types of mice used as controls – C57BL/6J and LysM-Cre (n=3). The only measurement that was significantly different, left ventricle dP/dt min, was between the PBS-treated controls. It is unclear why this is, but as seen in **Figure 3-14**, the main comparisons of interest involved the other groups, which showed that the value for the DEP-treated KO mice remained significantly different from the other two groups (PBS-treated KO and DEP-treated control). Nevertheless, it could be worthwhile to pursue looking at whether this particular difference would remain with increased numbers of samples from n=3.

Primer	Sequence	Roche Probe #
Nrf2 forward primer	GAGCAGGACATGGAGCAAGT	51
Nrf2 reverse primer	GCTTGTTTTTCGGTATTAAGACACTG	
β -actin forward primer	AAGGCCAACCGTGAAAAGAT	56
β -actin reverse primer	GTGGTACGACCAGAGGCATAC	
Gclm forward primer	TGGAGCAGCTGTATCAGTGG	18
Gclm reverse primer	CAAAGGCAGTCAAATCTGGTG	
Hmox1 forward primer	AGGCTAAGACCGCCTTCCT	17
Hmox1 reverse primer	TGTGTTCCCTCTGTCAGCATCA	
Il6 forward primer	GCTACCAAACCTGGATATAATCAGGA	6
Il6 reverse primer	CCAGGTAGCTATGGTACTCCAGAA	
Mip2 forward primer	AAAATCATCCAAAAGATACTGAACAA	26
Mip2 reverse primer	CTTTGGTTCTTCCGTTGAGG	
Srxn1 forward primer	AGGGGCTTCTGCAAACCTA	79
Srxn1 reverse primer	TGGCATAGCTACCTCACTGCT	

Table 3-2: Primers and probes for quantitative real-time PCR. Probes were purchased from the Roche Molecular Systems, Inc. (Pleasanton, CA) Universal ProbeLibrary System.

	PBS-Treated Control Mice	DEP-Treated Control Mice	PBS-Treated KO Mice	DEP-Treated KO Mice
Alveolar Macrophages 1	883	1006	735	762
Alveolar Macrophages 2	39	48	40	41
B Cells	801	1124	699	463
Basophils	10	8	4	10
Dendritic Cells	32	54	84	34
Endothelial Cells 1	8	16	22	35
Endothelial Cells 2	1	72	1	17
Endothelial Cells 3	10	71	36	55
Endothelial Cells (Kdr Marker)	106	585	59	231
Endothelial Cells (Tmem100 Marker)	615	2064	778	1282
Endothelial Cells (Vwf Marker)	36	114	27	58
Interstitial Macrophages	13	18	26	26
Monocytes 1	165	242	311	212
Monocytes 2	180	88	251	120
Neutrophils	245	111	176	698
NK Cells	161	347	108	246
NKT Cells	69	161	166	150
Stromal Cells 1	5	26	8	18
Stromal Cells 2	10	9	3	15
T Cells	331	624	342	422
TOTAL	3720	6788	3876	4895

Table 3-3: Distribution of lung cell types for scRNA-seq. The most abundant cell types acquired from the lung dissociation and Drop-seq procedures were endothelial cells (Tmem100 marker) and alveolar macrophages 1, while basophils and stromal cells 1 and 2 were the least abundant cell types.

Cell Type	# of DEGs	Enriched Pathways	Pathway DEGs*
Alveolar Macrophages 1	109 (90/19)	Immune system	S100a9, S100a9, Calr, Hspa5, Hsp90b1, Cstb, Cd74, Hspa8, Tnf, Lyz2
		Scavenging by class A receptors	Calr, Hsp90b1, Marco
		Regulation of TLR by endogenous ligand	S100a8, S100a9, Cd14, Cd36
		Nonsense-Mediated Decay	Rpl41, Rps19, Rps28, Rpl35a, Rpl22, Rpl27, Rps3a1
		Neutrophil degranulation	S100a8, S100a9, Cstb, Hspa8, Lyz2, Ctsc, Tyrobp, Serpinb1a, Cxcl1, Cd14
Neutrophils	96 (74/22)	Immune system	S100a8, S100a9, Ifitm1, Ifitm6, Prdx5, Fpr1, Pglyrp1, Ifitm2, Chi311, S100a11
		Detoxification of reactive oxygen species	Prdx5, Gpx1, Sod2
		Immunoregulatory interactions between a lymphoid and a non-lymphoid cell	Ifitm1, Ifitm6, Ifitm2, Ifitm3, Pilra
		Neutrophil degranulation	S100a8, S100a9, Prdx5, Fpr1, Pglyrp1, Chi311, S100a11, Lrg1, Mmp8, Lyz2
Endothelial Cells (Tmem100 Marker)	95 (40/55)	Metabolism	Lpl, Serinc3, Lyve1, Plcb4, Cyp1a1, Cyp26b1, Marcks, Sult1a1, Ucp2, Ptgs1
Monocyte 2	17 (12/5)	Metal sequestration by antimicrobial proteins	S100a8, S100a9
B Cells	15 (7/8)	Metal sequestration by antimicrobial proteins	S100a8, S100a9
		Regulation of TLR by endogenous ligand	S100a8, S100a9
T Cells	13 (10/3)	Metal sequestration by antimicrobial proteins	S100a8, S100a9
		Toll-Like Receptors Cascades	S100a8, S100a9, Hmgb1
		Nonsense-Mediated Decay	Rpl35, Rpl41, Rps28
Endothelial Cells (Kdr Marker)	8 (4/4)	Sema3A PAK dependent Axon repulsion	Hsp90ab1, Plxna2
Monocyte 1	3 (1/2)	Toll-Like Receptors Cascades	S100a8, Cd36
NK Cells	3 (2/1)	Antimicrobial peptides	S100a8, S100a9
		Toll-Like Receptors Cascades	S100a8, S100a9
Endothelial Cells (Vwf Marker)	1 (1)	none	Hbb-bs

Table 3-4: DEP-treated vs. PBS-treated control DEGs and enriched pathways. Significantly enriched pathways (FDR < 0.05) were acquired from REACTOME analysis. In the “# of DEGs” column, green represents the number of upregulated genes with DEP treatment, while in the “Pathway DEGs” column, green represents an upregulated gene with DEP treatment. For those same columns, red represents downregulation with DEP treatment. *Up to the top ten DEGs are listed per pathway, per cell type.

Cell Type	# of DEGs	Enriched Pathways	Pathway DEGs*
Endothelial Cells (Tmem100 Marker)	<u>124</u> (67/57)	none	Lpl, mt-Rnr2, Cd36, Ly6c1, Serinc3, Cdkn1a, Qsox1, Timp3, mt-Rnr1, Ehd4
Alveolar Macrophages 1	<u>33</u> (12/21)	Metal sequestration by antimicrobial proteins	S100a8, S100a9
Neutrophils	<u>25</u> (9/16)	Developmental biology	Gm5483, Actb, BC100530, Stfa2, Stfa211, Stfa1, Stfa3
Monocytes 2	<u>21</u> (8/13)	Antimicrobial peptides	S100a8, S100a9, Ccr2
Monocytes 1	<u>9</u> (4/5)	none	Gm10036, Chi313, Malat1, mt-Rnr2, S100a8, Serinc3, mt-Rnr1, Apoe, Pla2g7
B Cells	<u>7</u> (5/2)	none	Gm10036, Rps3a1, Plek, H60b, Crem, Rel, Rps3a3
T Cells	<u>6</u> (3/3)	none	Gm10036, Rps3a1, Samsn1, Ifngr1, H60b, Rpl5
Endothelial Cells (Kdr Marker)	<u>4</u> (3/1)	none	mt-Rnr2, Cdkn1a, mt-Rnr1, Nin
Dendritic Cells	<u>3</u> (3)	none	Ccl22, Ccl17, Rgs1
NK Cells	<u>1</u> (1)	none	Gm10036

Table 3-5: DEP-treated vs. PBS-treated KO DEGs and enriched pathways. Significantly enriched pathways (FDR < 0.05) were acquired from REACTOME analysis. In the “# of DEGs” column, green represents the number of upregulated genes with DEP treatment, while in the “Pathway DEGs” column, green represents an upregulated gene with DEP treatment. For those same columns, red represents downregulation with DEP treatment. *Up to the top ten DEGs are listed per pathway, per cell type.

Cell Type	# of DEGs	Enriched Pathways	Pathway DEGs
Alveolar Macrophages 1	75 (57/18)	Immune system	Lyz2, Cd74, S100a8, Clec4d, Sqstm1, S100a9, Calr, Cxcl3, Il1b, Hspa5
		Arachidonate production from DAG	Abhd12, Mgl1
		N-glycan trimming in the ER and Calnexin/Calreticulin cycle	Calr, Pdia3, Ubc
		Antigen Presentation: Folding, assembly and peptide loading of class I MHC	Calr, Hspa5, Pdia3, H2-Q7
		ER-Phagosome pathway	Calr, Pdia3, H2-Q7
		Detoxification of Reactive Oxygen Species	Txnrd1, Prdx1, Gsr
		Iron uptake and transport	Hmox1, Fth1, Ftl1, Ubc
		Chemokine receptors bind chemokines	Cxcl3, Cxc110, Cxcl1
		Signaling by Interleukins	Sqstm1, Il1b, Hsp90b1, Il1rn, Trf, Ubc
Neutrophil degranulation	Lyz2, S100a8, Clec4d, S100a9, Cxcl3, Hspa8, Fth1, Gp49a, Ftl1, H2-Q7		
Neutrophils	75 (60/15)	Insulin effects increased synthesis of Xylulose-5-Phosphate	Taldo1, Tkt
		Metabolism of carbohydrates	Taldo1, Pgd, Pkm, Adpgk, Tkt, Calm1
		Immune system	Lyz2, Actb, S100a8, Ifitm6, Nfkb1a, Itgam, Tnf, Fpr1, Slpi, Plaur
		Signaling by Rho GTPases	Actb, Arhgdib, Pfn1, Calm1, Ywhab, Arpc1b, Cyba
		Hemostasis	Itgam, Actn1, Plaur, Srgn, Plek, Atp2b1, Calm1, Cd177, Anxa2
Monocytes 2	32 (17/15)	Immune system	Lyz2, S100a8, Ifitm3, S100a9, B2m, Actb, Ctss, Ccr2, Anxa2, Fth1
		Neutrophil degranulation	Lyz2, S100a8, S100a9, B2m, Ctss, Anxa2, Fth1, Cst3, Pglyrp1
Endothelial Cells (Tmem100 Marker)	29 (7/22)	none	Rps3a3, mt-Rnr2, Lyve1, Lpl, Ly6c1, S100a8, mt-Nd5, Cyp1a1, Hpgd, Ly6a
Monocytes 1	10 (6/4)	none	Lyz2, Rps3a3, Apoe, Nfe2l2, Slc38a2, S100a8, Rps3a1, mt-Rnr2, Bcl2a1b, Hmox1
B Cells	9 (3/6)	Metal sequestration by antimicrobial proteins	S100a8, S100a9
		Regulation of TLR by endogenous ligand	S100a8, S100a9
T Cells	6 (3/3)	none	Rps3a3, Rps3a1, H60b, S100a8, Rgcc, Ubb
Endothelial Cells (Kdr Marker)	3 (3)	none	mt-Rnr2, Ybx1, mt-Nd5
NK Cells	3 (1/2)	none	Rps3a3, Rps3a1, Ccl5
Dendritic Cells	2 (1/1)	none	Rps3a3, Lyz2
Alveolar Macrophages 2	1 (1)	none	Lyz2
Interstitial Macrophages	1 (1)	none	Lyz2

Table 3-6: PBS-treated KO vs. PBS-treated control DEGs and enriched pathways. Significantly enriched pathways (FDR < 0.05) were acquired from REACTOME analysis. In the “# of DEGs” column, green represents the number of upregulated genes in the KO mice, while in the “Pathway DEGs” column, green represents an upregulated gene in the KO mice. For those same columns, red represents downregulation in KO mice. *Up to the top ten DEGs are listed per pathway, per cell type.

Cell Type	# of DEGs	Enriched Pathways	Pathway DEGs*
Endothelial (Tmem100)	161 (74/87)	Immune system	S100a9, S100a8, Lrg1, Ptpnb, Cd74, Actb, Nfkbia, Cxcl2, Tuba1b, Socs3
		FMO oxidises nucleophiles	Fmo1, Fmo2
		Developmental Biology	Sema7a, Sptbn1, Actb, Tuba1b, Ubc, Hsp90aa1, Sptan1, Cttna1, Stk4, Rhoc
		Programmed Cell Death	Fas, Ubc, Vim, Sptan1, Tnfsf10
		Signal Transduction	Cdkn1a, Arhgap29, Sptbn1, Actb, Ybx1, Lpl, Ier3, Nfkbia, Bmpr2, Calcr1
		Signaling by Receptor Tyrosine Kinases	Actb, Ubc, Hsp90aa1, Nedd4, Cttna1, Stk4, Stat1, Kitl, Plat, Kdr
		Semaphorin interactions	Sema7a, Hsp90aa1, Stk4, Rhoc, Tln1
		G1 Phase	Cdkn1a, Tuba1b, Ubc, Hsp90aa1, Tubb4b, Cdkn1b, Ccnd1
		Signaling by Non-Receptor Tyrosine Kinases	Socs3, Ubc, Cdkn1b, Ccnd1
		HSP90 chaperone cycle for steroid hormone receptors (SHR)	Tuba1b, Hsp90aa1, Tubb4b, Nr3c1
		Formation of the ternary complex, and subsequently, the 43S complex	Rps3a1, Rps28, Rps2, Rps18
		The role of G1/S in G2/M progression after G2 checkpoint	Cdkn1a, Tuba1b, Ubc, Hsp90aa1, Tubb4b
		SCF(Skp2)-mediated degradation of p27/p21	Cdkn1a, Ubc, Cdkn1b, Ccnd1
		Nonsense-Mediated Decay (NMD)	Rpl41, Rps3a1, Rps28, Rps2, Rps18, Rpl32
		Death Receptor Signalling	Nfkbia, Fas, Ubc, Tnfsf10, Tnf, Arhgef2
		RHO GTPases activate IQGAPs	Actb, Tuba1b, Cttna1, Tubb4b
		Neutrophil degranulation	S100a9, S100a8, Lrg1, Ptpnb, Cxcl2, Fth1, Hsp90aa1, Cd97, Qsox1, Sptan1
Alveolar Macrophages 1	76 (33/43)	Immune system	Lyz2, S100a8, S100a9, Mrc1, Cd74, Cd63, Cxcl3, Clec4d, Cd36, Creg1
		Regulation of TLR by endogenous ligand	S100a8, S100a9, Cd36, Tlr2
		Detoxification of Reactive Oxygen Species	Txnrd1, Prdx1, Gpx1
		Hemostasis	Cd74, Cd63, Slc7a11, Fn1, Cd36, Srgu, Cd47, F10, Serpine1, Trem1
		Cell surface interactions at the vascular wall	Cd74, Slc7a11, Fn1, Cd47, Trem1
		Neutrophil degranulation	Lyz2, S100a8, S100a9, Cd63, Cxcl3, Clec4d, Cd36, Creg1, Cd47, Fcgr4
Neutrophils	44 (25/19)	Immune system	S100a8, Lyz2, S100a9, Mmp8, Lrg1, Fth1, Ifitm2, Prdx5, Pglyrp1, Hp
		Keratinization	Stfa21l, BC100530, Stfa2, Gm5483, Stfa1
		Neutrophil degranulation	S100a8, Lyz2, S100a9, Mmp8, Lrg1, Fth1, Prdx5, Pglyrp1, Hp
Endothelial Cells (Kdr Marker)	21 (12/9)	Metal sequestration by antimicrobial proteins	S100a8, S100a9
B Cells	17 (8/9)	Translation	Rps3a1, Rps26, Rps8
		Ribosomal scanning and start codon recognition	Rps3a1, Rps26, Rps8
		Nonsense-Mediated Decay (NMD)	Rps3a1, Rps26, Rps8
Monocytes 2	17 (7/10)	Innate immune system	Lyz2, S100a8, S100a9, C5ar1, Mmp8, Lrg1
		Regulation of TLR by endogenous ligand	S100a8, S100a9
		Neutrophil degranulation	Lyz2, S100a8, S100a9, C5ar1, Mmp8, Lrg1
Monocytes 1	15 (7/8)	Antimicrobial peptides	Lyz2, S100a8, S100a9, Lyz1
		Regulation of TLR by endogenous ligand	S100a8, S100a9
NK Cells	14 (9/5)	Metal sequestration by antimicrobial proteins	S100a8, S100a9
		Regulation of TLR by endogenous ligand	S100a8, S100a9
T Cells	10 (6/4)	none	Rps3a3, Rps3a1, Gm10036, mt-Rnr2, mt-Rnr1, Rgcc, Macf1, Slc38a2, Tmsb10, Irf2bp2
Endothelial Cells (Vwf Marker)	5 (1/4)	Antimicrobial peptides	S100a9, S100a8
		Regulation of TLR by endogenous ligand	S100a9, S100a8
Alveolar Macrophages 2	2 (2)	none	Lyz2, Nfe2l2
Dendritic Cells	2 (1/1)	none	Rps3a3, Rps3a1
Endothelial Cells 2	1 (1)	none	Rps3a3
Endothelial Cells 3	1 (1)	none	Rps3a3
Interstitial Macrophages	1 (1)	none	Lyz2

Table 3-7: DEP-treated KO vs. DEP-treated control DEGs and enriched pathways. Significantly enriched pathways (FDR < 0.05) were acquired from REACTOME analysis. In the “# of DEGs” column, green represents the number of upregulated genes in the KO mice, while in the “Pathway DEGs” column, green represents an upregulated gene in the KO mice. For those same columns, red represents downregulation in the KO mice. *Up to the top ten DEGs are listed per pathway, per cell type.

References

- Adhyapak, S. M. and V. R. Parachuri (2014). "Stroke volume paradox in heart failure: mathematical validation." Asian Cardiovasc Thorac Ann **22**(3): 288-295.
- Alphonse, R. S., A. Vadivel, S. Zhong, S. McConaghy, R. Ohls, M. C. Yoder and B. Thebaud (2015). "The isolation and culture of endothelial colony-forming cells from human and rat lungs." Nat Protoc **10**(11): 1697-1708.
- Aoki, Y., H. Sato, N. Nishimura, S. Takahashi, K. Itoh and M. Yamamoto (2001). "Accelerated DNA adduct formation in the lung of the Nrf2 knockout mouse exposed to diesel exhaust." Toxicol Appl Pharmacol **173**(3): 154-160.
- Araujo, J. A., B. Barajas, M. Kleinman, X. Wang, B. J. Bennett, K. W. Gong, M. Navab, J. Harkema, C. Sioutas, A. J. Lusis and A. E. Nel (2008). "Ambient particulate pollutants in the ultrafine range promote early atherosclerosis and systemic oxidative stress." Circ Res **102**(5): 589-596.
- Asimakopoulos, G., P. L. Smith, C. P. Ratnatunga and K. M. Taylor (1999). "Lung injury and acute respiratory distress syndrome after cardiopulmonary bypass." Ann Thorac Surg **68**(3): 1107-1115.
- Banerjee, I., J. W. Fuseler, R. L. Price, T. K. Borg and T. A. Baudino (2007). "Determination of cell types and numbers during cardiac development in the neonatal and adult rat and mouse." Am J Physiol Heart Circ Physiol **293**(3): H1883-1891.
- Beyer, T. A., W. Xu, D. Teupser, U. auf dem Keller, P. Bugnon, E. Hildt, J. Thiery, Y. W. Kan and S. Werner (2008). "Impaired liver regeneration in Nrf2 knockout mice: role of ROS-mediated insulin/IGF-1 resistance." Embo j **27**(1): 212-223.
- Bhatia, M. and S. Moochhala (2004). "Role of inflammatory mediators in the pathophysiology of acute respiratory distress syndrome." J Pathol **202**(2): 145-156.
- Biswas, M. and J. Y. Chan (2010). "Role of Nrf1 in antioxidant response element-mediated gene expression and beyond." Toxicol Appl Pharmacol **244**(1): 16-20.
- Bodzioch, M., K. Lapicka-Bodzioch, B. Zapala, W. Kamysz, B. Kiec-Wilk and A. Dembinska-Kiec (2009). "Evidence for potential functionality of nuclearly-encoded humanin isoforms." Genomics **94**(4): 247-256.
- Bryant, D., L. Becker, J. Richardson, J. Shelton, F. Franco, R. Peshock, M. Thompson and B. Giroir (1998). "Cardiac failure in transgenic mice with myocardial expression of tumor necrosis factor-alpha." Circulation **97**(14): 1375-1381.
- Butler, A., P. Hoffman, P. Smibert, E. Papalexi and R. Satija (2018). "Integrating single-cell transcriptomic data across different conditions, technologies, and species." Nat Biotechnol **36**(5): 411-420.

Cesta, M. F. (2006). "Normal structure, function, and histology of the spleen." Toxicol Pathol **34**(5): 455-465.

Chan, K. and Y. W. Kan (1999). "Nrf2 is essential for protection against acute pulmonary injury in mice." Proc Natl Acad Sci U S A **96**(22): 12731-12736.

Chen, L. C. and J. S. Hwang (2005). "Effects of subchronic exposures to concentrated ambient particles (CAPs) in mice. IV. Characterization of acute and chronic effects of ambient air fine particulate matter exposures on heart-rate variability." Inhal Toxicol **17**(4-5): 209-216.

Cho, H. Y., A. E. Jedlicka, S. P. Reddy, T. W. Kensler, M. Yamamoto, L. Y. Zhang and S. R. Kleeberger (2002). "Role of NRF2 in protection against hyperoxic lung injury in mice." Am J Respir Cell Mol Biol **26**(2): 175-182.

Chuang, K. J., C. C. Chan, G. M. Shiao and T. C. Su (2005). "Associations between submicrometer particles exposures and blood pressure and heart rate in patients with lung function impairments." J Occup Environ Med **47**(11): 1093-1098.

Clausen, B. E., C. Burkhardt, W. Reith, R. Renkawitz and I. Forster (1999). "Conditional gene targeting in macrophages and granulocytes using LysMcre mice." Transgenic Res **8**(4): 265-277.

Cross, M. and R. Renkawitz (1990). "Repetitive sequence involvement in the duplication and divergence of mouse lysozyme genes." Embo j **9**(4): 1283-1288.

Deiuliis, J. A., T. Kampfrath, J. Zhong, S. Oghumu, A. Maiseyeu, L. C. Chen, Q. Sun, A. R. Satoskar and S. Rajagopalan (2012). "Pulmonary T cell activation in response to chronic particulate air pollution." Am J Physiol Lung Cell Mol Physiol **302**(4): L399-409.

Delfino, R. J., N. Staimer and N. D. Vaziri (2011). "Air pollution and circulating biomarkers of oxidative stress." Air Qual Atmos Health **4**(1): 37-52.

Devlin, R. B., A. J. Ghio, H. Kehrl, G. Sanders and W. Cascio (2003). "Elderly humans exposed to concentrated air pollution particles have decreased heart rate variability." Eur Respir J Suppl **40**: 76s-80s.

Di Valentin, E., C. Crahay, N. Garbacki, B. Hennuy, M. Gueders, A. Noel, J. M. Foidart, J. Grooten, A. Colige, J. Piette and D. Cataldo (2009). "New asthma biomarkers: lessons from murine models of acute and chronic asthma." Am J Physiol Lung Cell Mol Physiol **296**(2): L185-197.

Ensembl (2018). Transcript: Nfe2l2-201 ENSMUST00000102672.4, EMBL-EBI.

Foltz, C. J. and M. Ullman-Cullere (1999). "Guidelines for Assessing the Health and Condition of Mice." Lab Animal **28**(4).

Franks, T. J., T. V. Colby, W. D. Travis, R. M. Tuder, H. Y. Reynolds, A. R. Brody, W. V. Cardoso, R. G. Crystal, C. J. Drake, J. Engelhardt, M. Frid, E. Herzog, R. Mason, S. H. Phan, S.

H. Randell, M. C. Rose, T. Stevens, J. Serge, M. E. Sunday, J. A. Voynow, B. M. Weinstein, J. Whitsett and M. C. Williams (2008). "Resident cellular components of the human lung: current knowledge and goals for research on cell phenotyping and function." Proc Am Thorac Soc **5**(7): 763-766.

Gebhardt, C., J. Nemeth, P. Angel and J. Hess (2006). "S100A8 and S100A9 in inflammation and cancer." Biochem Pharmacol **72**(11): 1622-1631.

Gleason, W. L. and E. Braunwald (1962). "Studies on the first derivative of the ventricular pressure pulse in man." J Clin Invest **41**: 80-91.

Graff, D. W., W. E. Cascio, A. Rappold, H. Zhou, Y. C. Huang and R. B. Devlin (2009). "Exposure to concentrated coarse air pollution particles causes mild cardiopulmonary effects in healthy young adults." Environ Health Perspect **117**(7): 1089-1094.

Grommes, J. and O. Soehnlein (2011). "Contribution of neutrophils to acute lung injury." Mol Med **17**(3-4): 293-307.

Grunig, G., L. M. Marsh, N. Esmaeil, K. Jackson, T. Gordon, J. Reibman, G. Kwapiszewska and S. H. Park (2014). "Perspective: ambient air pollution: inflammatory response and effects on the lung's vasculature." Pulm Circ **4**(1): 25-35.

Han, X., R. Wang, Y. Zhou, L. Fei, H. Sun, S. Lai, A. Saadatpour, Z. Zhou, H. Chen, F. Ye, D. Huang, Y. Xu, W. Huang, M. Jiang, X. Jiang, J. Mao, Y. Chen, C. Lu, J. Xie, Q. Fang, Y. Wang, R. Yue, T. Li, H. Huang, S. H. Orkin, G. C. Yuan, M. Chen and G. Guo (2018). "Mapping the Mouse Cell Atlas by Microwell-Seq." Cell **172**(5): 1091-1107.e1017.

Harada, C., T. Kawaguchi, S. Ogata-Suetsugu, M. Yamada, N. Hamada, T. Maeyama, R. Souzaki, T. Tajiri, T. Taguchi, K. Kuwano and Y. Nakanishi (2011). "EGFR tyrosine kinase inhibition worsens acute lung injury in mice with repairing airway epithelium." Am J Respir Crit Care Med **183**(6): 743-751.

Heng, T. S. and M. W. Painter (2008). "The Immunological Genome Project: networks of gene expression in immune cells." Nat Immunol **9**(10): 1091-1094.

Hoit, B. D. (1998). Invasive Hemodynamic Studies in Open and Closed Chest Mice. Cardiovascular Physiology in the Genetically Engineered Mouse. B. D. Hoit and R. A. Walsh. Norwell, Massachusetts, Kluwer Academic Publishers: 111-124.

Hoit, B. D., N. Ball and R. A. Walsh (1997). "Invasive hemodynamics and force-frequency relationships in open- versus closed-chest mice." Am J Physiol **273**(5 Pt 2): H2528-2533.

Ishikawa, T. (2014). "Genetic polymorphism in the NRF2 gene as a prognosis marker for cancer chemotherapy." Front Genet **5**: 383.

Jonasson, L., H. Grauen Larsen, A. K. Lundberg, B. Gullstrand, A. A. Bengtsson and A. Schiöpu (2017). "Stress-induced release of the S100A8/A9 alarmin is elevated in coronary artery disease patients with impaired cortisol response." Sci Rep **7**(1): 17545.

Kadl, A., A. K. Meher, P. R. Sharma, M. Y. Lee, A. C. Doran, S. R. Johnstone, M. R. Elliott, F. Gruber, J. Han, W. Chen, T. Kensler, K. S. Ravichandran, B. E. Isakson, B. R. Wamhoff and N. Leitinger (2010). "Identification of a novel macrophage phenotype that develops in response to atherogenic phospholipids via Nrf2." Circ Res **107**(6): 737-746.

Kensler, T. W., N. Wakabayashi and S. Biswal (2007). "Cell survival responses to environmental stresses via the Keap1-Nrf2-ARE pathway." Annu Rev Pharmacol Toxicol **47**: 89-116.

Kobayashi, T., Y. Watanabe, Y. Saito, D. Fujioka, T. Nakamura, J. E. Obata, Y. Kitta, T. Yano, K. Kawabata, K. Watanabe, H. Mishina, S. Ito and K. Kugiyama (2010). "Mice lacking the glutamate-cysteine ligase modifier subunit are susceptible to myocardial ischaemia-reperfusion injury." Cardiovasc Res **85**(4): 785-795.

Koike, E., S. Hirano, N. Shimojo and T. Kobayashi (2002). "cDNA microarray analysis of gene expression in rat alveolar macrophages in response to organic extract of diesel exhaust particles." Toxicol Sci **67**(2): 241-246.

Leung, L., M. Kwong, S. Hou, C. Lee and J. Y. Chan (2003). "Deficiency of the Nrf1 and Nrf2 transcription factors results in early embryonic lethality and severe oxidative stress." J Biol Chem **278**(48): 48021-48029.

Li, N., J. Alam, M. I. Venkatesan, A. Eiguren-Fernandez, D. Schmitz, E. Di Stefano, N. Slaughter, E. Killeen, X. Wang, A. Huang, M. Wang, A. H. Miguel, A. Cho, C. Sioutas and A. E. Nel (2004). "Nrf2 is a key transcription factor that regulates antioxidant defense in macrophages and epithelial cells: protecting against the proinflammatory and oxidizing effects of diesel exhaust chemicals." J Immunol **173**(5): 3467-3481.

Li, Y. J., H. Takizawa, A. Azuma, T. Kohyama, Y. Yamauchi, S. Takahashi, M. Yamamoto, T. Kawada, S. Kudoh and I. Sugawara (2008). "Disruption of Nrf2 enhances susceptibility to airway inflammatory responses induced by low-dose diesel exhaust particles in mice." Clin Immunol **128**(3): 366-373.

Liu, J., X. Ye, D. Ji, X. Zhou, C. Qiu, W. Liu and L. Yu (2018). "Diesel exhaust inhalation exposure induces pulmonary arterial hypertension in mice." Environ Pollut **237**: 747-755.

Long, S. S. (2012). Respiratory Tract Symptom Complexes. Principles and Practice of Pediatric Infectious Diseases. S. S. Long. New York, Elsevier Health Sciences: 162-171.

Mackness, M. I., P. N. Durrington and B. Mackness (2004). "The role of paraoxonase 1 activity in cardiovascular disease: potential for therapeutic intervention." Am J Cardiovasc Drugs **4**(4): 211-217.

- Macosko, E. Z., A. Basu, R. Satija, J. Nemesh, K. Shekhar, M. Goldman, I. Tirosh, A. R. Bialas, N. Kamitaki, E. M. Martersteck, J. J. Trombetta, D. A. Weitz, J. R. Sanes, A. K. Shalek, A. Regev and S. A. McCarroll (2015). "Highly Parallel Genome-wide Expression Profiling of Individual Cells Using Nanoliter Droplets." Cell **161**(5): 1202-1214.
- Mannaa, F. A. and K. G. Abdel-Wahhab (2016). "Physiological potential of cytokines and liver damages." Hepatoma Research **2**: 131-143.
- Marzec, J. M., J. D. Christie, S. P. Reddy, A. E. Jedlicka, H. Vuong, P. N. Lancken, R. Aplenc, T. Yamamoto, M. Yamamoto, H. Y. Cho and S. R. Kleeberger (2007). "Functional polymorphisms in the transcription factor NRF2 in humans increase the risk of acute lung injury." Faseb j **21**(9): 2237-2246.
- Murphy, K., P. Travers and M. Walport (2008). Janeway's Immunobiology. New York, Garland Science, Taylor & Francis Group, LLC.
- Park, S. K., M. S. O'Neill, P. S. Vokonas, D. Sparrow and J. Schwartz (2005). "Effects of air pollution on heart rate variability: the VA normative aging study." Environ Health Perspect **113**(3): 304-309.
- Pasipoularides, A. (2018). "Challenges and Controversies in Hypertrophic Cardiomyopathy: Clinical, Genomic and Basic Science Perspectives." Rev Esp Cardiol (Engl Ed) **71**(3): 132-138.
- Pawar, R. D., A. Ramanjaneyulu, O. P. Kulkarni, M. Lech, S. Segerer and H. J. Anders (2007). "Inhibition of Toll-like receptor-7 (TLR-7) or TLR-7 plus TLR-9 attenuates glomerulonephritis and lung injury in experimental lupus." J Am Soc Nephrol **18**(6): 1721-1731.
- Peel, J. L., M. Klein, W. D. Flanders, J. A. Mulholland, G. Freed and P. E. Tolbert (2011). "Ambient air pollution and apnea and bradycardia in high-risk infants on home monitors." Environ Health Perspect **119**(9): 1321-1327.
- Peters, A., S. Perz, A. Doring, J. Stieber, W. Koenig and H. E. Wichmann (1999). "Increases in heart rate during an air pollution episode." Am J Epidemiol **150**(10): 1094-1098.
- Petrie, M. C., L. Caruana, C. Berry and J. J. McMurray (2002). "'Diastolic heart failure' or heart failure caused by subtle left ventricular systolic dysfunction?" Heart **87**(1): 29-31.
- Pinto, A. R., A. Ilinykh, M. J. Ivey, J. T. Kuwabara, M. L. D'Antoni, R. Debuque, A. Chandran, L. Wang, K. Arora, N. A. Rosenthal and M. D. Tallquist (2016). "Revisiting Cardiac Cellular Composition." Circ Res **118**(3): 400-409.
- Pope, C. A., 3rd, R. L. Verrier, E. G. Lovett, A. C. Larson, M. E. Raizenne, R. E. Kanner, J. Schwartz, G. M. Villegas, D. R. Gold and D. W. Dockery (1999). "Heart rate variability associated with particulate air pollution." Am Heart J **138**(5 Pt 1): 890-899.

Rangasamy, T., C. Y. Cho, R. K. Thimmulappa, L. Zhen, S. S. Srisuma, T. W. Kensler, M. Yamamoto, I. Petrache, R. M. Tudor and S. Biswal (2004). "Genetic ablation of Nrf2 enhances susceptibility to cigarette smoke-induced emphysema in mice." J Clin Invest **114**(9): 1248-1259.

Raphael, R., D. Purushotham, C. Gastonguay, M. A. Chesnik, W. M. Kwok, H. E. Wu, S. J. Shah, S. P. Mirza and J. L. Strande (2016). "Combining patient proteomics and in vitro cardiomyocyte phenotype testing to identify potential mediators of heart failure with preserved ejection fraction." J Transl Med **14**: 18.

Reddy, N. M., H. R. Potteti, T. J. Mariani, S. Biswal and S. P. Reddy (2011). "Conditional deletion of Nrf2 in airway epithelium exacerbates acute lung injury and impairs the resolution of inflammation." Am J Respir Cell Mol Biol **45**(6): 1161-1168.

Reddy, Y. N. V., V. Melenovsky, M. M. Redfield, R. A. Nishimura and B. A. Borlaug (2016). "High-Output Heart Failure: A 15-Year Experience." J Am Coll Cardiol **68**(5): 473-482.

Risom, L., P. Moller and S. Loft (2005). "Oxidative stress-induced DNA damage by particulate air pollution." Mutat Res **592**(1-2): 119-137.

Satija, R., J. A. Farrell, D. Gennert, A. F. Schier and A. Regev (2015). "Spatial reconstruction of single-cell gene expression data." Nat Biotechnol **33**(5): 495-502.

Strieter, R. M. and S. L. Kunkel (1994). "Acute lung injury: the role of cytokines in the elicitation of neutrophils." J Investig Med **42**(4): 640-651.

Strom, J. and Q. M. Chen (2017). "Loss of Nrf2 promotes rapid progression to heart failure following myocardial infarction." Toxicol Appl Pharmacol **327**: 52-58.

Sussan, T. E., T. Rangasamy, D. J. Blake, D. Malhotra, H. El-Haddad, D. Bedja, M. S. Yates, P. Kombairaju, M. Yamamoto, K. T. Liby, M. B. Sporn, K. L. Gabrielson, H. C. Champion, R. M. Tudor, T. W. Kensler and S. Biswal (2009). "Targeting Nrf2 with the triterpenoid CDDO-imidazole attenuates cigarette smoke-induced emphysema and cardiac dysfunction in mice." Proc Natl Acad Sci U S A **106**(1): 250-255.

The Jackson Laboratory (2013). "12 Things You Don't Know About Cre-Lox." <https://www.jax.org/news-and-insights/jax-blog/2013/september/a-dozen-facts-you-didnt-know-about-cre-lox> 2018.

van der Maaten, L. and G. Hinton (2008). "Visualizing Data using t-SNE." Journal of Machine Learning Research **9**: 2579-2605.

Watson, A. D., J. A. Berliner, S. Y. Hama, B. N. La Du, K. F. Faull, A. M. Fogelman and M. Navab (1995). "Protective effect of high density lipoprotein associated paraoxonase. Inhibition of the biological activity of minimally oxidized low density lipoprotein." J Clin Invest **96**(6): 2882-2891.

Widlitz, A. and R. J. Barst (2003). "Pulmonary arterial hypertension in children." Eur Respir J **21**(1): 155-176.

Wilson, J. N., J. D. Pierce and R. L. Clancy (2001). "Reactive oxygen species in acute respiratory distress syndrome." Heart Lung **30**(5): 370-375.

Wu, J., R. Lin, J. Huang, W. Guan, W. S. Oetting, P. Sriramarao and M. N. Blumenthal (2014). "Functional Fcγ receptor polymorphisms are associated with human allergy." PLoS One **9**(2): e89196.

Xue, P., Y. Hou, Y. Chen, B. Yang, J. Fu, H. Zheng, K. Yarborough, C. G. Woods, D. Liu, M. Yamamoto, Q. Zhang, M. E. Andersen and J. Pi (2013). "Adipose deficiency of Nrf2 in ob/ob mice results in severe metabolic syndrome." Diabetes **62**(3): 845-854.

Yamamoto, T., K. Yoh, A. Kobayashi, Y. Ishii, S. Kure, A. Koyama, T. Sakamoto, K. Sekizawa, H. Motohashi and M. Yamamoto (2004). "Identification of polymorphisms in the promoter region of the human NRF2 gene." Biochem Biophys Res Commun **321**(1): 72-79.

Yin, F., A. Lawal, J. Ricks, J. R. Fox, T. Larson, M. Navab, A. M. Fogelman, M. E. Rosenfeld and J. A. Araujo (2013). "Diesel exhaust induces systemic lipid peroxidation and development of dysfunctional pro-oxidant and pro-inflammatory high-density lipoprotein." Arterioscler Thromb Vasc Biol **33**(6): 1153-1161.

Zhang, M., K. Nakamura, S. Kageyama, A. O. Lawal, K. W. Gong, M. Bhetaratana, T. Fujii, D. Sulaiman, H. Hirao, S. Bolisetty, J. W. Kupiec-Weglinski and J. A. Araujo (2018). "Myeloid HO-1 modulates macrophage polarization and protects against ischemia-reperfusion injury." JCI Insight **3**(19).

Zhou, P. and W. T. Pu (2016). Recounting Cardiac Cellular Composition. Circ Res. United States. **118**: 368-370.

Zile, M. R., W. H. Gaasch, J. D. Carroll, M. D. Feldman, G. P. Aurigemma, G. L. Schaer, J. K. Ghali and P. R. Liebson (2001). "Heart failure with a normal ejection fraction: is measurement of diastolic function necessary to make the diagnosis of diastolic heart failure?" Circulation **104**(7): 779-782.

CHAPTER 4 –
CARDIOVASCULAR EFFECTS OF ELECTRONIC CIGARETTES

Introduction

The health effects of electronic cigarettes (e-cigs) is a growing field of study. To this day, we still have a limited knowledge base as to what impacts, adverse or not, these new devices have on our health as described in Chapter 1. The study in this chapter is a collaborative project between the labs of Holly Middlekauff, M.D., and Jesus Araujo, M.D., Ph.D., to assess the clinical and biochemical markers of cardiovascular health following e-cig use.

In this study, 42 volunteers, 23 of whom were habitual e-cig users and 19 were non-smokers, underwent clinical measures of heart rate variability and assessment of oxidative stress in the circulating blood. Dr. Middlekauff's team led the clinical aspect, while our lab was in charge of the biochemical assays. My role was to lead the processing of the subjects' nearly 200 plasma samples and perform the downstream assays, which included testing for hemolysis, low-density lipoprotein (LDL) oxidizability, high-density lipoprotein (HDL) antioxidant capacity, and paraoxonase 1 (PON1) activity.

I assessed the degree of hemolysis, LDL oxidizability, and HDL antioxidant capacity by performing various assays together with Fen Yin, Ph.D. The level of hemolysis, which is the rupture of red blood cells, was quantified by measuring the plasma sample's absorbance at 410 nm. A high level of red blood cell lysis, which is often due to issues during the blood draw or processing of the blood, can adversely affect the readings of other assays and so is an important quality control measure for our samples. The LDL oxidizability and HDL antioxidant capacity assays test the functional aspects of LDL and HDL, respectively, which are lipoproteins that act conversely to each other. LDL oxidation and accumulation lead to atherosclerotic plaque

formation and cardiovascular disease, while HDL has antioxidant and anti-inflammatory properties, and transports cholesterol back from the tissues to the liver for excretion. Both the LDL and HDL assays have been described previously (Yin et al. 2013). Briefly, dextran sulfate beads were used to pull down ApoB-containing molecules such as LDL (Yin et al. 2013). The ApoB-rich fraction underwent oxidization by air, and the level of DCF (2', 7'-dichlorofluorescein) fluorescence was measured and reported as LDL oxidizability (Yin et al. 2013). For the HDL antioxidant capacity assay, the supernatant fraction that was not pulled down by the dextran sulfate beads, which would contain molecules that do not contain ApoB, such as HDL, was used (Yin et al. 2013). A standard concentration of LDL was added to the HDL-enriched fraction, and the ability of HDL to prevent the oxidation of LDL was measured with the DCF assay (Yin et al. 2013).

I also performed the PON1 activity assay on all samples. The method for this assay was described in Chapter 3 and is also described in the methods section of the publication included in this chapter. Briefly, the PON1 activity assay measures the capacity of plasma samples to convert paraoxon to *p*-nitrophenol, as measured by kinetic absorbance readings at 405 nm over a 15-minute period (Moheimani et al. 2017). High PON1 activity has been associated with reduced risk for cardiovascular disease (Mackness et al. 2004). My contributions, as detailed above, earned a co-first authorship in the attached *Journal of the American Medical Association (JAMA) Cardiology* article, which overall demonstrated that chronic e-cig use decreased heart rate variability and increased systemic oxidative stress evidenced by increased LDL oxidizability (Moheimani et al. 2017).

Since the publication of this study, our labs have demonstrated that even acute use of nicotine-containing e-cigs induces effects on heart rate variability, which led to a co-authored

publication in the *Journal of the American Heart Association (JAHA)* (Moheimani et al. 2017). Additionally, we have also shown that chronic e-cig use also affects organs besides the heart; in our publication in *Physiological Reports*, habitual e-cig users exhibited increased metabolic activity in the spleen as well as the aorta, suggesting that e-cig use leads to activation of inflammatory cells (Boas et al. 2017).

What follows is our JAMA Cardiology article and corresponding supplemental material, which is reproduced with permission from JAMA Cardiology. 2017. 2(3): 278-284. Copyright © 2017 American Medical Association. All rights reserved.

Increased Cardiac Sympathetic Activity and Oxidative Stress in Habitual Electronic Cigarette Users

Implications for Cardiovascular Risk

Roya S. Moheimani, BS; May Bhetraratana, MHS; Fen Yin, PhD; Kacey M. Peters, BS; Jeffrey Gornbein, DrPH; Jesus A. Araujo, MD, PhD; Holly R. Middlekauff, MD

IMPORTANCE Electronic cigarettes (e-cigarettes) have gained unprecedented popularity, but virtually nothing is known about their cardiovascular risks.

OBJECTIVE To test the hypothesis that an imbalance of cardiac autonomic tone and increased systemic oxidative stress and inflammation are detectable in otherwise healthy humans who habitually use e-cigarettes.

DESIGN, SETTING, AND PARTICIPANTS Cross-sectional case-control study of habitual e-cigarette users and nonuser control individuals from 2015 to 2016 at the University of California, Los Angeles. Otherwise healthy habitual e-cigarette users between the ages of 21 and 45 years meeting study criteria, including no current tobacco cigarette smoking and no known health problems or prescription medications, were eligible for enrollment. Healthy volunteers meeting these inclusion criteria who were not e-cigarette users were eligible to be enrolled as control individuals. A total of 42 participants meeting these criteria were enrolled in the study including 23 self-identified habitual e-cigarette users and 19 self-identified non-tobacco cigarette, non-e-cigarette user control participants.

MAIN OUTCOMES AND MEASURES Heart rate variability components were analyzed for the high-frequency component (0.15-0.4 Hz), an indicator of vagal activity, the low-frequency component (0.04-0.15 Hz), a mixture of both vagal and sympathetic activity, and the ratio of the low frequency to high frequency, reflecting the cardiac sympathovagal balance. Three parameters of oxidative stress were measured in plasma: (1) low-density lipoprotein oxidizability, (2) high-density lipoprotein antioxidant/anti-inflammatory capacity, and (3) paraoxonase-1 activity.

RESULTS Of the 42 participants, 35% were women, 35% were white, and the mean age was 27.6 years. The high-frequency component was significantly decreased in the e-cigarette users compared with nonuser control participants (mean [SEM], 46.5 [3.7] nu vs 57.8 [3.6] nu; $P = .04$). The low-frequency component (mean [SEM], 52.7 [4.0] nu vs 39.9 [3.8] nu; $P = .03$) and the low frequency to high frequency ratio (mean [SEM], 1.37 [0.19] vs 0.85 [0.18]; $P = .05$) were significantly increased in the e-cigarette users compared with nonuser control participants, consistent with sympathetic predominance. Low-density lipoprotein oxidizability, indicative of the susceptibility of apolipoprotein B-containing lipoproteins to oxidation, was significantly increased in e-cigarette users compared with nonuser control individuals (mean [SEM], 3801.0 [415.7] U vs 2413.3 [325.0] U; $P = .01$) consistent with increased oxidative stress, but differences in high-density antioxidant/anti-inflammatory capacity and paraoxonase-1 activity were not significant.

CONCLUSIONS AND RELEVANCE In this study, habitual e-cigarette use was associated with a shift in cardiac autonomic balance toward sympathetic predominance and increased oxidative stress, both associated with increased cardiovascular risk.

JAMA Cardiol. 2017;2(3):278-285. doi:10.1001/jamacardio.2016.5303
Published online February 1, 2017. Corrected on March 22, 2017.

← Editorial page 237

+ Supplemental content

Author Affiliations: David Geffen School of Medicine, University of California, Los Angeles (Moheimani); Division of Cardiology, Department of Medicine, David Geffen School of Medicine, University of California, Los Angeles (Bhetraratana, Yin, Peters, Araujo, Middlekauff); Department of Biomathematics, David Geffen School of Medicine, University of California, Los Angeles (Gornbein); Department of Environmental Health Sciences, School of Public Health, University of California, Los Angeles (Araujo).

Corresponding Author: Holly R. Middlekauff, MD, Division of Cardiology, Department of Medicine, David Geffen School of Medicine, University of California, Los Angeles, 650 Charles Young Dr S, A2-237 CHS, Los Angeles, CA 90025 (hmiddlekauff@mednet.ucla.edu).

jamacardiology.com

Copyright 2017 American Medical Association. All rights reserved.

Electronic cigarettes (e-cigarettes), first marketed in the United States in 2006, have gained unprecedented popularity, especially among young people.^{1,2} E-cigarettes are not actually cigarettes at all: there is no combustion and they contain no tobacco. Electronic cigarettes are handheld devices that, when puffed, deliver a heated, aerosolized mixture of nicotine, flavorings, and a humectant into the mouth and lungs of the user. Electronic cigarettes have created significant controversy in the medical community. They have been viewed as either a safer alternative to lethal tobacco cigarettes or as a gateway to expanding tobacco cigarette addiction.³⁻⁵ Unfortunately, scientific data supporting either side of the controversy are sparse.

More than 50 years ago, based on decades of observational data in habitual tobacco cigarette users, the Surgeon General of the United States warned the public about the lethality of tobacco cigarettes.⁶ Only years later were the mechanisms by which tobacco cigarettes led to adverse cardiovascular effects uncovered such as increased oxidative stress and inflammation, increased sympathetic activity, and enhanced platelet activity.⁷⁻⁹ Although tobacco cigarettes are widely recognized as the most common preventable cause of cardiovascular disease in the world, virtually nothing is known about the cardiovascular risks of e-cigarettes. Rather than wait decades for epidemiological data in habitual e-cigarette users to become available, we reasoned that investigations into several of the known mechanisms by which tobacco cigarettes increase cardiovascular risk would provide insights in the health risks of e-cigarettes.

In this study of habitual e-cigarette users, we focus on 2 critical mechanisms by which tobacco cigarettes are known to promote cardiovascular disease: (1) a shift in the cardiac sympathetic-vagal balance toward sympathetic predominance as assessed by heart rate variability (HRV)⁹ and (2) increased systemic oxidative stress and inflammation.⁸ Abnormal HRV is present in tobacco cigarette smokers^{10,11} and has been shown in populations with and without known cardiac disease to identify those at increased risk for myocardial infarction and sudden cardiac death.¹²⁻¹⁴ Additionally, increased oxidative stress and inflammation are major mechanisms by which tobacco cigarettes initiate and propagate atherosclerosis. Each puff of tobacco cigarette smoke contains greater than 10¹⁵ free radicals.¹⁵ This promotes oxidative modification of low-density lipoprotein (LDL). Oxidized LDL is then taken up by macrophages forming foam cells, the instigators of atherosclerosis.⁸ The purpose of this study was to test the hypothesis that an imbalance of cardiac autonomic tone and increased systemic oxidative stress and inflammation are detectable in otherwise healthy humans who habitually use e-cigarettes.

Methods

Study Population

Otherwise healthy habitual e-cigarette users between the ages of 21 and 45 years, who had used e-cigarettes most days for a minimum of 1 year, were eligible for the study if they met the following criteria: (1) no current tobacco cigarette smoking, (2) nonobese (body mass index ≤ 30 [calculated as weight in kilograms divided by height in meters squared]), (3) no known

Key Points

Question Do habitual electronic cigarette users have increased cardiac sympathetic activity and oxidative stress, both risk factors for future adverse cardiac events?

Findings In this cross-sectional case-control study of 42 otherwise healthy habitual electronic cigarette users and nonuser control individuals, heart rate variability was shifted toward increased sympathetic predominance, with the low frequency to high frequency ratio significantly increased. Furthermore, low-density lipoprotein oxidizability, which is a measure of oxidative stress, was significantly increased in habitual electronic cigarette users.

Meaning Habitual electronic cigarette use is associated with physiologic effects. Further research into potential adverse health effects of electronic cigarettes is warranted.

health problems, (4) not taking prescription medications except oral contraceptive pills, (5) alcoholic intake 2 or fewer drinks per day and no illicit drug use, and (6) not exposed to secondhand smoke or using licensed nicotine replacement therapies. Participants who were former tobacco cigarette smokers were eligible for the study if they had quit smoking more than 1 year prior to the study. Healthy volunteers meeting these inclusion criteria who were not e-cigarette users were eligible to be enrolled as control participants.

The experimental protocol was approved by the institutional review board at the University of California, Los Angeles, and written informed consent was obtained from each participant.

A total of 42 participants meeting these criteria were enrolled in the study including 23 self-identified habitual e-cigarette users and 19 self-identified non-tobacco cigarette, non-e-cigarette user control participants. Two of the 23 e-cigarette users were eliminated when their plasma carboxy-hemoglobin levels were found to be elevated, consistent with recent tobacco cigarette use.¹⁶ One of the 19 control participants was eliminated when his plasma cotinine level was elevated, consistent with recent exposure to cigarettes.

Because the goal of the study was to investigate the effects of chronic, not acute, e-cigarette exposure, participants were asked not to use their e-cigarette on the day of the study. After abstaining from caffeine and e-cigarette use for at least 12 hours, volunteers were placed in a supine position in a quiet, temperature-controlled (21°C) room in the Human Physiology Laboratory located in the University of California, Los Angeles Clinical Translational Research Center. No cell phones or digital stimuli were permitted during the study, and during data acquisition, there was no unnecessary talking.

Heart Rate Variability

To avoid the potential influence of circadian rhythm or menstrual cycle phases on autonomic tone, participants were studied midday (between 10 AM-2 PM), and women were studied during the early follicular phase, confirmed by plasma estrogen and progesterone levels. All women had negative urine pregnancy test results on the day of the study.

Electrocardiogram electrodes were placed on the chest, and the participants then rested undisturbed for 10 minutes. The

Table 1. Baseline Characteristics

Characteristic	Mean (SD)		P Value
	E-Cigarette User (n = 16)	Nonuser Control Participant (n = 18)	
Age, y	28.6 (1.4)	26.6 (1.5)	.35
Sex, No.			
Male	13	7	.02
Female	3	11	
BMI	25.2 (0.8)	23.0 (0.9)	.85
Race/ethnicity, No.			
African American	1	2	NA
Asian	2	3	NA
Hispanic	2	2	NA
White (non-Hispanic)	11	11	NA
Former smoker, No.	10	2	NA
Pack-years	1.9 (0.5)	0.6 (0.4)	NA
Interval since quitting, y	2.3 (0.8)	13 (7)	NA
E-cigarette use			
Min/d	241 (158)	NA	NA
Duration, y	1.6 (0.5)	NA	NA
SBP, mm Hg	115.8 (2.5)	109.0 (2.6)	.07
DBP, mm Hg	73.5 (2.3)	70.0 (2.0)	.27
MAP, mm Hg	87.6 (2.3)	83.0 (2.0)	.15
HR, bpm	64.0 (2.0)	63.0 (2.0)	.73

Abbreviations: BMI, body mass index (calculated as weight in kilograms divided by height in meters squared); bpm, beats per minute; DBP, diastolic blood pressure; HR, heart rate; MAP, mean arterial pressure; NA, not applicable; SBP, systolic blood pressure.

electrocardiogram was then recorded for 5 minutes during quiet rest and during 5 minutes of controlled breathing at a rate of 12 breaths per minute, a known stimulus for vagal tone.^{17,18} During controlled breathing, participants were cued visually by watching the second hand on a large clock to inhale every 5 seconds. Five-minute electrocardiogram recordings were analyzed using standard commercial software (LabChart7; Ad Instruments) in the frequency domain according to published guidelines.¹⁹ Three main spectral components were distinguished: high frequency (HF; 0.15-0.4 Hz), low frequency (LF; 0.04-0.15 Hz), and very LF (0.003-0.04 Hz). As recommended in the published guidelines, HRV is presented in normalized units to correct for differences in total power between the groups and in absolute units (microseconds squared).¹⁹ Time domain analysis was not applied to these recordings because a minimum of 20-minute recordings, and preferentially 24-hour recordings, are recommended for this methodology.¹⁹

Blood Tests

Venipuncture was performed by trained Clinical Translational Research Center nurses. Blood was drawn into preiced heparinized vacutainers and placed on ice. Blood was centrifuged to separate into plasma samples, which were frozen at -80°C in a cryopreservative solution²⁰ for later analysis for the following antioxidant parameters: (1) LDL oxidizability, indicative of susceptibility of apolipoprotein B-containing lipoproteins to oxidation as previously reported,²¹ (2) high-density lipoprotein (HDL) antioxidant/anti-inflammatory capacity, expressed as an HDL antioxidant in-

dex, which assesses the ability of HDL to inhibit LDL oxidation monitored by conversion of a nonfluorescent dihydrodichloro-fluorescein probe into the fluorescent dichlorofluorescein, performed as previously reported,^{22,23} and (3) paraoxonase-1 activity, a protective ester hydrolase enzyme associated with HDL in blood that prevents the formation of oxidized LDL,²⁴ assayed by its ability to hydrolyze paraoxon substrate,²³ described in detail in the eMethods in the Supplement.

Blood was also sent to the University of California, Los Angeles Clinical Laboratory for measurement of (1) nicotine ($t_{1/2}$ 1-2 hours) and the nicotine metabolite cotinine ($t_{1/2}$ 20 hours), (2) plasma carboxyhemoglobin (marker for tobacco cigarette but not e-cigarette use), and (3) inflammatory markers including C-reactive protein and fibrinogen.

Statistical Analysis

The Shapiro-Wilk statistic and normal quantile plots (not shown) were examined to determine whether continuous variables followed the normal distribution. If so, *P* values for comparing non-user control individuals with e-cigarette users were computed using the *t* test, and the mean and its standard error are reported. Otherwise, *P* values were computed using the nonparametric Wilcoxon rank sum test, and the median and its standard error are reported. For binary data, such as sex, *P* values for nonuser control vs e-cigarette user comparisons were computed using Fisher exact test. For within-group paired comparisons (eg, controlled breathing and spontaneous breathing), the parametric *P* value was computed via the paired *t* test and the nonparametric *P* value was computed via the Wilcoxon signed rank test. Associations between 2 continuous variables were assessed using the nonparametric Spearman correlation. Missing data values were not imputed; only the observed data were used. Differences or associations were considered statistically significant when *P* was less than or equal to .05.

Results

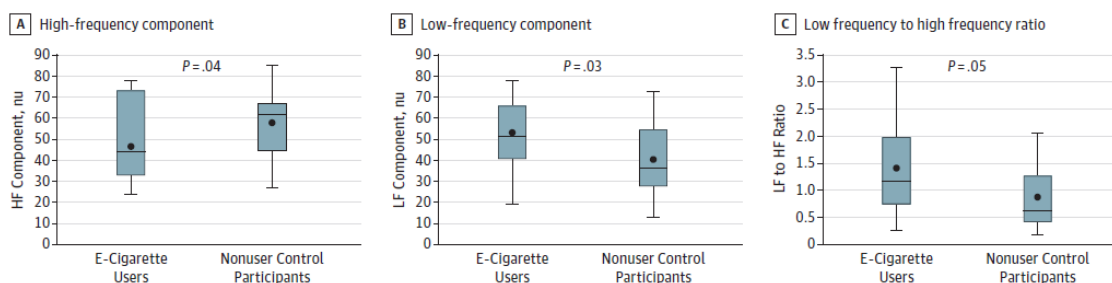
Baseline Characteristics

Although e-cigarette users were asked to abstain from using their e-cigarette on the day of the study, nicotine was present in plasma in 5 habitual e-cigarette users, consistent with recent use (range, 2.6-27.3 mg/L [to convert to micromoles per liter, multiply by 6.164]). These 5 e-cigarette users were excluded from further analysis; an analysis inclusive of these additional 5 e-cigarette users is available in eTables 1-5 in the Supplement. Plasma cotinine levels were elevated on the day of the study in 12 of the remaining 16 e-cigarette users, (range, 3.8-139 ng/mL, eFigure in the Supplement). Baseline characteristics of the 16 e-cigarette users and 18 nonusers are compared in Table 1. All parameters were within normal limits.

Heart Rate Variability

Heart rate variability components were analyzed for the HF component, an indicator of vagal activity, the LF component, a mixture of both vagal and sympathetic activity, and the ratio of the LF to HF, reflecting the cardiac sympathovagal balance (Figure 1; Table 2).¹⁹ The HF component was significantly decreased in

Figure 1. Heart Rate Variability Components



A. The high-frequency (HF) component, an indicator of vagal activity, was significantly decreased in the e-cigarette users compared with nonuser control individuals (mean [SEM], 46.5 [3.7] nu vs 57.8 [3.6] nu, $P = .04$). B and C. The low-frequency (LF) component (mean [SEM], 52.7 [4.0] nu vs 39.9 [3.8] nu, $P = .03$), and the LF to HF

ratio (1.37 [0.19] vs 0.85 [0.18], $P = .05$), were significantly increased in the e-cigarette users compared with nonuser controls, consistent with sympathetic predominance. These findings were present even in the absence of recent e-cigarette use, as verified by the absence of detectable nicotine in the plasma.

the e-cigarette users compared with nonuser control participants (mean [SEM], 46.5 [3.7] nu vs 57.8 [3.6] nu; $P = .04$). The LF component (mean [SEM], 52.7 [4.0] nu vs 39.9 [3.8] nu; $P = .03$), and the LF to HF ratio (mean [SEM], 1.37 [0.19] vs 0.85 [0.18]; $P = .05$), were significantly increased in the e-cigarette users compared with nonuser control participants, consistent with sympathetic predominance even in the absence of recent e-cigarette use as verified by the absence of detectable nicotine in the plasma (Figure 1). Controlling for e-cigarette or nonuser control group, sex had no significant effect (data not shown) on HRV components.

Correlation of HRV With E-Cigarette Burden

Plasma cotinine levels, an estimate of e-cigarette use, were significantly correlated with each of the HRV components: plasma cotinine levels were inversely related to HF component ($r_s, -0.34$; $P = .04$) and directly related to the LF component ($r_s, 0.35$; $P = .03$) and LF to HF ratio ($r_s, 0.36$; $P = .03$).

Controlled Breathing (Vagal Maneuver)

Within each group (e-cigarette users and nonuser control individuals), the HF component was significantly increased during controlled breathing compared with spontaneous breathing. Similarly, within each group, the LF and LF to HF ratio were decreased during controlled breathing compared with spontaneous breathing, consistent with a relative increase in cardiac vagal tone and decline in cardiac sympathetic influence (Figure 2). However, between e-cigarette users and nonuser groups, the magnitude of the increase in HF and decrease in LF and LF to HF ratio during controlled breathing were not different (Figure 2).

Oxidative Stress and Inflammation

Low-density lipoprotein oxidizability, indicative of susceptibility of apolipoprotein B-containing lipoproteins to oxidation, was significantly increased in e-cigarette users ($n = 12$) compared with nonuser control participants ($n = 18$) (mean [SEM], 3801.0 [415.7] U vs 2413.3 [325.0] U, $P = .01$), consistent with increased oxidative stress (Figure 3). Paraonase-1 activity tended to be lower in the e-cigarette users ($n = 12$) compared with nonuser control individuals ($n = 18$) (mean [SEM],

Table 2. Heart Rate Variability (Absolute Units)^a

HRV Parameter	Mean (SD), μs^2		P Value
	E-Cigarette User (n = 16)	Nonuser Control Participant (n = 18)	
High frequency	833.6 (295.7)	1376.5 (574.2)	.33
Low frequency	455.5 (258.2)	1316.0 (504.0)	.08
Very low frequency	896.0 (524.2)	987.1 (432.5)	.59
Total power	1652.0 (720.5)	4502.0 (1279.8)	.04

Abbreviation: HRV, heart rate variability.

^a Median values are displayed because these data followed a nonparametric distribution.

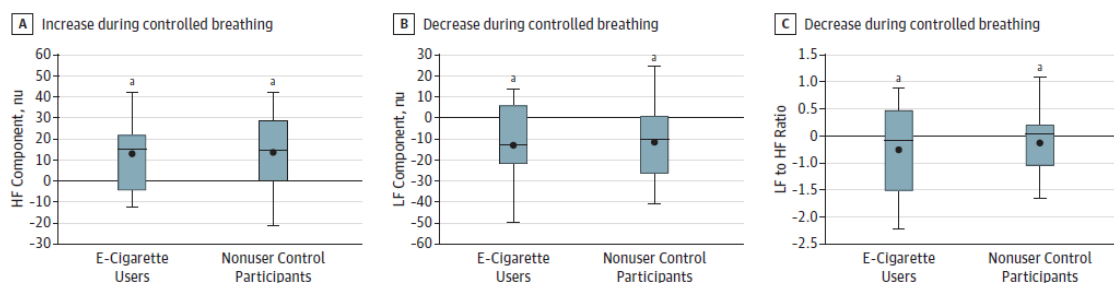
649.9 [125.7] nmol p-nitrophenol/min/mL vs 892.8 [110.0] nmol p-nitrophenol/min/mL; $P = .17$), consistent with decreased protection against oxidative stress, although this difference did not meet statistical significance. High-density lipoprotein antioxidant index was not different between the groups (e-cigarette users [$n = 12$] vs nonusers [$n = 18$]: mean [SEM], 0.42 [0.05] U vs 0.38 [0.04] U; $P = .55$). Inflammatory markers, including fibrinogen (e-cigarette users [$n = 15$] vs nonusers [$n = 17$]: mean [SEM], 270.9 [12.6] mg/dL vs 251.9 [10.4] mg/dL; $P = .24$ [to convert to micromoles per liter, multiply by 0.0294]) and C-reactive protein levels were not different between e-cigarette users and nonusers (abnormal in 3 e-cigarette users [$n = 15$] and 1 nonuser [$n = 17$]; $P = .15$).

Plasma cotinine levels were directly related to LDL oxidizability ($r_s, 0.35$; $P = .05$) but not the other indices of oxidative stress measured.

Discussion

The major new findings in this study are that in otherwise healthy, habitual e-cigarette users compared with nonsmoking healthy control participants (1) HRV components are shifted toward sympathetic predominance and decreased vagal tone, the pattern found in patients with increased cardiovascular risk, including tobacco cigarette smokers,^{10,12-14} (2) systemic oxidative

Figure 2. Heart Rate Variability During Controlled Breathing

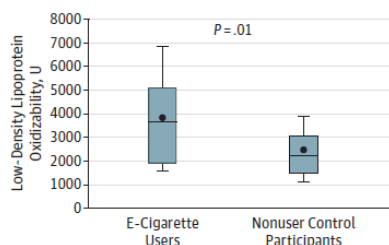


A. Within each group (e-cigarette users and nonuser control participants), the high-frequency (HF) component was significantly increased during controlled breathing compared with spontaneous breathing. Similarly, within each group, the low frequency (LF) (B), and LF to HF ratio (C) were decreased during controlled compared with spontaneous breathing, consistent with a relative increase in cardiac vagal and decline in cardiac sympathetic influence. However, between e-cigarette user

and nonuser groups, the magnitude of the increase in HF and decrease in LF and LF to HF ratio during controlled breathing were not different.

^a $P = .05$, within-group difference between controlled breathing and spontaneous breathing.

Figure 3. Oxidative Stress



Low-density lipoprotein oxidizability, indicative of susceptibility of apoB-containing lipoproteins to oxidation, was significantly increased in e-cigarette users ($n = 12$) compared with nonuser ($n = 18$) control participants (mean [SEM], 3801.0 [415.7] U vs 2413.3 [325.0] U, $P = .01$), consistent with increased oxidative stress.

stress is increased, and (3) abnormalities of both HRV and oxidative stress are directly associated with e-cigarette burden. Importantly, these findings are not attributable to a transient pharmacological effect of nicotine because plasma nicotine levels were nondetectable at the time of the study. These findings are important for 2 reasons: first, because both increased cardiac sympathetic activity and increased oxidative stress are known mechanisms by which tobacco cigarettes increase cardiovascular risk,^{8,9} these findings have critical implications for the long-term cardiac risks associated with habitual e-cigarette use. Second, these findings mandate a reexamination of aerosolized nicotine and its metabolites. Nicotine, which is the major bioactive ingredient in e-cigarette aerosol, with its metabolites, may harbor unrecognized, sustained adverse physiologic effects that lead to an increased cardiovascular risk profile in habitual e-cigarette users.

In the 1980s, clinical studies first recognized perturbations in HRV as a powerful independent predictor of increased mortality in patients following myocardial infarction.¹² These perturbations in HRV reflect a relative increase in cardiac sympathetic nerve activity and a decrease in vagal tone.¹⁹ Since these early

reports, abnormal HRV indicative of sympathetic predominance has been shown in numerous studies in diverse patient populations with and without known cardiac disease to identify patients who have increased cardiovascular mortality.^{14,25-28} In fact, this increased risk has been demonstrated to have a dose-response relationship, with the most severe HRV abnormalities conferring the greatest cardiovascular mortality.^{13,14} Adverse cardiovascular sequelae of increased sympathetic nerve activity include increased arrhythmia risk, heart failure, and fatal and nonfatal myocardial infarction.⁹

Habitual tobacco cigarette smokers have been found to have abnormal HRV, specifically, this same pattern of increased sympathetic cardiac activity accompanied by decreased cardiac vagal tone.¹⁸ This pattern of autonomic perturbation is found in habitual tobacco cigarette smokers who have abstained from tobacco cigarette smoking on the day of HRV measurement as well as in those who have smoked several tobacco cigarettes prior to the HRV measurement and in nonsmokers acutely and transiently exposed to secondhand smoke.^{11,29-31} Evidence supports the concept that nicotine exposure can alter HRV in tobacco cigarette smokers because acute oral nicotine ingestion in never-smokers also shifts the HRV balance toward sympathetic predominance.³² Acute nicotine exposure releases norepinephrine from postganglionic cardiac sympathetic nerve terminals, underlying this acute pharmacological effect.³³ Surprisingly, in tobacco cigarette smokers who refrain from smoking 8 hours prior to HRV measurement, the LF to HF ratio has also been reported to be shifted compared with nonsmoking control individuals, consistent with persistently increased cardiac sympathetic activity even in the absence of acute nicotine exposure.¹¹ Similarly, in our study of e-cigarette users, nicotine was not detectable in e-cigarette users at the time of the HRV recordings, consistent with a mechanism beyond the acute pharmacological effect of nicotine.

In this study, we also found evidence of increased oxidative stress in habitual e-cigarette users compared with nonusers. Low-density lipoprotein oxidizability is a measure of the susceptibility of LDL to oxidation, which increases in the presence of oxidative stress. The sensitivity of LDL to oxidation depends on its

antioxidant contents, which determine its antioxidant potential. It has been shown that patients with diabetes and smokers have increased LDL oxidation.³⁴ In addition, patients with diabetes have increased LDL oxidizability, as assessed by Cu²⁺-induced malondialdehyde formation in association with decreased LDL antioxidant potential, reflecting the presence of increased oxidative stress.³⁵ Therefore, LDL oxidizability constitutes a useful measure of early oxidative stress. Each puff of smoke from a combusted tobacco cigarette releases enormous quantities of free radicals, and evidence is accumulating that e-cigarette aerosol also carries significant oxidative stress burden.^{33,36} Lerner et al³⁶ have reported similar oxidants and reactive oxygen species reactivity in e-cigarette aerosols and tobacco cigarette smoke.³⁶ This oxidative stress reportedly led to a cytotoxic response in oral epithelial cells in vitro.³⁷ However, other reports showed significant variability between e-cigarette liquids, with only 1 in 11 liquids tested inducing significant oxidative stress in cultured human endothelial cells.³⁸ Nonetheless, it remains likely that the heated, aerosolized nicotine, the humectants (propylene glycol/glycerol), and/or flavorings, all known or potential airway irritants, could lead to the presence of reactive oxygen species in the human airway, in turn leading to systemic oxidative stress. Our e-cigarette users used a variety of flavored liquids and brands, all containing nicotine, suggestive of an oxidative effect that is ubiquitous from habitual e-cigarette use.

Limitations

Human studies rely on self-reporting for many of the behaviors that cannot be controlled when participants are away from the laboratory and thus are vulnerable to misstatements and misrecollections.³⁹ To circumvent this problem, we required biochemical verification of e-cigarette use and absence of tobacco cigarette use.^{16,39} Nonetheless, we cannot be completely certain that 1 or more of our participants was not surreptitiously consuming tobacco products. We did not perform toxicology screening to eliminate marijuana and other drug exposures. Quantifying e-cigarette exposure is more difficult than tobacco cigarette exposure, which can be quantified by the number of tobacco cigarettes smoked per day. Although we did ask e-cigarette users how much time per day they used their e-cigarettes and how much liquid they used per day, answers were vague and varied on repeated questioning and were unreliable overall. Although measured only once, plasma cotinine

levels seemed the most objective means to assess e-cigarette burden. There were more former smokers in the habitual e-cigarette user group compared with nonuser control individuals. This difference is unlikely to explain the difference in HRV or oxidative stress between the groups because several studies have confirmed that HRV components improve significantly, and cardiovascular risk similarly improves following tobacco cigarette cessation.⁴⁰⁻⁴⁴

Finally, the relative effect of tobacco cigarettes compared with e-cigarettes on autonomic balance and oxidative stress remains an important yet unanswered question. In contrast to our findings in e-cigarette users, Barutcu et al¹⁸ found that vagal modulation in response to controlled breathing was blunted in heavy tobacco cigarette smokers who had abstained from smoking the day of the study, compared with age-matched non-smoker control participants. In our study, vagal responses to controlled breathing were not different between e-cigarette users and nonusers, perhaps indicative of a less severe abnormality of autonomic function associated with e-cigarettes compared with tobacco cigarettes.

Conclusions

In summary, in this cross-sectional study of non-tobacco cigarette smoking adults who habitually use e-cigarettes compared with nonuser control participants, evidence is presented demonstrating that e-cigarette use is not harmless. Habitual e-cigarette use is associated with a shift in cardiac autonomic balance toward sympathetic predominance and increased oxidative stress, both associated with increased cardiovascular risk. Further studies are required to determine whether these risks are similar to those associated with habitual tobacco cigarette use. However, the nonlinear relationship between number of tobacco cigarettes smoked per day and cardiovascular risk suggests that there may be a low threshold above which underlying physiologic processes are saturated⁴⁵; habitual e-cigarette users may cross this threshold. On the basis of these studies, we can conclude that habitual e-cigarette use is associated with physiologic effects. Nonetheless, we cannot confirm causality on the basis of this single, small study; further research into the potential adverse cardiovascular health effects of e-cigarettes is warranted.

ARTICLE INFORMATION

Accepted for Publication: November 15, 2016.

Published Online: February 1, 2017.

doi:10.1001/jamacardio.2016.5303

Correction: This article was corrected on March 22, 2016, to reflect changes to the author contributions section.

Author Contributions: Dr Middlekauff had full access to all the data in the study and takes responsibility for the integrity of the data and the accuracy of the data analysis. Mss Moheimani and Bhetharatana contributed equally to the research and are considered cofirst authors. *Concept and design:* Moheimani, Araujo, Middlekauff.

Acquisition, analysis, or interpretation of data:

Moheimani, Bhetharatana, Yin, Peters, Gornbein, Araujo, Middlekauff.

Drafting of the manuscript: Moheimani, Middlekauff.

Critical revision of the manuscript for important intellectual content: Moheimani, Bhetharatana, Yin, Peters, Gornbein, Araujo, Middlekauff.

Statistical analysis: Moheimani, Gornbein.

Obtained funding: Araujo, Middlekauff.

Administrative, technical, or material support: Moheimani, Yin, Peters.

Supervision: Moheimani, Araujo, Middlekauff.

Conflict of Interest Disclosures: All authors have completed and submitted the ICMJE Form for Disclosure of Potential Conflicts of Interest and none were reported.

Funding/Support: This study was supported by the Tobacco-Related Disease Research Program under the contract number TRDRP-XT 320833 (Dr Middlekauff), American Heart Association, Western States Affiliate, Grant-in-Aid 15GRNT22930022 (Dr Middlekauff), the National Institute of Environmental Health Sciences, National Institutes of Health R56 ES016959-06 (Dr Araujo), Training Grant in Molecular Toxicology (Ms Bhetharatana), Irma and Norman Switzer Dean's Leadership in Health and Science Scholarship (Ms Moheimani) and the University of California, Los Angeles Clinical and Translational Science Institute grant UL1TR000124.

Role of the Funder/Sponsor: The funding sources had no role in the design and conduct of the study; collection, management, analysis, and interpretation of the data; preparation, review, or approval of the

manuscript; and decision to submit the manuscript for publication.

Disclaimer: The content is solely the responsibility of the authors and does not necessarily represent the official views of the National Institutes of Health.

Additional Contributions: We are grateful to G. Ramanathan, PhD, Department of Environmental Health Sciences, School of Public Health, University of California, Los Angeles, who contributed to the early stages of this work in blood collection and storage. No compensation was received.

REFERENCES

1. Bhatnagar A, Whitsel LP, Ribisl KM, et al; American Heart Association Advocacy Coordinating Committee, Council on Cardiovascular and Stroke Nursing, Council on Clinical Cardiology, and Council on Quality of Care and Outcomes Research. Electronic cigarettes: a policy statement from the American Heart Association. *Circulation*. 2014;130(16):1418-1436.
2. Singh T, Marynak K, Arrazola RA, Cox S, Rolle IV, King BA. Vital signs: exposure to electronic cigarette advertising among middle school and high school students: United States, 2014. *MMWR Morb Mortal Wkly Rep*. 2016;64(52):1403-1408.
3. Avdalovic MV, Murin S. POINT: does the risk of electronic cigarettes exceed potential benefits? Yes. *Chest*. 2015;148(3):580-582.
4. Middlekauff HR. COUNTERPOINT: does the risk of electronic cigarettes exceed potential benefits? No. *Chest*. 2015;148(3):582-584.
5. Green SH, Bayer R, Fairchild AL. Evidence, policy, and e-cigarettes: will England reframe the debate? *N Engl J Med*. 2016;374(14):1301-1303.
6. Schroeder SA, Koh HK. Tobacco control 50 years after the 1964 surgeon general's report. *JAMA*. 2014;311(2):141-143.
7. Ambrose JA, Barua RS. The pathophysiology of cigarette smoking and cardiovascular disease: an update. *J Am Coll Cardiol*. 2004;43(10):1731-1737.
8. Csordas A, Bernhard D. The biology behind the atherothrombotic effects of cigarette smoke. *Nat Rev Cardiol*. 2013;10(4):219-230.
9. Middlekauff HR, Park J, Moheimani RS. Adverse effects of cigarette and noncigarette smoke exposure on the autonomic nervous system: mechanisms and implications for cardiovascular risk. *J Am Coll Cardiol*. 2014;64(16):1740-1750.
10. Lucini D, Bertocchi F, Malliani A, Pagani M. A controlled study of the autonomic changes produced by habitual cigarette smoking in healthy subjects. *Cardiovasc Res*. 1996;31(4):633-639.
11. Hayano J, Yamada M, Sakakibara Y, et al. Short- and long-term effects of cigarette smoking on heart rate variability. *Am J Cardiol*. 1990;65(1):84-88.
12. Kleiger RE, Miller JP, Bigger JT Jr, Moss AJ. Decreased heart rate variability and its association with increased mortality after acute myocardial infarction. *Am J Cardiol*. 1987;59(4):256-262.
13. Tsuji H, Larson MG, Venditti FJ Jr, et al. Impact of reduced heart rate variability on risk for cardiac events. The Framingham Heart Study. *Circulation*. 1996;94(11):2850-2855.
14. Hillebrand S, Gast KB, de Mutsert R, et al. Heart rate variability and first cardiovascular event in populations without known cardiovascular disease: meta-analysis and dose-response meta-regression. *Europace*. 2013;15(5):742-749.
15. Pryor WA, Stone K. Oxidants in cigarette smoke: radicals, hydrogen peroxide, peroxyxynitrate, and peroxyxynitrite. *Ann N Y Acad Sci*. 1993;686:12-27.
16. SRNT Subcommittee on Biochemical Verification. Biochemical verification of tobacco use and cessation. *Nicotine Tob Res*. 2002;4(2):149-159.
17. Driscoll D, Diccio G. The effects of metronome breathing on the variability of autonomic activity measurements. *J Manipulative Physiol Ther*. 2000;23(9):610-614.
18. Barutcu I, Esen AM, Kaya D, et al. Cigarette smoking and heart rate variability: dynamic influence of parasympathetic and sympathetic maneuvers. *Ann Noninvasive Electrocardiol*. 2005;10(3):324-329.
19. Task Force of the European Society of Cardiology and the North American Society of Pacing and Electrophysiology. Heart rate variability: standards of measurement, physiological interpretation and clinical use. *Circulation*. 1996;93(5):1043-1065.
20. Breton CV, Yin F, Wang X, Avol E, Gilliland FD, Araujo JA. HDL anti-oxidant function associates with LDL level in young adults. *Atherosclerosis*. 2014;232(1):165-170.
21. Yin F, Lawal A, Ricks J, et al. Diesel exhaust induces systemic lipid peroxidation and development of dysfunctional pro-oxidant and pro-inflammatory high-density lipoprotein. *Arterioscler Thromb Vasc Biol*. 2013;33(6):1153-1161.
22. Ramanathan G, Yin F, Speck M, et al. Effects of urban fine particulate matter and ozone on HDL functionality. *Part Fibre Toxicol*. 2016;13(1):26.
23. Ramanathan G, Araujo JA, Gornbein J, Yin F, Middlekauff HR. Cigarette smoking is associated with dose-dependent adverse effects on paraoxonase activity and fibrinogen in young women. *Inhal Toxicol*. 2014;26(14):861-865.
24. Watson AD, Berliner JA, Hama SY, et al. Protective effect of high density lipoprotein associated paraoxonase. Inhibition of the biological activity of minimally oxidized low density lipoprotein. *J Clin Invest*. 1995;96(6):2882-2891.
25. La Rovere MT, Bigger JT Jr, Marcus FI, Mortara A, Schwartz PJ, ATRAMI (Autonomic Tone and Reflexes After Myocardial Infarction) Investigators. Baroreflex sensitivity and heart-rate variability in prediction of total cardiac mortality after myocardial infarction. *Lancet*. 1998;351(9101):478-484.
26. Bigger JT Jr, Fleiss JL, Steinman RC, Rolnitzky LM, Kleiger RE, Rottman JN. Frequency domain measures of heart period variability and mortality after myocardial infarction. *Circulation*. 1992;85(1):164-171.
27. Dekker JM, Crow RS, Folsom AR, et al. Low heart rate variability in a 2-minute rhythm strip predicts risk of coronary heart disease and mortality from several causes: the ARIC Study: Atherosclerosis Risk In Communities. *Circulation*. 2000;102(11):1239-1244.
28. Liao D, Carnethon M, Evans GW, Cascio WE, Heiss G. Lower heart rate variability is associated with the development of coronary heart disease in individuals with diabetes: the atherosclerosis risk in communities (ARIC) study. *Diabetes*. 2002;51(12):3524-3531.
29. Kobayashi F, Watanabe T, Akamatsu Y, et al. Acute effects of cigarette smoking on the heart rate variability of taxi drivers during work. *Scand J Work Environ Health*. 2005;31(5):360-366.
30. Wilson MD, McGlothlin JD, Rosenthal FS, Black DR, Zimmerman NJ, Bridges CD. Ergonomics: the effect of occupational exposure to environmental tobacco smoke on the heart rate variability of bar and restaurant workers. *J Occup Environ Hyg*. 2010;7(7):D44-D49.
31. Dinas PC, Koutedakis Y, Flouris AD. Effects of active and passive tobacco cigarette smoking on heart rate variability. *Int J Cardiol*. 2013;163(2):109-115.
32. Sjoberg N, Saint DA. A single 4 mg dose of nicotine decreases heart rate variability in healthy nonsmokers: implications for smoking cessation programs. *Nicotine Tob Res*. 2011;13(5):369-372.
33. Haass M, Kübler W. Nicotine and sympathetic neurotransmission. *Cardiovasc Drugs Ther*. 1997;10(6):657-665.
34. Mol MJ, de Rijke YB, Demacker PN, Stalenhoef AF. Plasma levels of lipid and cholesterol oxidation products and cytokines in diabetes mellitus and cigarette smoking: effects of vitamin E treatment. *Atherosclerosis*. 1997;129(2):169-176.
35. Singh N, Singh N, Kumar Singh S, Kumar Singh A, Kafle D, Agrawal N. Reduced antioxidant potential of LDL is associated with increased susceptibility to LDL peroxidation in type ii diabetic patients. *Int J Endocrinol Metab*. 2012;10(4):582-586.
36. Lerner CA, Sundar IK, Watson RM, et al. Environmental health hazards of e-cigarettes and their components: oxidants and copper in e-cigarette aerosols. *Environ Pollut*. 2015;198:100-107.
37. Ji EH, Sun B, Zhao T, et al. Characterization of electronic cigarette aerosol and its induction of oxidative stress response in oral keratinocytes. *PLoS One*. 2016;11(5):e0154447.
38. Putzhammer R, Doppler C, Jakschitz T, et al. Vapours of US and EU market leader electronic cigarette brands and liquids are cytotoxic for human vascular endothelial cells. *PLoS One*. 2016;11(6):e0157337.
39. Connor Gorber S, Schofield-Hurwitz S, Hardt J, Levasseur G, Tremblay M. The accuracy of self-reported smoking: a systematic review of the relationship between self-reported and cotinine-assessed smoking status. *Nicotine Tob Res*. 2009;11(1):12-24.
40. Stein PK, Rottman JN, Kleiger RE. Effect of 21 mg transdermal nicotine patches and smoking cessation on heart rate variability. *Am J Cardiol*. 1996;77(9):701-705.
41. Harte CB, Meston CM. Effects of smoking cessation on heart rate variability among long-term male smokers. *Int J Behav Med*. 2014;21(2):302-309.
42. Minami J, Ishimitsu T, Matsuoka H. Effects of smoking cessation on blood pressure and heart rate variability in habitual smokers. *Hypertension*. 1999;33(1 Pt 2):586-590.
43. Sandhu RK, Jimenez MC, Chiuve SE, et al. Smoking, smoking cessation, and risk of sudden cardiac death in women. *Circ Arrhythm Electrophysiol*. 2012;5(6):1091-1097.
44. Thun MJ, Carter BD, Feskanich D, et al. 50-year trends in smoking-related mortality in the United States. *N Engl J Med*. 2013;368(4):351-364.
45. Pope CA III, Burnett RT, Krewski D, et al. Cardiovascular mortality and exposure to airborne fine particulate matter and cigarette smoke: shape of the exposure-response relationship. *Circulation*. 2009;120(11):941-948.

Supplementary Online Content

Moheimani RS, Bhetraratana M, Yin F, et al. Increased cardiac sympathetic activity and oxidative stress in habitual electronic cigarette users: implications for cardiovascular risk. *JAMA Cardiol*. Published online February 1, 2017. doi:10.1001/jamacardio.2016.5303

eMETHODS: Paraoxonase-1 (PON-1) Enzymatic Activity

eTable 1: Baseline Characteristics (Includes 5 E-cigarette Users With Detectable Nicotine)

eTable 2: E-Cigarette Use in All E-cigarette Users Without Detectable Nicotine

eTable 3: Heart Rate Variability (Includes 5 E-cigarette Users With Detectable Nicotine) (Normalized Units)

eTable 4: Heart Rate Variability (Includes 5 E-cigarette Users With Detectable Nicotine) (Absolute Units)

eTable 5: Blood Tests (Includes 5 E-cigarette Users With Detectable Nicotine)

eFigure 1: Cotinine Levels in E-cigarette Users Without Detectable Nicotine

This supplementary material has been provided by the authors to give readers additional information about their work.

eMETHODS-SUPPLEMENT

Paraoxonase-1 (PON-1) enzymatic activity:

The enzymatic activity of human plasma PON-1 was determined by its capacity to hydrolyze paraoxon substrate to p-nitrophenol. Assays were performed in duplicate in clear, flat-bottom, 96-well plates (Corning® Costar®), and measurements were conducted using the BioTek Synergy Mx microplate reader and Gen5 software. From each plasma sample, 5 μ L was incubated with paraoxon (Chem Service Inc., catalog # N-12816-100MG) in the assay buffer (0.1 M Tris-HCl buffer at pH 8.5, with 2 M NaCl and 2 mM CaCl₂) at room temperature. The kinetics of p-nitrophenol formation were immediately measured every 15 seconds at 405 nm for a total of four minutes in the BioTek microplate reader. The absorbance readings (OD/min) were converted into nanomoles p-nitrophenol/min/ml with the use of the molar extinction coefficient for p-nitrophenol, determined to be 16,734 M⁻¹cm⁻¹ at a pH of 9.18, and considering a path length of 0.58 cm.

eTABLE 1-SUPPLEMENT
Baseline Characteristics (Includes 5 e-cigarette users with detectable nicotine)

	E-Cigarette User (n=21)	Non-User Control (n=18)	p value
Age (years)	28.7 ± 1.1	26.6 ± 1.5	0.25
Sex (M/F)	15/6	7/11	0.05
BMI (kg/m ²)	25.3 ± 0.7	23.0 ± 0.9	0.04
Ethnicity			
African American	1	2	
Asian	3	3	
Hispanic	2	2	
White (Non-Hispanic)	15	11	
Former smoker	15	2	
Pack-years	2.3 ± 0.5	0.6 ± 0.4	
Interval since quitting (years)	2.3 ± 0.6	13 ± 7	
E-cigarette use			
Minutes/day	247 ± 284 (5-960)		
Duration (years)	1.8 ± 0.6 (1-3)		
SBP (mmHg)	116.4 ± 2.2	109.0 ± 2.6	0.07
DBP (mmHg)	74.6 ± 2.3	70.0 ± 2.0	0.11
MAP (mmHg)	88.5 ± 2.0	83.0 ± 2.0	0.07
HR (bpm)	65.9 ± 2.3	63.0 ± 2.0	0.35

BMI = body mass index, bpm = beats per minute, DBP = diastolic blood pressure, HR = heart rate, MAP = mean arterial pressure, SBP = systolic blood pressure

eTable 2-SUPPLEMENT**E-Cigarette Use**

User	Device* Liquid/day (ml)	Flavor	Nicotine(mg)[†]	
1	Pen	Strawberry cheesecake, Unicorn	6	Unknown
2	Mod	Milk	3	15+
3	Cigalike, Pen Unknown	Blu, Cherry	2.4%, 3	
4	Pen	Fruit	6	2
5	Cigalike Unknown	Mint		18
6	Mod	Fruity	6	3
7	Pen	Menthol	12	3
8	Pen	Savory Flavors		3 3
9	Pen	Custards and Creams	8	Unknown
10	Pen	Gogurt	3	Unknown
11	Pen	Chase the Vapor	8	Unknown
12	Cigalike Unknown	Menthol		12
13	Unknown	Apple, Fruit	1.2%	5
14	Unknown	Vaping Rabbit, Milkman		3 2
15	Mod	Vapor Chef, Honeydew		3 4-7
16	Mod	Fruity, Menthol		3 6
**17	Pen	Vanilla	6	3-5
**18	Pen	Vapor nuvola, Guava banana	12	Unknown
**19	Mod	Enigma, Blueberry, Strawberry		3 22
**20	Pen	Vapism, White Girl	6	15
**21	Cigalike	Menthol Ice		2.4% 8

*E-cigarette devices are generally divided into 1st generation “Cigalike” devices, which come with a chamber preloaded with e-liquid; 2nd generation, “Pen” devices, in which the

user can mix and refill customized flavors; and 3rd generation, “Mods” in which the voltage of the heating element can be modified, providing a larger quantity of aerosol.

† Units of nicotine content is mgs in the eLiquid used in the Pen and Mods, % in the Cigalike devices

**17-21 were excluded from analysis since they had detectable nicotine levels consistent with recent e-cigarette use.

eTable 3-SUPPLEMENT

**Heart Rate Variability (Includes 5 e-cigarette users with detectable nicotine)
(normalized units)**

	E-Cigarette User (n=21)	Non-User Control (n=18)	<i>p</i> value
HF (nu)	48.2 ± 3.2	57.8 ± 3.5	<0.05
LF (nu)	51.0 ± 3.4	39.9 ± 3.6	0.03
LF/HF ratio	1.25 ± 0.16	0.85 ± 0.17	0.09

HF = high frequency, LF = low frequency, nu=normalized units; Mean values are displayed since these data followed a parametric distribution.

eTable 4-SUPPLEMENT

Heart Rate Variability (Includes 5 e-cigarette users with detectable nicotine)

(absolute units)

	E-Cigarette User	Non-User Control	<i>p</i> value
	(n=21)	(n=18)	
HF (μs^2)	615.0 \pm 259.8	1376.5 \pm 574.2	0.14
LF (μs^2)	483.0 \pm 220.6	1316.0 \pm 504.0	0.09
VLF (μs^2)	942.5 \pm 409.0	987.1 \pm 432.5	0.66
Total power (μs^2)	1970.0 \pm 601.8	4502.0 \pm 1279.8	0.03

HF = high frequency, LF = low frequency, VLF = very low frequency; Median values are displayed since these data followed a nonparametric distribution.

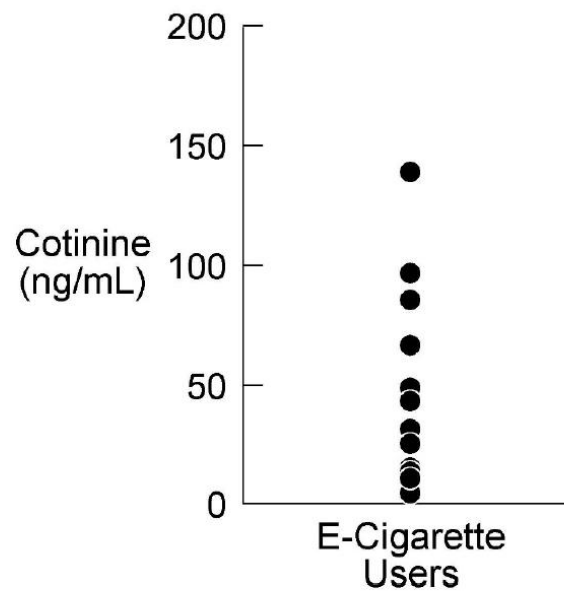
eTable 5-SUPPLEMENT

Blood tests (Includes 5 e-cigarette users with detectable nicotine)

	E-Cigarette User	Non-User Control	<i>p</i> value
	(n=12)	(n=18)	
LDL-Ox (units)	3741.7 ± 351.6	2413.3 ± 310.1	
0.008			
PON-1 (nmol p-nitrophenol/min/ml)	612.3 ± 109.3	892.8 ± 110.0	0.08
HOI (units)	0.49 ± 0.05	0.38 ± 0.04	0.09
Fibrinogen(mg/dL)	268.9 ± 9.7	251.4 ± 10.5	0.23

HOI = HDL anti-oxidant index, LDL-Ox = LDL-Oxidizability, PON-1 = Paraoxonase-activity; Mean values are displayed since these data followed a parametric distribution.

eFigure 1.



eFigure 1. Cotinine levels on the day of the study in e-cigarette users. Cotinine levels are well-distributed across the range of values from 3.8-139 ng/mL.

References (for the Introduction)

Boas, Z., P. Gupta, R. S. Moheimani, M. Bhetraratana, F. Yin, K. M. Peters, J. Gornbein, J. A. Araujo, J. Czernin and H. R. Middlekauff (2017). "Activation of the "Spleno-cardiac Axis" by electronic and tobacco cigarettes in otherwise healthy young adults." Physiol Rep **5**(17).

Mackness, M. I., P. N. Durrington and B. Mackness (2004). "The role of paraoxonase 1 activity in cardiovascular disease: potential for therapeutic intervention." Am J Cardiovasc Drugs **4**(4): 211-217.

Moheimani, R. S., M. Bhetraratana, K. M. Peters, B. K. Yang, F. Yin, J. Gornbein, J. A. Araujo and H. R. Middlekauff (2017). "Sympathomimetic Effects of Acute E-Cigarette Use: Role of Nicotine and Non-Nicotine Constituents." J Am Heart Assoc **6**(9).

Moheimani, R. S., M. Bhetraratana, F. Yin, K. M. Peters, J. Gornbein, J. A. Araujo and H. R. Middlekauff (2017). "Increased Cardiac Sympathetic Activity and Oxidative Stress in Habitual Electronic Cigarette Users: Implications for Cardiovascular Risk." JAMA Cardiol **2**(3): 278-284.

Yin, F., A. Lawal, J. Ricks, J. R. Fox, T. Larson, M. Navab, A. M. Fogelman, M. E. Rosenfeld and J. A. Araujo (2013). "Diesel exhaust induces systemic lipid peroxidation and development of dysfunctional pro-oxidant and pro-inflammatory high-density lipoprotein." Arterioscler Thromb Vasc Biol **33**(6): 1153-1161.

CHAPTER 5 –
CONCLUSIONS AND FUTURE DIRECTIONS

Our research demonstrated that DEPe induced peritoneal macrophages to have more of a Mox phenotype, commonly driven by the antioxidant transcription factor NRF2 across multiple mouse strains, as discussed in Chapter 2. To our knowledge, this identification of a Mox-like subtype in DEPe-treated macrophages had not been reported before. The Mox macrophage subtype is uniquely different from other known subtypes like M1 and M2. Thus, future studies could be conducted to determine the behavior of these DEP-treated cells, such as their migrating and phagocytic capabilities. Also, because of the importance of *Nrf2* in cell responses to DEPe, looking at gene expression profiles of macrophages that are deleted for *Nrf2* to determine if the Mox marker pattern would be ablated and if another macrophage subtype becomes more prominent would provide a better mechanistic understanding of air pollution responses especially in our mNrf2 KO mice.

In Chapter 3, hyperacute DEP exposures in the mNrf2 KO mice resulted in visually obvious symptoms of respiratory distress. Since we did not notice any definitive explanation for this, such as a distinct influx of inflammatory cells, we are aiming to collaborate with a pulmonary physiology lab to measure lung function and quantify their respiratory distress. These mice also had signs of diastolic dysfunction. To look at the risks for cardiovascular disease like atherosclerosis, a worthy future study would be to conduct chronic exposures with mNrf2 KO mice in an ApoE null background and to determine plaque formation, for instance. Additionally, data from scRNA-seq of our lungs identified potential genes that could explain the sickness observed in mNrf2 KO mice, including circulating factors such as S100A8/9 and humanin. Thus,

performing scRNA-seq on the heart tissue and more assays on circulating factors in the blood could help elucidate a clearer link between lung exposures and cardiovascular disease.

Finally, in Chapter 4 we demonstrated that chronic use of e-cigs can lead to dysfunctions in the cardiovascular system, specifically on heart rate variability and LDL oxidizability. In follow-up studies, we continued to further show an acute effect of e-cig use on heart rate variability. Other measures of cardiovascular function would be worth analyzing in future research to gauge the extent of harm that e-cigs may produce, especially in comparison to tobacco cigarettes.

This dissertation discussed the effects of two inhalation toxicants – DEP and e-cigs – each with their own cardiovascular risks. From a public health perspective, policies surrounding vehicular and industrial emissions as well as e-cig device manufacturing and marketing are important for the public’s safety, and based on our findings, I would urge for greater regulation. This is because trends of global air pollution levels have been mixed, and the prevalence of e-cig devices in society is rising. From a molecular toxicology perspective, the mechanistic process by which air pollutants cause cardiovascular disease and the extent of the risks caused by smoking e-cigs are both suggestive but remain uncertain, and thus more studies need to be done in both realms.